EMULSION TEMPLATING AS A ROUTE TO THE RELEASE OF ORGANIC MICRO- AND NANO-PARTICLES

Thesis submitted in accordance with the requirements of the University of Liverpool for the degree of Doctor in Philosophy

by

Neil Cameron Grant

November 2011

ABSTRACT

Many useful organic molecules such as drugs are poorly soluble in water. Novel ways of the deployment of these molecules are as stable nanodispersions. In our research we aim to produce a method for the creation of nanoparticles via a technique called emulsion-evaporation. These techniques include the creation of emulsions, polymerisation and freeze-drying. The production of these nanoparticles in-situ with templated porous polymers by these techniques was used. This avoids the problem of nanoparticle aggregation. These nanoparticles can be released into an aqueous medium by diffusing out of the porous scaffold or by a stimuli-sensitive trigger. We describe here the preparation of porous poly N-isopropylacrylamide. The swelling of the polymer and contraction above a solution temperature were explored for the uptake and release of polymeric colloids. The thesis discusses the application of readily soluble aqueous nanodispersions prepared by using a polyvinyl alcohol/sodium dodecyl sulphate (PVA/SDS) monolith prepared by emulsion templating. The monoliths can be prepared with the in-situ formation of drug nanoparticles which, readily solubilises the drug as nanodispersions. The thesis continues to explore stimuli as a method for the release of the organic nanoparticles: a chitosan based emulsion templated monolith was prepared which can release the formed nanoparticles from the scaffolds via control of pH. Finally, the use of a disulphide crosslinked polymer was explored for the release of organic nanoparticles. The particles could be released from the polymer by using a disulphide bond "cleaver" which degrades the polymer and thus releasing the internal organic nanoparticles.

ACKNOWLEDGEMENTS

Firstly, many thanks go to Dr Haifei Zhang who has given me his time guidance and encouragement and friendly support during some difficult times. Also my thanks go to Professor Andrew Cooper and his group for their participation in discussions and advice (and some office space!).The EPSRC is acknowledged for funding of the PhD.

To everyone in my year group at University of Liverpool it has been a brilliant 8 years altogether and it has been a privilege to have such a good set of friends whilst we have all struggled on!

On a more general manner, the author would like to thank all the staff at the Department of Chemistry for their involvement through technical support, in some cases analysis but above all friendship.

Most importantly, I'd like to thank my family, Mum and Dad especially for their support over the last few years, as difficult as it has been. Finally, I am indebted to the love and support of my wife (to be, at the time of writing!) Clare, without your support, encouragement and patience I would not have been able to have completed this PhD. I should also mention the kids – Faye and Sam who have taken me as their own father and I cannot understate how fantastic and understanding they have been whilst I have been writing up (Sam - It won't be long now before I'll let you on my computer!), you'll be a fantastic brother and sister to baby James. I cannot wait for all the fabulous years we will have with our family.

Publications/Proceedings Resulting from this Work

- Grant, N., Zhang, H.F., "Preparation of poorly water-soluble drug nanoparticles and instant formation of aqueous nanoparticle dispersions", manuscript submitted
- Grant, N., Cooper, A.I., Zhang, H.F., "Uploading and temperature-controlled release of polymeric colloids via hydrophilic emulsion-templated porous polymers", ACS Appl. Mater. Interfaces, 2010, 2 (5), 1400–1406
- Grant, N; Rannard, S, Cooper, A.I., Zhang, HF, "Preparation and pH-responsive release of organic nanoparticles", Journal of Pharmacy and Pharmacology, 2009, 61, A1-A1
- Grant, N., Cooper, A. I., Zhang, H.F., "Preparation of poorly water-soluble drug nanoparticles and release into aqueous solutions", Journal of Pharmacy and Pharmacology, 2009, 61, A14-A14
- Grant, N., Zhang, H., Cooper, A. I., "Thermoresponsive polymeric pumps for the release of drug nanoparticles", Materials Research Society Symposium Proceedings, 2008, 1095, 25-29

CONTENTS

LIST OF FIGURES

Chapter 1:

Chapter 4

List of Abbreviations

APS – Ammonium Persulfate

AM - Acrylamide

BAC – N, N' - bisacryloylcystamine

CH – Cyclohexane

CHIT - Chitosan

DLS – Dynamic Light Scattering

HIPE – high internal phase emulsion

IMC – Indomethacin

LCST – Lower critical solution temperature

MBAM – N,N-methylenebisacrylamide

MW – Molecular Weight

NIPAM – N-isopropylacrylamide

OR – Oil Red

O/W – Oil-in-water

PNIPAM – Poly N-isopropylacrylamide

PS - Polystyrene

PVA – Polyvinyl alcohol

SDS – Sodium dodecyl sulphate

SEM – Scanning Electron Microscopy

SS – Disulphide bond

TEM – Transmission Electron Microscopy

TMEDA – Tetramethylethylenediamine

UCST – Upper critical solution temperature

UV – Ultraviolet

W/O – Water-in-oil

XRD – X-ray Diffraction

XYL – o-xylene

1 INTRODUCTION

"These new compounds, like rocks, never dissolve in water".[1] It is estimated that approximately 40% of newly discovered drug candidates are difficult to formulate due to their lack of solubility in water.[2,3] Overcoming the issue of poor water solubility is of great interest in the pharmaceutical industry.

This thesis focuses on emulsion templated materials for: i) the uploading and release of polymeric colloids and ii) release of drug nanoparticles from porous composites.

LAYOUT OF THE THESIS

Within this thesis the research is split into 4 categories, each with its own introduction, results, discussion, and conclusion sections. Separating the chapters this way is intended to give the reader a clearer picture of each project.

The first experimental chapter, Chapter 2 investigates the uploading and release of polymeric colloids via thermoresponsive emulsion templated polyNIPAM. It was shown that microparticles can be uploaded and released on demand reproducibly from porous, thermoresponsive polyNIPAM.[4]

Chapter 3 looks at the preparation of IMC nano-dispersions through emulsion templating. Oil-in-water emulsions of PVA/SDS were prepared and freeze-dried. The freeze-dried materials were shown to rapidly dissolve into aqueous solutions.[5]

Chapter 4 focuses on the pH-dependent release of organic nanoparticles from emulsion templated Chitosan. Firstly, the biological dye Oil Red was used to model the release of nanoparticles from the templated material. After which the model drug Indomethacin (IMC) was used to be released from the prepared materials.

Finally, Chapter 5 investigates the redox-responsive release of Oil Red from disulphide cross-linked polymers. In aqueous conditions the material swells and slowly diffuses Oil Red (OR), however when treated with dithiothreitol, the materials degrade releasing the OR as nanoparticles.

Herein is an introduction to the key aspects and techniques employed throughout the research which are on common ground throughout the thesis.

1.1 Emulsions

Emulsions are a heterogeneous mix of two or more immiscible liquids.[6] One liquid can exist in the form of droplets within the other and usually one liquid will be water or an aqueous solution. The diameter of the droplets are typically in the range of >0.1 μm.[7,8] These immiscible fluids are generally stabilized by surface active agents (surfactants), solids and polymers. Emulsions are usually described as oil-in-water (O/W) or water-in-oil (W/O) reverse phase representing the internal phase and external phase respectively.[9]

There are three principle methods for the production of emulsions:

- physical emulsification (i.e. stirring)
- emulsification by phase inversion[10]

- spontaneous emulsification[11]

The latter two methods are chemical based processes where the final emulsions are controlled by the chemical makeup of the system while the first depends on the mechanical nature of the process.

In all emulsions, an emulsifier is needed to assist the droplet formation to the desired stability. An emulsifier has two primary functions:

- lower the energy requirements to form droplets (i.e. interfacial tension)
- hinder the reversal of drop formation

For an emulsifier to perform correctly it must be able to absorb at the interface between the droplet and the continuous phases. They must also form some kind of layer or barrier at the interface to prevent or slow down droplet coalescence.[12]

Emulsifiers can be split into four different classes: i) Ionic materials (figure 1a) – these usually have little effect on the interfacial tension. However, they can aid in the stabilization by inducing an electrostatic barrier between approaching drops; ii) colloidal solids (figure 1b) – do not directly affect the interfacial tension, yet can stabilize emulsions by absorbing at the interface and forming a barrier between droplets;[13] iii) polymeric materials (figure 1c) – these may aid emulsion formation as some polymers may have surface active properties; their main function is as stabilizers however, and their actions result from steric or electrostatic interactions. Finally, surfactants (figure 1d) – these decrease the interfacial tension and add stability to a system. An account of surfactants is given in chapter 1.2.

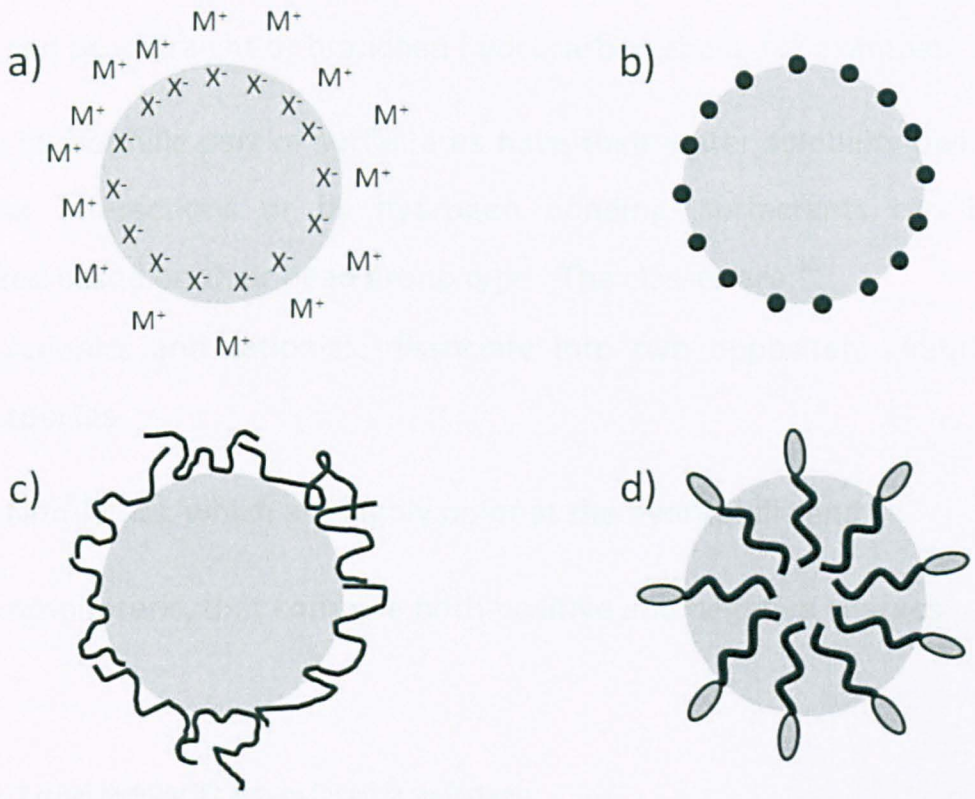

Figure 1-1 – Stabilisation methods for droplets; a) stabilisation by salts where M+ is a metal cation and X- is the corresponding counterion; b) stabilisation by colloidal particles; c) stabilisation by polymeric surfactants and d) by surfactants

1.2 Surfactants

Surfactants (short for surface active agents) are molecules which interact at an interface. They consist of two parts: a lyophilic ('solvent-loving') and a hydrophobic ('solvent fearing') group in the molecule.[14] Their structures consist of a hydrophobic tail, typically a hydrocarbon, with a polar hydrophilic head group which can be ionic or non-ionic. When surfactants are dissolved at low concentrations, they have the ability to absorb at interfaces, altering the physical properties observed at the interface.[15]

1.2.1 Classification of Surfactants

Several variations are possible within the structure of surfactants at both the head group and the tail group of the molecules. The head

group can be charged or neutral and relatively small in size. The tail group can be a straight or branched hydrocarbon chain, for example.

As the hydrophilic part of surfactants have their water solubility owing to ionic interactions or by hydrogen bonding, surfactants can be classified based on their head group type. The classes are:[15]

- Anionics and cationics, dissociate into two oppositely charged species
- Non-ionics, which are highly polar at the hydrophilic end
- Amphoteric, that combine both positive and negative charges

Table 1 – Typical hydrophilic groups found in surfactants

Class	Structure
Sulfate	$R\text{-}OSO_3^-M^+$
Carboxylate	$R\text{-}COO^-M^+$
Betaines	$RN^+(CH_3)_2CH_2COO^-$
Polyoxyethylene	$R\text{-}OCH_2CH_2(OCH_2CH_2)_nOH$
polyglycodyl	$R\text{-}(OCH_2CH(CH_2OH)CH_2)_n\text{-}OCH_2CH(CH_2OH)CH_2OH$

Table 2 – Typical hydrophobic groups found in surfactants

Class	Structure
Fatty acids	$CH_3(CH_2)_n$
Olefins	$CH_3(CH_2)_nCH{=}CH_2$
Alkylbenzenes	$CH_3(CH_2)_nCH_2\text{-}Bz\text{-}OH$
Fluorocarbons	$CF_3(CF_2)_nCOOH$

1.2.2 Uses of Surfactants

Synthetic surfactants are an essential component in many industrial formulations. The number and arrangement of the hydrocarbon groups together with the nature of the hydrophilic group can determine the surface active properties, for example emulsification, of the surfactants. Surfactants with hydrocarbon chains of C12 to C20 are optimum for detergency, where shorter chains are more useful for wetting and foaming. Anionics and nonionics at the head group, for example sulfates ($-OSO^{3-}$) and ethoxylates ($-(OCH_2CH_2)_mOH$) respectively can be applied to formulations as emulsifiers and soaps. Other uses of surfactants can have place in the Petroleum industry, paints and in pharmaceutical research, to name a few.[16]

1.3 Emulsion Stability

Emulsion instability can arise from a number of processes which take place individually or simultaneously. There are four main ways that an emulsion can become unstable: sedimentation, flocculation, coalescence and Ostwald ripening.[12,17]

1. Sedimentation (or Creaming) (Figure 2b)

Creaming occurs in all systems where there is a difference in densities between the two phases. The emulsion droplets can rise (cream) or fall (sediment) in an emulsion system.[17]

2. Flocculation (2c)

Flocculation is where droplets in an emulsion aggregate, without the rupturing of the stabilizing layer at the oil-water interface.[17]

3. Coalescence (2D)

Coalescence is where two or more droplets in the emulsion fuse together to form a single larger droplet, this step is irreversible. For this process to occur, the film that separates the droplets becomes sufficiently thin that the force of the droplets ruptures the film from which coalescence occurs.[17]

4. Ostwald Ripening

Ostwald ripening is the result of differences in chemical potential between droplets of different sizes where the two liquids have a mutual solubility. Smaller droplets have a greater solubility than larger droplets. Dispersed molecules from the smaller droplets will diffuse from the surface and join with the larger droplets. As a result a shift in interfacial area reduction is observed and as a result smaller droplets become smaller and larger droplets become larger.[18] Ostwald ripening was first described by Ostwald in the 1900s.[19]

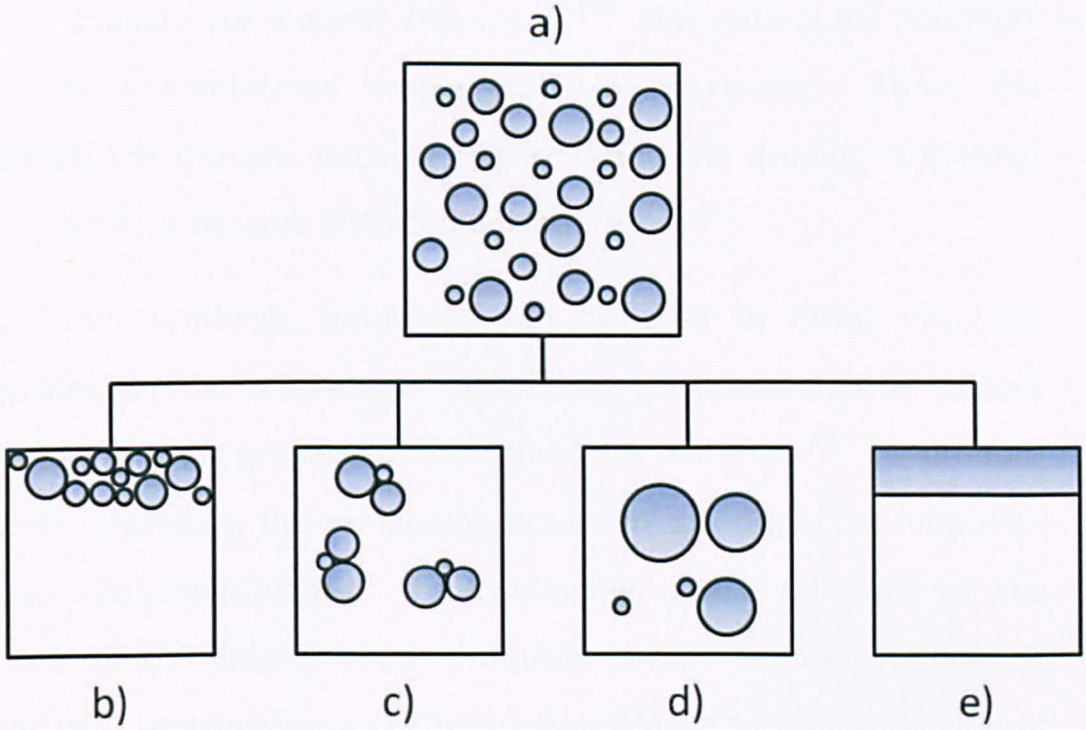

Figure 1-2 – An emulsion a) and stability issues associated: b) creaming (or sedimentation), c) flocculation, d) coalescence and e) complete phase separation of emulsions

1.4 Emulsion Templating

Emulsions are a mixture of two immiscible liquids with one phase dispersed in the other. Emulsions can range from as little as 5% up to 99% v/v (percentage of internal phase droplets in a continuous phase). Depending on the range, emulsions can be classified as having low, medium or high internal phase ratios. The continuous phase of the emulsions can be polymerised and a porous material prepared after drying to remove the internal phase. Bismarck classified polymerised low and medium phase emulsions as having internal phase ratios of <25 % and between 30 and 70 % respectively.[20] For higher internal phase ratios, the term HIPE was coined from much earlier publications.[21-24]

High internal phase emulsions (HIPEs) have been known for a number of years. Emulsions are all around us and are commonly seen in foods, paints, fuels and in the cosmetic industry.[16] The major aspect of HIPEs

is their droplet ratio is above 74% v/v.[17,22-29] This value is the maximum of which non-deformed droplet spheres are made. Above this threshold the droplets become distorted and the droplets are either non-uniform or become distorted polyhedra.[17,22-29]

In polymer synthesis, emulsions can be used in three ways: (1) templates for the preparation of colloids; (2) preparation of porous materials and (3) preparation of composite materials.[29] To produce colloidal materials, the templating occurs in the dispersed monomer phase. Polymerisation of the continuous phase followed by the removal of the droplet phase produces porous emulsion templated materials.[26] Polymerisation of both phases leads to the production of composite materials.[30] Figure 3 shows a representation of emulsion templated materials. The synthesis of porous materials is the focus of this thesis.

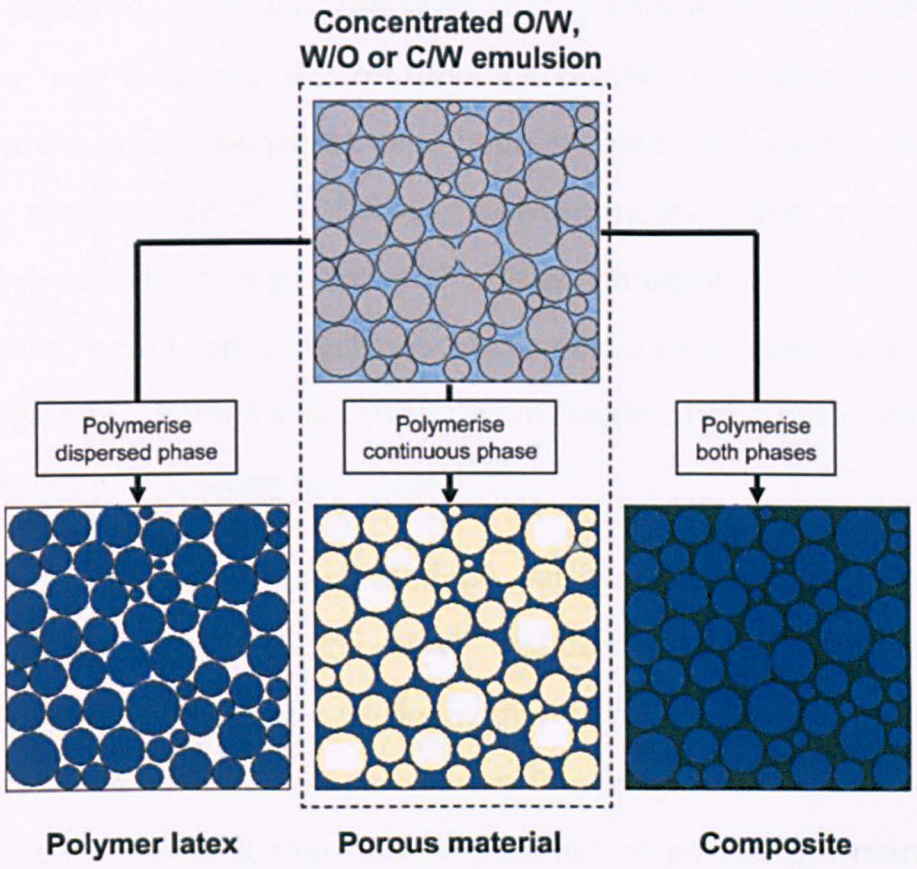

Figure 1-3 – Schematic representation of polymerisation of an emulsion in the dispersed phase, continuous phase, and both phases for the preparation of colloids, porous materials, and composites, respectively. C/W is supercritical carbon dioxide in water.[29]

1.4.1 Synthesis of Porous Emulsion Templated Materials

Porous polymeric materials prepared by emulsion templating are found in abundance in the literature. Emulsion template structures can be hydrophobic or hydrophilic and prepared from water-in-oil (W/O) and oil-in-water (O/W). In 1982, Unilever[25] patented a process for the preparation of a crosslinked polymeric material polymerised from high internal phase emulsions. The most widely investigated hydrophobic system is based on polymers containing styrene/divinylbenzene.[21,31-35] Other hydrophobic monomers include methylmethacrylate, 2-ethyl hexyl methacrylate and butyl acrylate. [28,36,37]

Hydrophilic O/W emulsions containing acrylic acid monomers have been prepared.[38] It was reported that a choice of surfactant and initiator can influence the morphology of the templated materials. Hydrophilic porous polymers have been prepared using poly(urethane urea) nanoparticles.[39] Porous polyurethanes have also been synthesised within high internal phase emulsions.[40] Hydrophilic polyHIPEs based on 2-hydroxyethyl methacrylate have also been investigated.[41] Porous silica and titanium oxide can be prepared using the emulsion templating technique.[42,43]

Emulsions can also be stabilised by particles, commonly known as Pickering Emulsions.[44-47] Binks et al[48] first demonstrated stabilisation of emulsions with Pickering particles with volume fractions of 65 and 70 vol%. Porous polymers prepared from Pickering emulsions have been prepared.[49] Bismarck reported preparation of porous polymers with Pickering particles with an internal phase of up to 92 vol%.[50]

1.4.2 Applications of Emulsion Templated Materials

Tissue engineering and Cell Culture

Styrene/di-vinylbenzene polyHIPEs have been prepared and used as scaffolds to culture hepatocyte cells.[51] A hydrophilic HIPE based on a poly(ε-caprolactone) oligomer with terminal vinyl groups was used as a crosslinking comonomer for a polyHIPE based on t-butyl acrylate which was reported to exhibit enhanced cell adhesion and growth.[28]

Purification

PolyHIPEs based on 4-vinylbenzyl chloride and divinylbenzene were functionalised by a flow through method. Columns with immobilized tris(2-aminoethyl)amine were applied for the effective removal of acid

chlorides from the solution pumped through the column. High effectiveness of columns were demonstrated by an over 90% of acid chloride removal from the solution after a single pass-flow of the solution through the column. The morphology of the column material was characterized by scanning electron microscopy and showed no damage of the material after the flow-through utilization.[52] The removal of atrazine from water by a solid phase extraction technique using insoluble polymers was described.[53] Porous crosslinked polymers bearing piperazine prepared from the precursor 4-nitrophenylacrylate. Polymers were applied to sequester atrazine from aqueous solutions with a concentration of 33 ppb and irreversible covalent bonding to the polymers was achieved. The dynamics of atrazine uptake were monitored and it was found that almost complete removal of atrazine was accomplished with an excess of polymer after 48 hours at room temperature.

Reactions and separations

Poly(glycidyl methacrylate-co-ethylene glycol dimethacrylate) based monolithic columns were prepared for liquid chromatography with microsized particles.[54] Yang et al,[55] recently prepared poly(vinyl ester) stabilised by poloxamer 127 polyHIPEs for potential applications in separation. A palladium based organosilica polyHIPE was prepared and reported to improve the yield, turnover and cycling performances of the Suzuki-Miyaura and Mizoroki-Heck reactions.[56]

Other applications

Cohen and Silverstein,[57] have recently prepared polyHIPEs based on acrylonitrile polymers for the production of carbon nanotubes. HIPEs have also been prepared by Bismarck as polymer scaffolds for setting

cements.[32] The Bismarck group also have published several articles on the preparation of tough macroporous polymers through stabilisation with silica and titania particles.[58,59]

There are extensive reviews on the synthesis and applications of emulsion templated materials, the most recent from Kimmins and Cameron,[27] older reviews which can be of interest to the reader can also be found in the literature. [22,29]

1.5 Poorly Water Soluble Drugs

A wide range of organic materials are poorly soluble in water or water-miscible solvents. Lipinski reported that 31.2 % of a group of 2246 compounds had a solubility equal to or less than 20 μg/ml.[60] Such low water solubility results in low bioavailability which is of great concern in the pharmaceutical industry. It is estimated that >40% of marketed drugs are poorly water soluble.[61,62] Based on the biopharmaceutical classification system (BCS), drugs can be placed into four categories (see Figure 4).

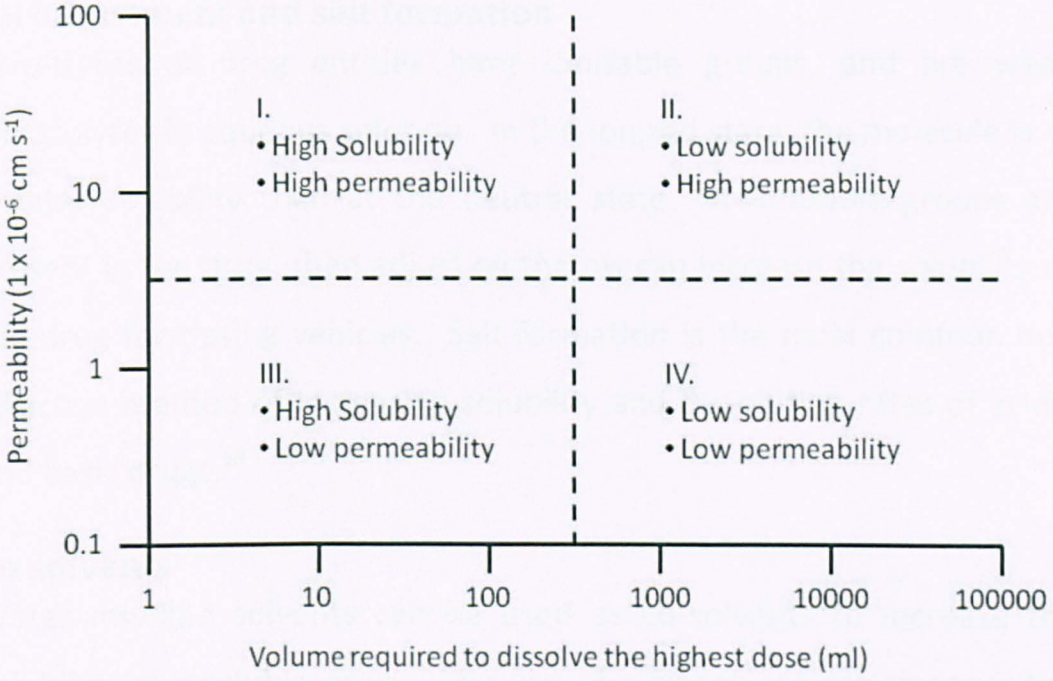

Figure1-4 The Biopharmaceutical classification system[62]

The four categories are: Class I - High intestinal permeability and high solubility, such compounds are well absorbed into the body; Class II – high permeability and low solubility. The bioavailability of such products is limited by their solvation rates; Class III – Low permeability and High Solubility, these are limited by the permeation rate but the drug is solvated at a fast rate and finally Class IV – Low permeability and low solubility.[62]

Drugs which have low solubility but reasonable membrane permeability are characterized as BCS class II. The drug dissolution step is the rate limiting step.[62]

1.5.1 Formulations of Poorly Water Soluble Drugs

Poorly water soluble drugs can be formulated in a vast array of techniques. Below gives an account of the techniques employed to improve the water solubility of poorly water soluble drugs.

pH adjustment and salt formation

Two-thirds of drug entities have ionisable groups, and are weak electrolytes in aqueous solution. In the ionized state, the molecule is of greater solubility than at the neutral state. If ionisable groups are present in the drug, then adjusting the pH can increase the solubility of the drug for dosing vehicles. Salt formation is the most common and effective method of increasing solubility and dissolution rates of acidic and basic drugs.[63]

Co solvents

Water miscible solvents can be used as co-solvents to increase the solubility of insoluble drugs. The use of a co-solvent can improve the solubility of a non-polar solute by many orders of magnitude. Whereas salt formation aids the solubilisation of molecules with ionisable groups, molecules with no ionisable groups can be used in the co-solvent approach. The most commonly used solvents in the co-solvent approach are Polyethyleneglycol-400 (PEG-400), polypropyleneglycol (PPG), Ethanol, glycerin and dimethylacetamide (DMA).[64,65]

Although the use of co-solvents can increase the solubility of drugs; they have their limitations and disadvantages: firstly, upon dilution in water, precipitation can occur which can affect the drugs bioavailability, another disadvantage to co-solvents is their high toxicity levels associated with the solvent choice.[66]

Complexation

Complexations using cyclodextrins (CDs, figure 5) are widely used for solubilisation of poorly soluble drug compounds. Cyclodextrins are from a family of naturally occurring oligosaccharides which consist of 6-8 D-Glucopyranose units.[67] The presence of such units gives CDs a

hydrophilic exterior and a lyophilic cavity. This cavity is useful for complexation owing to the fact that a guest molecule can form a complex with the CD.[67]

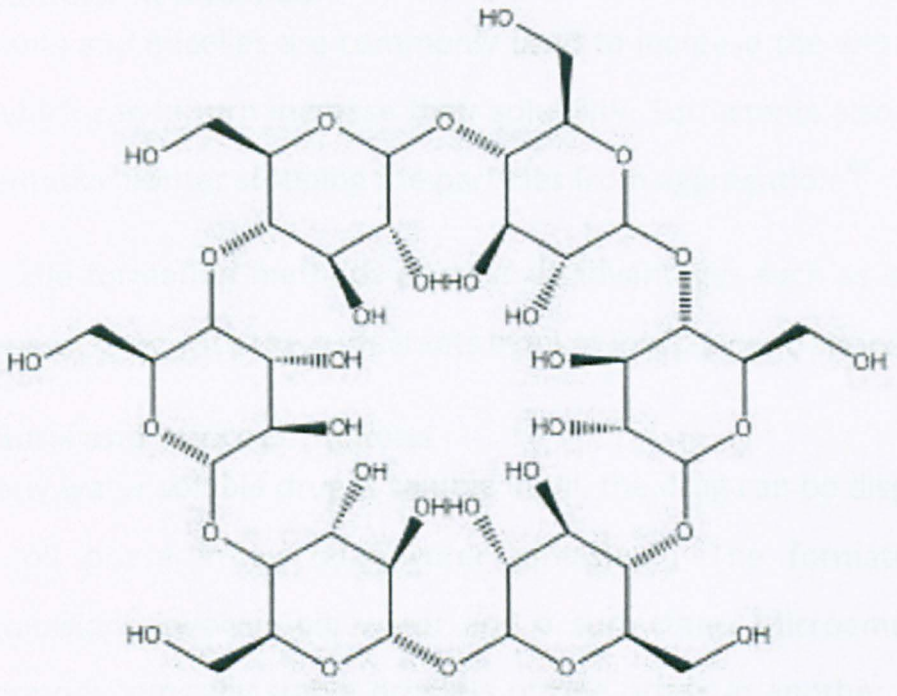

Figure 1-5 – An example of a cyclodextrin

Cyclodextrins are capable of interacting with large variety of guest molecules to form non-covalent inclusion complexes. The outer surface is hydrophilic due to the presence of hydroxyl groups and the interior of the cone is hydrophobic due to presence of glycosidic ether oxygen at O-4 and the hydrogen attached to C-3 and C-5 and thereby provides an environment into which drug can enter and can be partially or fully included without covalent bonding, while outer hydrophilic environment contributes to drug dissolution.[64] The drug molecule and cyclodextrin complex combine in a 1:1 complex:[68]

Disadvantages of cyclodextrins include there having to be a strict correlation between the structure of the guest molecule and the size of the cyclodextrin and cyclodextrins limited solubility in water.[68]

Surfactants and micelles

Surfactants and micelles are commonly used to increase the wetting of drugs which can in turn increase their solubility. Surfactants also act as a preventative barrier stopping the particles from aggregation.[69]

The micelle formation methods possess disadvantages such as toxicity effects associated with the surfactants even at low concentrations.

Emulsions and microemulsions

If a poorly water soluble drug is soluble in oil, the drug can be dispersed in the oil phase in an oil-in-water emulsion. The formation of microemulsions involves oil, water and a surfactant. Microemulsions are thermodynamically stable droplets of one phase in another with a droplet diameter of less than 500 nm.[70] With the disadvantages above regarding the surfactants, the inclusion of a drug within oil diminishes the pharmacokinetics of the incorporated drug.

Nanosuspensions and nanoparticles

Nanosuspensions are a sub-micron dispersion of pure drug particles, which possess a large surface area for enhanced dissolution. A more detailed account of drug nanoparticles and nanosuspensions will be discussed in section 1.6.

1.6 Drug Nanoparticles

Overcoming the issue of poor water solubility is of great interest in the pharmaceutical field. Engineering drug nanoparticles to produce micron and nano-sized particles has been researched to address this

problem.[71,72] The Nernst-Brunner/Noyes-Whitney equation can describe how the dissolution rate of an organic compound is proportional to the surface area available for dissolution.[73]

$$\frac{dX}{dt} = \left(\frac{A.D}{h}\right).\left(\frac{C_s - X_d}{V}\right)$$

where dX/dt=dissolution rate, X_d=amount dissolved, A=particle surface area, D=diffusion coefficient, V=volume of fluid available for dissolution, C_s=saturation solubility, h=effective boundary layer thickness.

Through this principle decreasing the size of particles down to sub-micron range will further increase the dissolution rate due to the increase of particle surface area.[74] For a drug with dissolution limitation, particle size reduction can significantly improve the pharmacokinetics of the drug.[75]

1.6.1 Preparation of Drug Nanoparticles

Drug nanoparticles can be prepared by "top-down" and "bottom-up" approaches. The top-down approach, the size of large drug nanoparticles are reduced to micrometer and nanometer scale by means of high pressure homogenization, milling, or microfluidization.[76-78] For the bottom-up approach, the drug nanoparticles are formed from molecules in a solution or in an emulsion. Emulsion evaporation, solvent displacement, solvent diffusion and rapid freezing have been widely used to prepare drug nanoparticles.[79-81] As a type of green and sustainable solvents, supercritical fluids (particularly supercritical carbon dioxide) have been explored to produce drug particles in the processes of rapid expansion, rapid expansion to aqueous solutions, and anti-solvent effect on organic drug solutions.[71,82-84]

1.6.2 Emulsion Evaporation (or Precipitation)

In this research the organic nanoparticles are prepared via methods similar to emulsion-evaporation. Preparation of nanoparticles via this method is performed by dissolving the active compound in oil with an emulsifier. The solvent is then removed by distillation. The precipitation of the compound takes place when the solubility limit is achieved. Sjostrom et al[85] produced Cholesteryl acetate particles stabilized by lecithin and bile salts. Choi[86] prepared poly(d,l-lactic-co-glycolic acid) (PLGA) nanoparticles by emulsion/solvent diffusion method. Lemoine and Preat[87] also prepared PLGA nanoparticles from dichloromethane and PVA or Span 20 as the stabilising agent. Although the solvent evaporation method can be a simple method for the preparation of nanoparticles, it is time consuming and possible coalescence of the nanodroplets during the evaporation process may affect the final particle size and morphology.[88]

We expand this method by using freeze-drying as the method for removing the solvent. An account of freeze-drying is given in section 1.7.

1.7 Freeze-Drying

Freeze drying (or lyophilisation) is a drying process where solvents are crystallized at low temperatures and sublimed from the solid phase into the gaseous phase.

Water is the most commonly used solvent for freeze-drying. The phase diagram for water is shown below (figure 6). If a system contains two or more components, phase diagrams will become more complicated, therefore a simplified model is used here. The drying transforms the ice

or amorphous water directly into vapour. The idea of freeze-drying is to produce a dry material.[89]

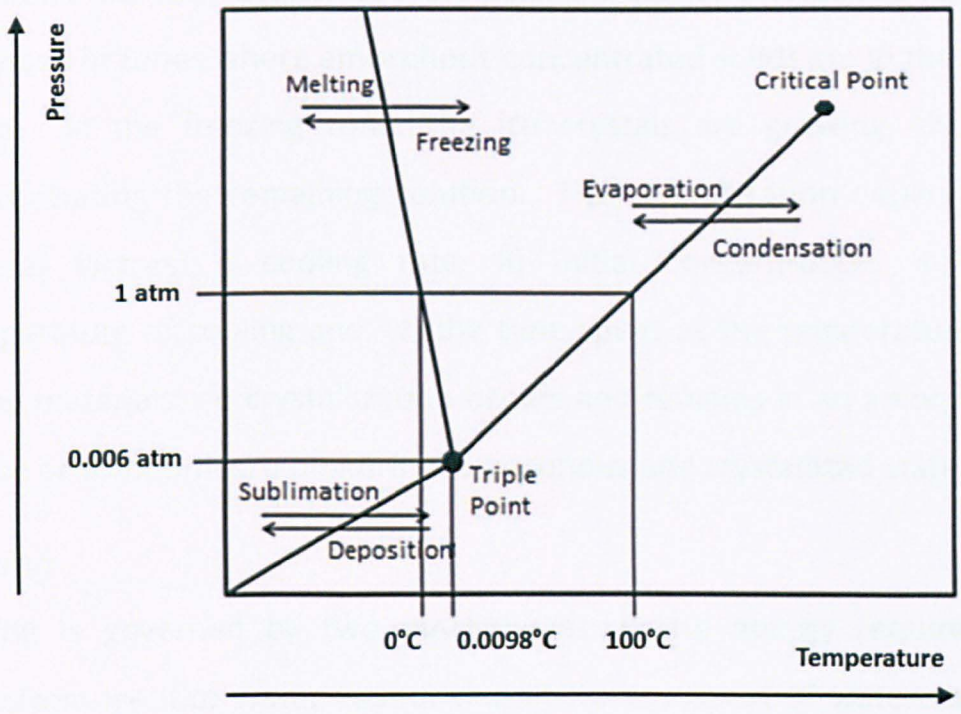

Figure 1-6 - Simplified phase diagram of water

There are advantages and disadvantages associated with freeze drying. Advantages include:

- Drying at low temperatures reduces degradation of heat-sensitive products
- Freeze-drying helps preserve any desired morphologies of the materials

Conversely, disadvantages include:

- High investment, operating and maintenance costs

There are two stages to freeze-drying. An account of these will be discussed below:

Freezing

To freeze a material, it must be cooled to a temperature where the solutions are fully crystallized or, where areas of crystallized ice are enclosed in zones where amorphous concentrated solids are in the solid state. In the freezing zone, the ice crystals are growing, thereby concentrating the remaining solution. The crystallization depends on several factors: i) cooling rate, ii) initial concentration, iii) end temperature of cooling and, iv) the time spent at the temperature. In many materials, no crystallization occurs and remains in an amorphous phase or sometimes, a mixture of amorphous and crystallized states.[89]

Drying

Drying is governed by two mechanisms: i) the energy required to transform ice into water vapour and ii) the transport of water vapour through the material into the drying chamber for condensation. After the ice has been sublimed, the water that is absorbed is desorbed from the solid. This is a separate process to the main drying. The two drying method are discussed below.[89]

Primary (Sublimation) Drying

During this stage the pressure is lowered to the millibar region. Enough energy is supplied to the system for the solids to be sublimed. The amount of energy for sublimation depends on the sublimation temperature. Energy is consumed to heat the vapour during the transport through the material that has already been dried in the process. Energy can be translated to the ice in four different forms:

1. By radiation of heated surfaces
2. Conduction from heated plates

3. Gas convection
4. Dielectric loss in the ice

About 95% of the water in the material is sublimed in this first stage of drying. This part of the drying process is slow owing to the fact that if the heating was too rapid, the material that is being dried would lose its structure. As the system is in vacuum, this aids the speed of the sublimation. The addition of a condenser in the chamber also aids the speed of sublimation due to the fact that these provide a surface for the vapours to solidify on. The condenser stops water vapour from passing through the system and ultimately damaging the vacuum pump.[89]

Secondary Drying

This drying stage removes all unfrozen water molecules. The stage of drying is governed individually to the sample. Each sample has its own adsorption isotherm. In this step of the drying the temperature is raised slightly higher. This increase in heat breaks any physical or chemical interactions that may have formed between water and the material that was frozen.

Despite the two drying stages, it is not always possible to remove 100% of the waters in the material. There will always be 1-4% water remaining in the sample. Therefore the storage of a freeze-dried product starts at the end of the secondary drying stage. The materials can either be sealed or stored in an inert environment or in a dessicator.[89]

1.8 Polymers

Polymerisation methods can be split into two sections: chain growth and step growth.[90-92] Chain growth polymerisation is highly used for industrial synthetic polymers such as poly(vinyl chloride) and acrylics.

Three methods are common for the chain polymerisation method. These are: free-radical, cationic and anionic. They all possess the same basic steps: initiation, where a reactive species is generated; propagation where more monomer units are added to give a lengthening chain which has a reactive end-group and termination where the growing chains are deactivated.

1.8.1 Free Radical Polymerisation

The polymerisations found in chapters 2 and 5 are prepared via free radical polymerisation. This section discusses the mechanisms in which free radical polymerisation occurs. A free radical is a molecular species that has an unpaired electron. This electron is very reactive and reacts rapidly with an olefinic monomer to create a chain (polymer).

A radical initiator is a molecule which undergoes homolytic fission, typically via temperature to form an unpaired electron which is highly reactive. These radicals proceed to attack alkene monomers initiating the propagation.[93] Typically in aqueous solutions persulphates are used.

1.8.2 Mechanism of Free Radical Polymerisation

Free-radical polymerization occurs over three steps: initiation, propagation and termination, and these are complete in a matter of seconds. Because of this, radical concentrations are always very low and separating these out is always inaccessible.

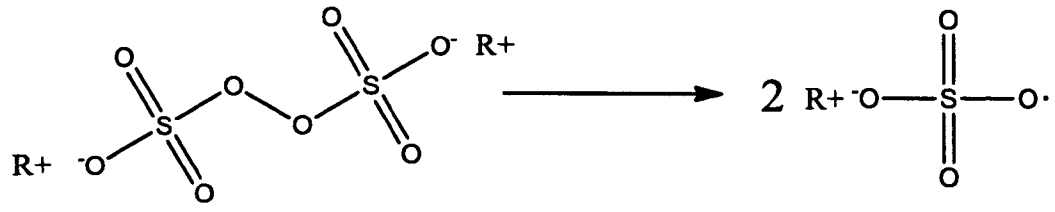

Figure 1-7 - Mechanism of peroxide decomposition upon heating

Persulphates are used in aqueous polymerisation systems. The persulphate molecule (figure 7) undergoes thermal decomposition, typically above 50°C.

Upon initiation, the initiator free radical reacts with the monomer by opening the double bond (Figure 8):

Figure 1-8 - Initiation of a vinyl monomer

This monomer radical can then react further with another vinyl monomer (also known as propagation, figure 9):

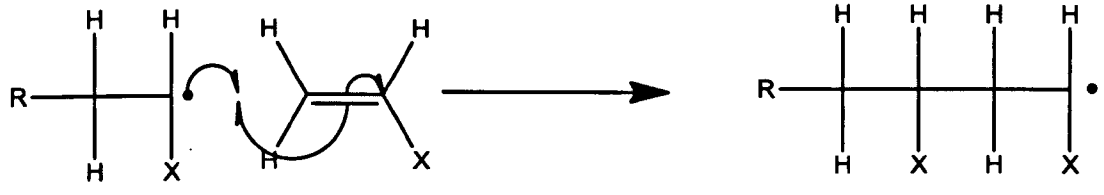

Figure 1-9 - Propagation of a vinyl monomer by addition of a monomer radical to a monomer unit

Termination occurs when two radical species meets to terminate the radicals and produce a polymer chain (figure 10)

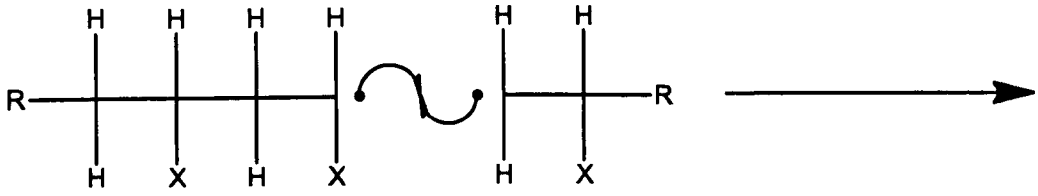

Figure 1-10 - Termination of a monomer chain by two radicals meeting

The other form of polymerisation which is not encountered in this thesis is polymerisation via step growth. These were previously known as condensation polymerisations due to the elimination of a small molecule during polymerisation, commonly water.

The main feature of step growth polymerisation is that any two molecules in a system can react. The monomer is part of the chain from an early stage of the reaction. Usually, an initiator is not required however catalysts may assist the reaction. The mechanisms and rates of initiation, propagation and termination are similar.

1.8.3 Solution Behaviour of Polymers

When the solubility of a solute in a solvent is considered, it is well known that the solubility increases as a function of temperatures or conversely as the system is cooled the solubility is decreased. This pattern is observed with polymer materials in a good solvent. When the system is cooled to below what is known as the Θ-temperature, the solvent becomes poorer and two phases will be observed with the polymer phase being swollen with solvent.[94] This phase boundary is known as the upper critical solution temperature (UCST, figure 11). In many aqueous systems another phase is observed called the Lower critical solution temperature (LCST, figure 11) where the phase separation occurs when the system is heated. Water-soluble polymers can possess certain polar groups such as hydroxyl, amide or ether

groups which partake in H-bonding in the structure of water. Above the LCST the H-bonding is decreased and phase separation occurs[95] Figure 11 shows a general solubility diagram of polymers

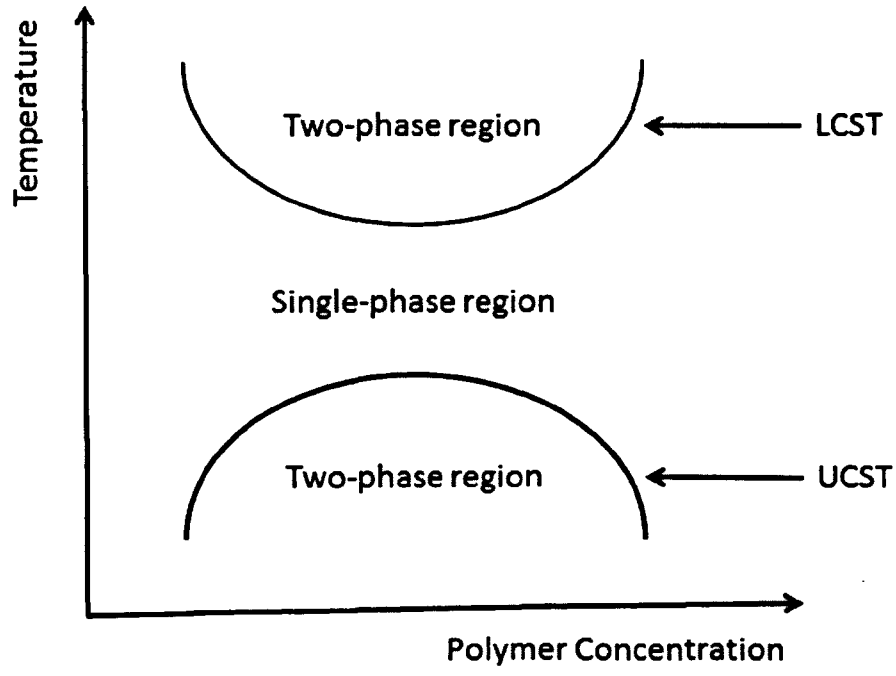

Figure 1-11 – General solution phase diagram showing the LCST and UCST of polymers as a function of polymer concentration and solution temperature.

1.9 Characterisation Principles

1.9.1 UV Spectroscopy

Most organic molecules and functional groups are transparent in the ultraviolet and visible regions (190 nm – 800 nm). When radiation passes through these molecules, some of the radiation may be absorbed. As a result of this absorption, atoms or molecules in compounds pass from a low energy state to a higher energy state.[96]

In UV-vis Spectroscopy, as a result of the absorption of electromagnetic radiation the transitions that occur are between electronic energy levels. As molecules absorb the energy – an electron is promoted from the low energy state (occupied orbitals) to a higher state (unoccupied orbitals). Generally these transitions are between the Highest occupied

molecular orbital (HOMO) and the lowest unoccupied molecular orbital (LUMO).

The lowest-energy occupied molecular orbitals are the σ orbitals (corresponding to σ bonds). The π orbitals are at higher energy levels and higher again are the n orbitals (orbitals with a shared lone pair of electrons). The corresponding unoccupied orbitals are the π* and the σ* orbitals.[96]

Figure 12 shows electronic energy levels and transitions. Certain restrictions apply with transitions, called selection rules. The n→π* transition is the most common type of forbidden transition.

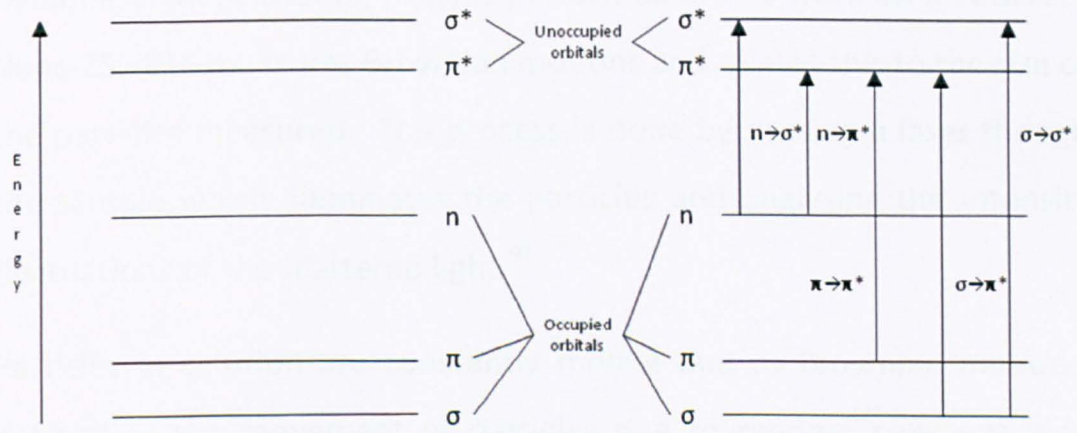

Figure 1-12 – Electronic energy levels and transitions

For molecules, UV absorption occurs over a range of wavelengths as molecules have many excited modes of vibration and rotation at ambient temperatures. As there are so many possible transitions in a molecule which differ by only a small amount; rather than then tracing all the transitions, a UV spectrum consist of a band with the centre of the band is near the wavelength of the major transition.

The more molecules in a compound that absorbs light at a specific wavelength, the greater the extent of the absorption. From this the expression of the Beer-Lambert Law is given:

$$A = \log({}^{I_\circ}/_{I}) = \varepsilon c l$$

A = absorbance, I_o = intensity of light incident on cell, I = intensity of light leaving sample, c = molar concentration, l = length of sample cell, ε = molar absorptivity

1.9.2 Particle Sizing

1.9.2.1 DLS

Dynamic Light Scattering (DLS) is performed in this work on a Zetasizer Nano ZS. DLS measures Brownian motions and relates this to the size of the particles measured. The process is done by passing a laser though the sample which illuminates the particles and analysing the intensity fluctuations of the scattered light.[97]

Particles in solution are constantly mobile due to Brownian motions, defined as the movement of particles due to random collisions with other molecules of the liquid that surrounds those particles. One important feature of Brownian motion which governs DLS is that smaller particles move more quickly than larger particles. The relationship between particle size and its speed due to Brownian motions is defined in the Stoke-Einstein-Sutherland equation:[98]

$$D = \frac{k_B T}{6\pi \eta R}$$

Where D is the diffusion constant K_B is the Boltzmann constant, T is the absolute temperature, η is the viscosity and R being the radius of the spherical particle. As the particles are in constant movement, the constructive and destructive phase of the scattered light will cause intensity fluctuations. The Zetasizer Nano systems measure this rate of intensity fluctuation and calculate the size of the particles.

The intensity fluctuations can be assessed by a digital correlator. This measures the degree of similarity between two signals over a short period of time. At two times close together (i.e t and t+δt) the signals would be very similar (or correlated). If the time was continued to t+2δt, there would still be good correlation however not as strong as the correlation of t+δt, therefore the correlation is reducing with time. If you were to continue to measure the correlation at t+3δt, t+4δt and so on, the correlation would eventually reach zero. A typical correlation function against time is shown below:

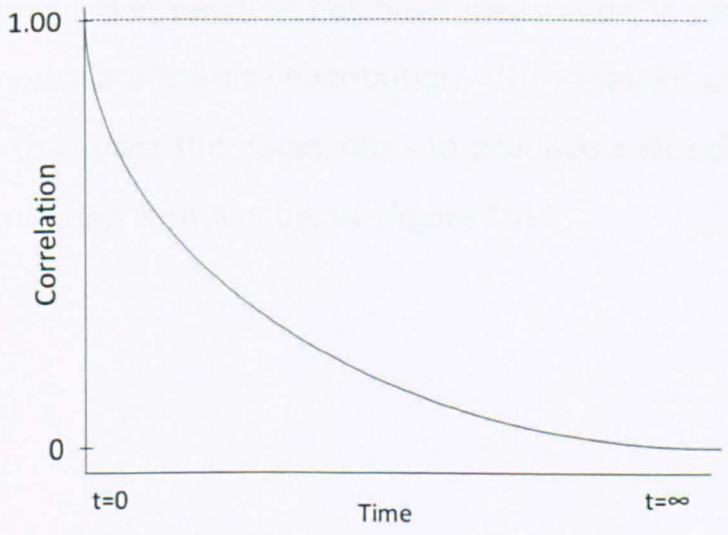

Figure 1-13 - Correlation of particles as a function of time

The speed of the particles affects the correlation function. Larger particles move slowly and therefore the intensities and the fluctuations

happen slowly. Conversely, smaller particles move much quicker and as a result fluctuations happen quicker. This is exemplified in figure 14 which shows the correlation function for small and larger particles. The rate of decay is directly related to the size of the particles.[97]

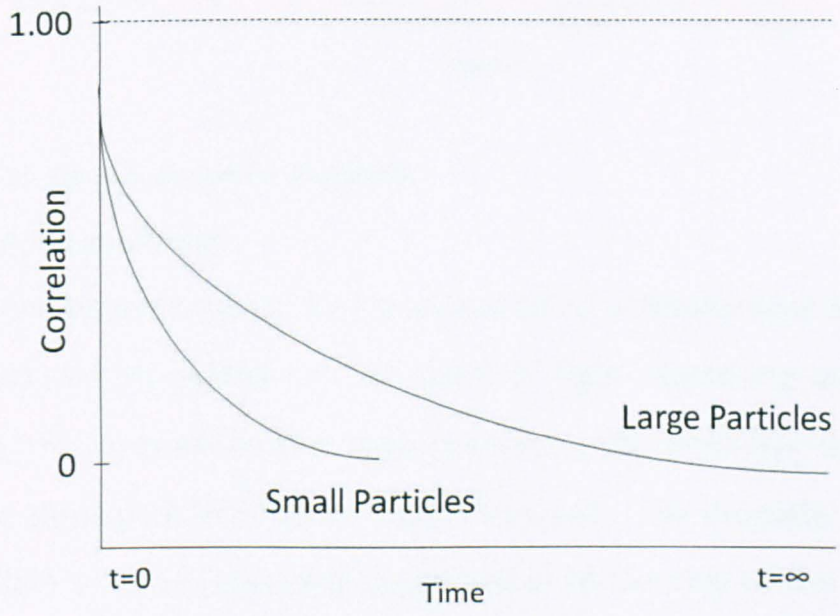

Figure 1-14 - changes in correlation for large and small particles.

After the correlation function has been measured the information can be used to calculate the size distribution. The Zetasizer uses a series of algorithms to extract the decay rates to produce a size distribution. A typical distribution is shown below (figure 15):

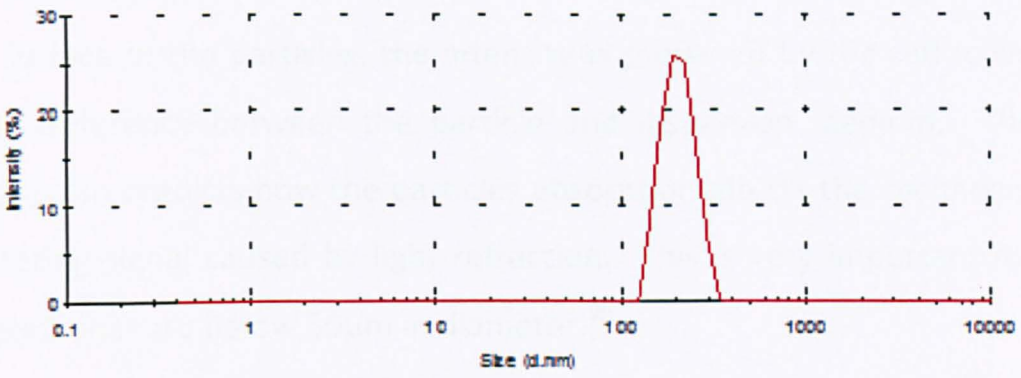

Figure 1-15 - Example particle size distribution

1.9.2.2 Mastersizer

Emulsion dispersions can be measured using a Mastersizer S2000. The droplets are measured on the basis of light scattering using lasers. During the laser diffraction measurements, the emulsion droplets are passed through a laser beam that is focused. The droplets scatter the laser light which is inversely proportional to the size of the droplets.[97] The angular intensity of the scattered light is measured by a series of photosensitive detectors. The scattering intensity versus the angle is the primary source of information to calculate the droplet sizes. The scattering of the droplets are predicted using the Mie scattering model. The Mie theory provides a solution for the calculation of droplet size distributions. It predicts the scattering intensities for all the particles based on the following assumptions:[99]

- Droplets are spherical
- Suspension is dilute
- The optical properties of the dispersion and the medium surrounding is known
- Homogeneous particles.

The Mie theory predicts the primary scattering response observed from the surface of the particles, the intensity is predicted by the refractive index difference between the particle and dispersion medium. The theory also predicts how the particles absorption affects the secondary scattering signal caused by light refraction. This is very important for droplets that are below 50μm in diameter.[99]

1.9.3 Zeta Potential (Electrophoresis)

Zeta potential is derived by determining the Electrophoretic Mobility and applying the Henry equation. The mobility is obtained by performing an electrophoresis experiment and measuring the particles using Laser Doppler Velocimetry (LDV). Herein is a discussion of Electrophoresis and how LDV is employed to measure Electrophoresis.

By developing a charge on the surface of a particle the distribution of ions in the surrounding interfacial region becomes affected. This results in an increased concentration of counter ions close to the surface of the particle. From this an electrical double layer is formed around each particle.[100]

The layer surrounding the particle has two components: firstly an inner region which is called the Stern Layer, this is where the ions are strongly bound to the particle; Secondly, an outer diffuse region where ions are less firmly attached to the particle. When a particle moves, these ions are attached as a stable entity and move together with the particle. Ions beyond the boundary of the outer diffuse layer do not move with the particle entity. This boundary is called the hydrodynamic shear or a slipping plane. The potential that is found at this boundary is called the zeta potential.[100]

The potentials magnitude gives an indication of the particles stability. If a particle in suspension has a large negative or positive potential, the particles thus have repulsive properties and are able to repel other particles and have no tendency to flocculate. Conversely, if particles were to have a low zeta potential then there is no force of repulsion to prevent the particles from flocculating together. The dividing line which is given between a stable and unstable system is between -30 mV and +30 mV. [100]

One important factor that affects the zeta potential is the pH of the system. A zeta potential value is meaningless without a quoted pH. If a particle in suspension has a negative zeta potential, and more alkali is added the suspension will acquire more negative charge. If acid was to be added to the suspension, a point will be reached where the alkali becomes neutralized. Further addition of acid can build up a positive charge. The point at which the plot passes through the zero-zeta potential is known as the isoelectric point. This is the point at which the particles are at their least stable.[100]

1.9.4 Mercury Intrusion Porosimetry

Mercury has a high surface tension (485 dyne/cm^3) and also exhibits a high contact angle (approximately 130°) When mercury is in contact with a pore of circular cross-section, the surface tension of the mercury acts along the circle of contact for a length equal to the perimeter of the circle. Thus, the force with which mercury resists entering the pores is equal to $-\pi D\gamma \cos\theta$, where D is the diameter of the pore, γ is the surface tension and θ being the contact angle. The force from an external pressure acts over the circle of contact and is expressed by

$\pi D^2P/4$ where P is the applied Pressure. As at equilibrium the forces are equal, this gives the equation:

$$-\pi D\gamma \cos\theta = \frac{\pi D^2 P}{4}$$

Or simply

$$D = \frac{-4\gamma \cos\theta}{P}$$

Being the Washburn equation were D=pore diameter, γ=surface tension of mercury, P=applied pressure and Θ=contact angle.

Porous monoliths can be fractured and weighed accurately into a penetrometer. The penetrometer was then sealed and placed into the low pressure port of the instrument where the sample and penetrometer were evacuated to 50 mmHg and then filled with mercury. A pressure cycle from 0.5 to 60,000 psi was then performed on the assembly in predefined steps. As mercury does not enter the porous structure by capillary action, the filling occurs when a pressure is applied to a system. At each pressure step the volume of mercury pushed into the sample is detected by a change in capacitance between the penetrometer ends. Each measurement is the inverse proportion to a pore diameter (the Washburn equation).

The low pressure port is used to apply pressure to 25 psi whereas the high pressure chamber is used for pressures up to 60,000 psi. After the low pressure analysis the penetrometer is reweighed so the volume of mercury uptake is calculated. Through a calibration process carried out on the penetrometers before the samples were analysed, capacitance changes due to the contraction of the sealed apparatus can be

subtracted. The data obtained reliability is thus increased. Using the volume calibration and the weights recorded, the pore size distributions and pore volumes can be calculated.[101]

1.9.5 Scanning (Transmission) Electron Microscopy

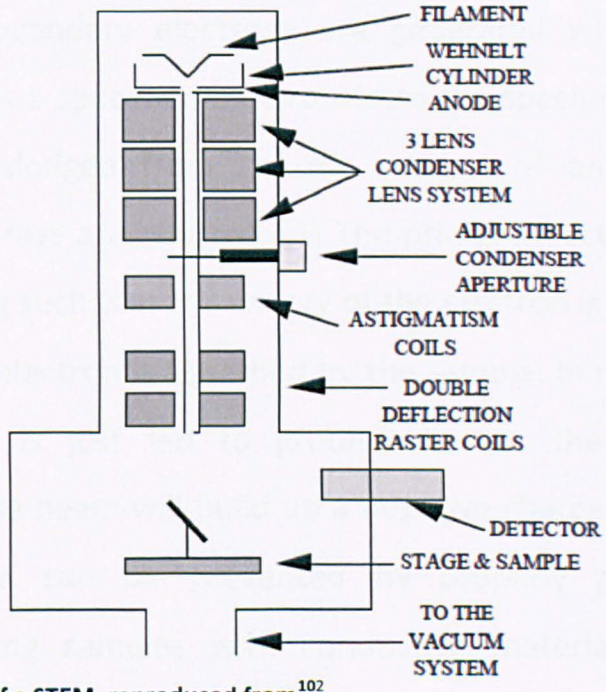

Figure 1-16 – Diagram of a STEM, reproduced from[102]

The basic components of a STEM are shown in Figure 16. These components are part of seven primary operational systems: vacuum, beam generation, beam manipulation, beam interaction, detection, signal processing, and display and record. These systems function together to determine the results and qualities of a micrograph such as magnification, resolution, depth of field, contrast, and brightness. A vacuum is needed when using electron beams as the beam of electrons can quickly disperse or scatter due to collisions with other molecules. An electron beam generator can be found at the top of the microscope which generates the beam of electrons known as the primary electron

beam. The produced beam has to be manipulated. This is done so by a series of electromagnetic lenses and coils which control the position, size and shape of the electron beam.[102]

When the beam hits the specimen one of several things can occur to the beam: (1) a primary beam electron may be scattered in such a way that it escapes back from the specimen but does not go through the specimen; (2) Secondary electrons are generated when a primary electron dislodges a specimen electron from the specimen surface; (3) electrons are dislodged from specific orbitals of an atom in the specimen, and X-rays are omitted; (4) The primary electron undergoes enough scattering such that the energy of the electron is decreased to a point where the electron is absorbed by the sample. In most cases, the induced current is just led to ground. If not, the region being bombarded by the beam will build up a negative charge. This is known as Charging and can be prevented by properly grounding and sometimes coating samples with conductive material; (5) primary electrons may pass through the specimen. These electrons are known as transmitted electrons and they provide some atomic density information.

SEM can consist of several different detectors to detect different energy emissions that occur from the sample. The signals produced are processed and transformed into a visualisation of the electronic signal.[102]

1.10 Previous Work

This thesis continues from previous work which has seen temperature responsive materials release nanoparticles from porous structures. Release of organic nanoparticles using porous emulsion template poly(N-isopropylacrylamide) (polyNIPAM) has been investigated previously. Oil Red (OR), a biological stain which is insoluble in water was used as the organic model material. This dissolved in the water immiscible Cyclohexane (CH) was chosen as the internal organic phase. The OR-CH solution was emulsified into an aqueous phase containing NIPAM and a crosslinker methylene-bis-acrylamide (MBAM), the surfactant Triton X-405 was used to stabilize the emulsions. The prepared emulsions where placed into an oven at 60 °C overnight. The polymerized samples where frozen and freeze-dried. Both the internal organic phase and the water phase are removed by the process of freeze-drying. During the freeze-drying OR nanoparticles are formed within the pore structure in a way which is similar to emulsification-evaporation techniques.[103].

To investigate the thermo-responsive properties of the material swollen in water the polymer was swollen rapidly and frozen to lock the morphology. In comparison, piece of the swollen polymer was heated above its LCST and frozen rapidly. Both samples where freeze-dried and the morphologies investigated. Figure 17 shows the morphologies of the polymer in the dry state, swollen and heated to 45 °C.

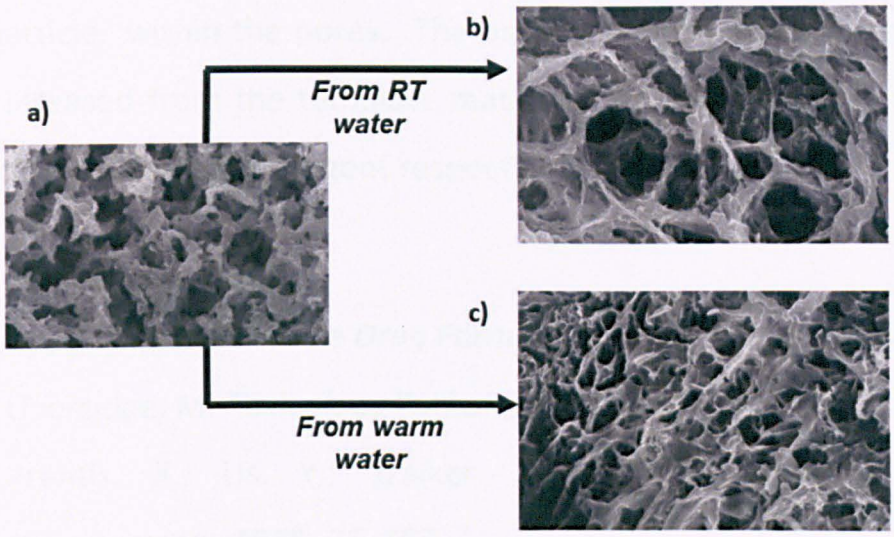

Figure 1-17 - SEM figures of the prepared NIPAM (a) and swollen in water (b) then heated above the LCST (c)

The work was further extended to produce and release drug nanoparticles and polymer microparticles. Ketoprofen, Carbamazepine and polystyrene were used as examples. When preparing the emulsions: Ketoprofen (0.05 wt% in 6ml o-xylene), Carbamazepine (0.2 wt% in 6ml o-xylene) or polystyrene (5 wt% in 6ml o-xylene) was used. The procedure for releasing these particles was followed as before by heating in a water bath [104].

The initial aim of the thesis was to extend the responsive systems that can be used in an emulsion template to release organic nanoparticles of poorly water soluble compounds. We extended the concept of the work to include the uptake and release of polymeric colloids using the temperature responsive NIPAM. We also aimed to investigate the preparation of drug nanodispersions within templated hydrophilic polyvinyl alcohol. To complement the original idea of using responsive systems to control the release of organic nanoparticles – a pH dependent chitosan and a redox responsive emulsion templated polymer were prepared with the insitu preparation of organic

nanoparticles within the pores. The organic nanoparticles were aimed to be released from the template materials via the change of pH and the inclusion of a redox reagent respectively.

1.11 References

1. Liu, R. *Water Insoluble Drug Formulations*; CRC Press, 2008.
2. Liversidge, M. *Toxicology Pathology* **2008**, *36*, 43.
3. Prentis, R.; Lis, Y.; Walker, S. *British Journal of Clinical Pharmacology* **1988**, *25*, 387.
4. Grant, N.; Cooper, A. I.; Zhang, H. *ACS Applied materials and Interfaces* **2010**, *2*, 573.
5. Grant, N.; Zhang, H. *Journal of Colloids and Interfacial Science* **2011**, *356*, 573.
6. Utada, A. S.; Lorenceau, E.; Link, D. R.; Kaplan, P. D.; Stone, H. A.; Weitz, D. A. *Science* **2005**, *308*, 537.
7. J. QIU; B. CHARLEUX; MATYJASZEWSKI, K. *Progress in Polymer Science* **2001**, *26*, 2083.
8. McAuliffe, C. *Journal of Petroleum Technology* **1973**, *25*, 727.
9. Bibette, J. *Emulsion Science: Basic Principles*; Springer, 2007.
10. Kunieda, K.; Shinoda, K. *J. Dispersion Sci. Technology* **1982**, *3*, 233.
11. Kunieda, H. *Langmuir* **1996**, *12*, 2136.
12. Myers, D. *Surfaces, Interfaces and Colloids*; Wiley, 1999.
13. R. Aveyard; B. P. Binks; Clint, J. H. *Advances in Colloid and interface Science* **2003**, *100-102*, 503.
14. Farn, R. *Chemistry and technology of surfactants*; Blackwell Publishing, 2006.
15. Rosen, M. J. *Surfactants and Interfacial Phenomena*; Wiley, 2004.
16. Myers, D. *Surfactant Science and Technology*; Wiley, 2006.

17.Sjoblom, J. *Emulsions and Emulsion Stability*; Taylor & Francis, 2006.

18.Jiao, J.; Burgess, D. J. *Journal of Colloids and Interfacial Science* **2003**, *264*, 509.

19.Ostwald, W. *Z. Phys. Chem.* **1900**, *34*, 495.

20.Manley, S.; Graeber, N.; Grof, Z.; Menner, A.; Hewitt, G. F.; Stepanek, F.; Bismarck, A. *Soft Matter* **2009**, *5*, 4780.

21.Williams J. M.; Gray, A. J.; H., W. M. *Langmuir* **1990**, *6*, 437.

22.Cameron, N. R. *Polymer* **2005**, *46*, 1439.

23.Cameron, N. R.; Sherrington, D. C. *Journal of The Chemical Society - Faraday Transactions* **1996**, *92*, 1543.

24.Cameron, N. R.; Sherrington, D. C. *Advances in Polymer Science* **1996**, *126*, 162.

25.Barby, D.; Haq, Z. In *Eur Pat Appl 60138* 1982.

26.Cameron, N. R.; Sherrington, D. C. *Advanced Polymer Science* **1996**, *126*, 163.

27.Kimmins, S.; R., C. N. *Advanced Functional Materials* **2011**, *21*, 211.

28.Lumelsky, Y.; Lalush-Michael, I.; Levenberg, S. S., M. S. *Journal of Polymer Science, Part A: Polymer. Chemistry* **2009**, *47*, 7043.

29.Zhang, H.; Cooper, A. I. *Soft Matter* **2005**, *1*, 107.

30.Ruckenstein, E. *Polymer Composites* **1997**, *18*, 320.

31.Abbasian, Z. *Journal of Applied Polymer Science* **2010**, *116*, 986.

32.Shirshova, N.; Menner, A.; Funkhouser, G. P.; Bismarck, A. *Cement and Concrete Research* **2011**, *41*, 443.

33.Hainey, P.; Huxham, I.; Rowatt, B.; Sherrington, D. C.; Tetley, L. *Macromolecules* **1991**, *24*, 117.

34.Barbetta, A.; Cameron, N. R.; Cooper, S. J. *Chem Comm* **2000**, *3*, 221.

35.Busby, W.; Cameron, N. R.; Jahoda, C. A. B. *Polymer International* **2002**, *51*, 871.

36.Zhang, S.; Chen, J. *Chemical Communications* **2009**, *16*, 2217.

37.Krajnc, P.; Leber, N.; Setefanec, D.; Kontrec, S.; Podgornik, A. *Journal of Chromatography A* **2005**, *1065*, 69.

38.Kranjc. P *Macromolecular rapid communication* **2005**, *26*, 1289.

39.Zhu, Y.; Zhang, S.; Y, H.; Chen, J.; Pu Hu, C. *Polymer* **2010**, *51*, 3612.

40.David, D.; Silverstein, M. *Journal of Polymer Science, Part A: Polymer. Chemistry* **2009**, *47*, 5806.

41.Kulygin, O.; Silverstein, M. S. *Soft Matter* **2007**, *3*, 1525.

42.Strohm, H.; Lobmann, P. *Journal of Materials* **2004**, *14*, 2667.

43.Zhang, H.; Hardy, G. C.; Khimyak, Y. Z.; Rosseinsky, M. J.; Cooper, A. I. *Chemistry of Materials* **2004**, *16*, 4245.

44.Binks, B. *Current Opinion in Colloids interface science* **2002**, *7*, 21.

45.Binks, B.; Lumsdon, S. O. *Langmuir* **2001**, *17*, 4540.

46.Vignati, E.; Piazza, R.; Lockhart, T. *Langmuir* **2003**, *19*, 6650.

47.Melle, S.; Lask, M.; Fuller, G. *Langmuir* **2005**, *21*, 2158.

48.Binks, B. *Langmuir* **2000**, *16*, 2539.

49.Gurevitch, I.; Silverstein, M. S. *Journal of Polymer Science, Part A: Polymer. Chemistry* **2010**, *19*, 1516.

50.Ikem, V.; A., M.; Bismarck, A. *Angewangte Chemie International Edition* **2008**, *47*, 8277.

51.KBokhari, M.; Carnachan, R.; R., C. N.; Przyborski, A. *BioChem. Biophys Res Commun* **2007**, *354*, 1095.

52. Kavacic, S.; P, K. *Journal of Polymer Science, Part A: Polymer. Chemistry* **2009**, *47*, 6726.

53. Pulko, I. *Science of the total environment* **2007**, *386*, 114.

54. Yao, C.; Qi, L.; Yang, G.; Wang, F. *Journal of Separation Science* **2010**, *3*, 475.

55. Xu, P.; Yao, P.; L., L. *Journal of Applied Polymer Science* **2011**, *119*, 412.

56. Ungureanu, S.; Deleuze, H.; Babot, O.; Achard, M.; Sanchez, C.; Popa, M.; Backov, R. *Applied Catalysis, A: General* **2010**, *390*, 51.

57. Cohen, N.; Silverstein, M. *Polymer* **2011**, *52*, 282.

58. Wu, R.; A., M.; Bismarck, A. *Journal of Polymer Science, Part A: Polymer. Chemistry* **2010**, *48*, 1979.

59. Menner, a.; Verdejo, R.; Shaffer, M.; Bismarck, A. *Langmuir* **2010**, *26*, 8836.

60. Lipinski, C. *AAPS Press: Arlington Virginia* **2004**.

61. Giliyar, C.; Fikstad, D. T.; Tyavanagimatt *Drug Deliv. Technol.* **2006**, *6*, 57.

62. Lipinski, C.; Lombardo, F.; GDominy, B.; Feeny, P. *Journal of Advanced Drug Delivery Reviews* **2001**, *46*, 3.

63. Serajuddin, A. *Advanced Drug Delivery Reviews* **2007**, *59*, 603.

64. Saharan, V.; Kukkar, V.; Kataria, M.; Gera, M.; Choudhury, P. *International Journal of Health Research* **2009**, *2*, 207.

65. Basit, A.; Newton, J.; Short, M.; Waddington, W.; Ell, P.; Lacey, L. *Pharmaceutical Research* **2001**, *18*, 1146.

66. Maas, J. *European Journal of Pharm. Biopharm.* **2007**, *66*, 1.

67. Szente, L. *Advanced Drug Delivery Reviews* **1999**, *1999*, 17.

68. Del Valle, E. M. M. *Process Biochemistry* **2004**, *39*, 1033.

69. Gaucher, G.; Satturwar, P.; Jones, M.-C.; RFurtos, A.; Leroux, J.-C. *European Journal of Pharmaceutics and Biopharmaceutics* **2010**, *76*, 147.

70. He, C.-X.; He, Z.-G.; Gao, J.-Q. *Expert Opinion on Drug Delivery* **2010**, *7*, 445.

71. Date, A. *Current Opinion Colloids Interface Science* **2004**, *9*, 222.

72. Chow, A.; Tong, H.; Chattopadhyay, P.; Shekunov, B. *Pharmaceutical Research* **2007**, *24*, 411.

73. Kesisoglou, F.; Panmai, S.; Wu, Y. *Advanced Drug Delivery Reviews* **2007**, *59*, 631.

74. Patravale, V.; Date, A.; Kulkarni, R. *J. Pharm. Pharmacol.* **2004**, *56*, 827.

75. Liversidge, G. *International Journal of Pharmacology* **1995**, *125*, 91.

76. Eerdenbrugh, B.; Mooter, G.; Augustijns, P. *International Journal of Pharmacology* **2008**, *364*, 64.

77. Verma, S.; Gokhale, R.; Burgess, D. J. *International Journal of Pharmacology* **2009**, *380*, 216.

78. Sepassi, S. *J. Pharm. Sci.* **2007**, *96*, 2655.

79. Kumar, M.; Bakowsky, U.; Lehr, C. *Biomaterials* **2004**, *25*, 1771.

80. Overhoff, K. *Eur. J. Pharm. Biopharm.* **2007**, *65*, 57.

81. Chen, X. *J. Pharm. Sci.* **2004**, *93*, 1867.

82. Reverchon, E. *Ind. Eng Chem. Res.* **2002**, *23*, 196.

83. Pathak, P. *JACS* **2004**, *136*, 10842.

84. Shekunov, B. *Pharmaceutical Research* **2006**, *23*, 196.

85. Sjostrom, J. *Pharmaceutical Research* **1995**, *12*, 39.

86. Choi, S. *Journal of Pharmaceutics* **2006**, *311*, 223.

87.Liu, Y. *Journal of Controlled Release* **1998**, *54*, 15.

88.Rao, J.; Geckeler, K. *Progress in Polymer Science* **2011**, *36*, 887.

89.Oetjen, G. *Freeze-Drying*; Wiley, 2004.

90.Flory, P. *Chem Rev* **1946**, *39*, 137.

91.Flory, P. *Chem. Rev.* **1931**, *8*, 353.

92.Carothers, W. *JACS* **1929**, *51*, 2548.

93.Cosgrove, T. *Colloid Science: Principles, Methods and Applications*; Blackwell Publishing, 2005.

94.Daoud, M.; Jannink, G. *JLe Journal De Physique* **1976**, *37*, 973.

95.Jones, R. *Soft Condensed Matter*; Oxford, 2002.

96.Pavia *Introduction to Spectroscopy*; 2009, 2009.

97.*DLS - Technical notes*; Malvern Instruments.

98.Cao, A. *Analytical Letters* **2003**, *36*, 3185.

99.*Analyzing Light Scattering Data*; Malvern Instruments Website.

100. Malvern Instruments.

101. Webb, P. *Analytical methods in fine particle technology*; Micromeritics, 1997.

102. Dunlap, M. Introduction to the Scanning Electron Microscope: Theory, Practice & Procedures. [Online Early Access]. Published Online: 1997.

103. Zhang, H.; Cooper, A. I. *Advanced Materials* **2007**, *19*, 2439.

104. Grant, N.; Zhang, H. In *Mater. Res. Soc. Symp. Proc.* 2008; Vol. 1095E, p 1095.

2 Preparation of a Macroporous Thermo-responsive Polymer and the Uploading and Release of Colloids

2.1 Chapter Overview

Thermoresponsive Poly N-isopropylacrylamide (PNIPAM) monoliths were prepared via an emulsion templating approach. The polymerised monoliths were seen to swell in aqueous media and contract above the polymers lower critical solution temperature (LCST, approximately 32 °C). These properties were utilised in the absorption and release of polystyrene colloids.

2.2 Introduction

Porous polymers can be used as scaffolds for tissue engineering and controlled drug release.[1,2] The release of an active from a porous material can be achieved by the use of a trigger or a combination of triggers. The sensitivity of such a trigger is an important parameter for the controlled release process. Porous polymers can be applied in an aqueous environment. Polymers with high porosity and thus higher interconnectivity can allow for the contact between water and the polymer and a free-flow of aqueous phases through the structures. Hydrophilic polymers can absorb water. As a result of large volumes of water being absorbed into hydrophilic material the polymers can become soft and have a very flexible network. With this flexibility, porous polymers may exhibit a higher sensitivity towards a trigger.

Highly interconnected porous structures can be prepared using a high internal phase emulsion (HIPE, which exhibits a droplet volume of greater than 74.07 v/v%)[3,4] as a template. The continuous phase can be polymerized (as discussed in 1.4) and a porous material with a high pore volume can be produced after the removal of the internal phase of the original emulsion. These materials are known as polyHIPEs.[3] There are a vast application for polyHIPEs including gas storage,[5] scaffolds for tissue engineering,[6] supports for organic synthesis[7], electrochemical sensing[8] and other applications.[4,9] An array of polyHIPE and polyHIPE-based materials have been synthesized including hydrophobic polymers,[9-11] hydrophilic polymers,[12,13] interpenetrating polymer networks (IPN),[14] biodegradable polymers[15,16] and organic-inorganic composites.[17,18]

PolyHIPE materials can be stabilized using surfactants. PolyHIPEs have also been stabilized using silica particles,[19] titania nanoparticles[20] and polymer nanoparticles,[21] known as Pickering emulsions.

A range of monomers can be used to produce polyHIPE materials which exhibit different functionalities. The surface properties of formed polyHIPEs can be modified by plasma treatment[22] or functionalized by click chemistry.[23]

Poly(N-isopropylacrylamide)(PNIPAM) has been the main focus for temperature responsive polymer systems.[24] PNIPAM exhibits a sharp phase transition with the lower critical solution temperature (LCST) at around 32 °C in water.[25] At temperatures below this threshold, PNIPAM exists in a flexible form soluble in water. Above this temperature, the polymer becomes hydrophobic and the chains collapse. NIPAM has

been polymerized for thermoresponsive delivery,[24,25] forming hydrogels for cell evaluation[26] and as a coating for controlled release from gold nanocages.[27] Crosslinked PNIPAM is a polymeric network which is capable of absorbing large amounts of water[28] whilst maintaining its distinct 3D structure. The presence of the hydrophilic acrylamide group gives rise to the capabilities.[29] Above the LCST, the swollen PNIPAM can contract in volume and expel absorbed waters out. Previously, thermoresponsive cross-linked PNIPAM with the *in-situ* formation of organic nanoparticles was prepared by polymerizing NIPAM followed by a freeze-drying process.[30] The organic nanoparticles were released from the polymer into water to form a stable nanoparticle suspension. The particles were released when the polymer contracts above the LCST. HIPEs were used as templates as crosslinked PNIPAM was prepared with high interconnectivity of macropores and a high pore volume. The PNIPAM was able to absorb a large amount of water, thus making the network flexible and highly sensitive in water.

In this study, we investigated the use of highly porous PNIPAM to load and release polymeric colloids by using temperature as a trigger. Unlike in the previous study where organic nanoparticles were formed simultaneously with the production of the porous material,[30] the PNIPAM is swollen in a suspension of colloids and then these can be released by altering the temperature of the system. HIPE-templated porous PNIPAM is prepared and used to load and release polymeric colloids for multiple cycles. The process discussed here utilizes preformed colloids, active ingredients such as drug molecules could be encapsulated into the colloids beforehand.[31] The process is very useful for the applications such as drug delivery. Polymeric microspheres,

nanoporous colloids, microgels and polymer vesicles have been used as carriers for drug delivery.

2.3 Experimental

2.3.1 Materials

N-isopropylacrylamide (NIPAM, 97%), N,N'-methylenebisacrylamide (MBAM, 99%), Triton X-405 (70% in water), Ammonium persulfate (APS, 98%), N,N,N,N-tetramethylethylenediamine (TMEDA, 99%) were all purchased from Sigma Aldrich Cyclohexane (CH) was purchased from VWR and used as received. Methacrylic acid-stabilized polystyrene (PS) colloids (10 wt%) with a zeta potential of -45.2 mV were prepared according to the previously reported method, briefly: in a glass reactor under nitrogen, styrene (60 g) methacrylic acid (0.6 g) and water 580 ml were stirred at approximately 250rpm. The vessel was left stirring and flushing with nitrogen until a reaction temperature of 70 °C was attained. Potassium persulfate (0.24g in water 20 ml) was added to the mixture. After 6 hours, 9g styrene, 6g methacrylic acid and 0.048g potassium persulfate were added to the vessel. The polymerization was left for 24 h under nitrogen until the reaction was complete. The colloids were stained with Rhodamine B dye by adding a few crystals to the PS colloidal suspension and sonicating for 20 minutes. Excess dye was removed by using a Gooch crucible with a pore size of 0.2μm and washed with copious amounts of water until no further dye was washed from the colloids. The colloids where redispersed into water to a concentration of 3 wt%. Centrifugation of the colloids confirmed the dye had been removed from the water. Distilled water was used in all cases.

2.3.2 Preparation of PNIPAM polyHIPEs

Aqueous solutions of NIPAM and MBAM were prepared with respective concentrations at 1M and 0.0xM (see table 1), these polymers were designated NIPAM-X (see table 1). The typical procedure for making PNIPAM with x% cross-linking co-monomer was: to aqueous NIPAM/MBAM (2ml), Triton X-405 (0.3ml) and APS (10% in H_2O, 0.1ml) were added in turn while stirring at approximately 600rpm using an overhead LabEgg paddle stirrer, after which CH (6ml) with TMEDA (30μl) was slowly dropped into the aqueous phase. The volume phase ratio was approximately 3:1. The emulsion was stirred for 5 minutes and placed into an oven at 60°C for at least 12 hours. The polymerized material was allowed to cool before freezing in liquid nitrogen and freeze-dried at -10°C in a freeze-dryer (Vir-tis Advantage, Biopharma) to produce the dry porous solid. The dried materials were Soxhlet extracted by refluxing of methanol and acetone (24 hours each) using a Soxhlet extractor, to remove surfactant, APS and unpolymerised materials.

Table 1 - Preparation Conditions for PNIPAM-X polyHIPE

Sample	NIPAM (M)	MBAM (M)
PNIPAM-1	1	0.01
PNIPAM-2	1	0.02
PNIPAM-5	1	0.05

2.3.3 Loading and release of PS colloids

Porous PNIPAM (0.05g) was soaked in an aqueous solution of RhB-stained PS colloids (10ml, concentration of colloids 3 ± 0.2 wt%) for 3 hours. The swollen polymer was filtered and the surface water removed. The colloid loaded polymer was dried through freeze-drying.

The mass loading of the colloids was calculated by the following equation:

$$Mass\ Loading = (\frac{M_S - M_P}{M_S})$$

Where M_S stands for the mass of that material after soaking and M_P stands for the mass of the polymer used.

PNIPAM with the PS colloids loaded were placed into a vial with 10 ml water. The vial was placed into a fridge at 4 °C. 0.2 ml of the aqueous suspension was taken at different times for 2 hours and stored for UV analysis. The polymer was then placed back into the fridge to cool before two more cycles of heating release (1 h cooling time). The removed medium samples were analysed by UV using a 96-well UV plate reader (μQuant, Bio-Tek instruments Inc). The height of absorption peak at 420nm was used to monitor the release of PS colloids.

2.3.4 Repeated loading and release of colloids

The porous PNIPAM samples (0.05g) were immersed in the PS colloidal suspensions (10ml at the concentration of 3 ± 0.2 wt%) for 3 hours. The swollen samples were then filtered, freeze dried, and then weighed to obtain the mass loading. The dry composites were soaked in water at 4°C for 2 hours and then transferred in a 45°C water bath for the release of PS colloids. After releasing, the polymer was collected, dried, and weighed to get the mass of PS colloids left in the PNIPAM. The polymer with some loading of PS colloids were immersed in the PS colloidal suspension again and processed for the release. This

procedure was repeated 4 times in order to test the multicycle capability of the porous PNIPAM to absorb and release PS colloids.

The released percentage of loaded PS colloids was calculated for each cycle of loading and release. The mass of the polymer used was noted as Mp. The mass of the polymer after the first upload of the colloids was noted as M_∞. Each subsequent mass was measured as Mx. The percentage release was calculated by the equation:

$$\%\, release = \frac{M_x - M_p}{M_\infty - M_p}\, x\, 100$$

2.3.5 Characterisation

The release of Rhodamine B stained PS colloids was monitored using a UV plate reader. The porous structures and PS colloids were observed using a Hitachi S-4800 scanning electron microscope (SEM). The porous polymers were adhered to SEM studs using double sided carbon tape and then coated with gold using a sputter-coater (EMITECH K550X0) for 3 minutes at 40μA before imaging. For particle analysis, 30 μl of the PS colloids suspension (3 wt% or as released into water) was deposited and allowed to dry on an SEM stud and coated likewise. The pore volume and pore size distribution of porous PNIPAM were characterized by mercury intrusion porosimetry (Micromeritics Autopore IV 9500). DSC thermograms of the PNIPAM polymer where performed using a Q2000 DSC, approximately 60mgs of the swollen polymer were weighed and heated between the temperatures of 20-40 °C at °C/min. To calculate the swelling ratios (i.e. the amount of water absorbed) below the LCST the extracted polymer was weighed and denoted Wd, the polymer was

allowed to swell in water for 3 hours and filtered and reweighed, denoted Ws. A sample of the swollen polymer in water was placed into a waterbath at 45 °C for 5 minutes. The contracted polymer was hot filtered and weighed, denoted Wc. The swelling and contracted ratios were calculated by:

$$Ratio\ (Swollen) = \frac{Ws - Wd}{Wd}$$

$$Ratio\ (Contracted) = \frac{Wc - Wd}{Wd}$$

The PS colloidal suspension was also analysed by dynamic laser scattering (DLS, Viscotek Model 802). Photographs of the polymer were taken using an Olympus C-5060 wide zoom digital camera.

2.4 Results and Discussion

2.4.1 Emulsion Templated PNIPAM

Porous PNIPAM was prepared using oil-in-water (O/W) HIPEs as templates. Triton X-405 was used to stabilize the emulsions. The thermoresponsive property and highly interconnected porosity of PNIPAM were utilized for the loading and release of PS colloids. The prepared dry porous PNIPAM was firstly soaked in the aqueous PS colloidal suspensions for the loading process. Porous PNIPAM could absorb a large amount of the suspension and swell at room temperature. The swollen sample was then dried and weighed to calculate the mass loading of PS colloids. During this soaking process, the surfactant Triton X-405 and the un-polymerized monomers could also diffuse out of the porous PNIPAM. Moreover, the presence of non-thermoresponsive Triton X-405 in PNIPAM might also reduce the

temperature sensitivity and the volume change capacity of PNIPAM. Therefore, all the samples were soxhlet extracted with acetone and methanol for 24 hours each to remove Triton X-405.[22] The mass losses for these samples were 4.3% for PNIPAm-1, 4.0% for PNIPAm-2, and 3.9% for PNIPAm-5. There was no further mass loss when these samples were subject to another cycle of extraction. The soxhlet-extracted samples were then used for all the loading and release processes.

Linear PNIPAM chains were crosslinked together by MBAM. Three levels of crosslinking ratios (MBAM/NIPAM = 1%, 2%, and 5% in mole) were investigated. At the lower crosslinking ratio (1 %), the PNIPAM was more flexible and more sensitive to temperature. DSC thermograms show how the crosslinking densities affect the responsiveness of the polyNIPAM (figure 1). Swelling and contraction ratios were also calculated (table 2). With the increase of crosslinking ratio, the structure became more rigid and the materials were mechanically more stable and therefore are more able to withstand higher pressures during mercury intrusion porosimetry. This is seen by the change in swelling/contraction ratios of the polymer. For 1% crosslinked polymer, the differences in the ratios are at its largest yet for 5% crosslinking the difference drastically reduces. For example, at the crosslinking ratio 5 %, a well-defined emulsion-templated porous structure was revealed (Fig. 2a). However, this also led to a reduced sensitivity and volume change. All the polymers show an endotherm around 32 °C owing to the polymers change in conformation at this temperature. The volume changes of the polymer also show how the polymers size changes with temperature. For polymers with a low crosslinking density the polymer shows a sharp transition at 30 °C and a larger endotherm. As the

Table 2 - Pore characterisation and swelling ratios of PNIPAM monoliths above and below the LCST

			Peak pore size (μm)		Pore volume (cm^3/g)		Swelling/Contraction Ratios	
Sample	NIPAM (M)	MBAM (M)	< LCST	>LCST	<LCST	>LCST	<LCST	>LCST
PNIPAm-1	1	0.01	60.4 ± 6.0, 1.6 ± 0.2	3.2 ± 0.3	12.3 ± 0.6	8.0 ± 0.4	14.38 ± 0.02	2.26± 0.03
PNIPAm-2	1	0.02	60.5 ± 6.1, 0.8 ± 0.1	3.9 ± 0.4	9.9 ± 0.5	4.7 ± 0.2	12.67± 0.01	3.55± 0.02
PNIPAm-5	1	0.05	10.0 ± 1.0	4.8 ±0.5	4.8 ± 2.4	3.5 ± 0.2	8.73± 0.05	3.66± 0.02

crosslinking density increases, the volume response is lower as is the endotherm confirming the polyNIPAMs lower response for higher crosslinking densities.

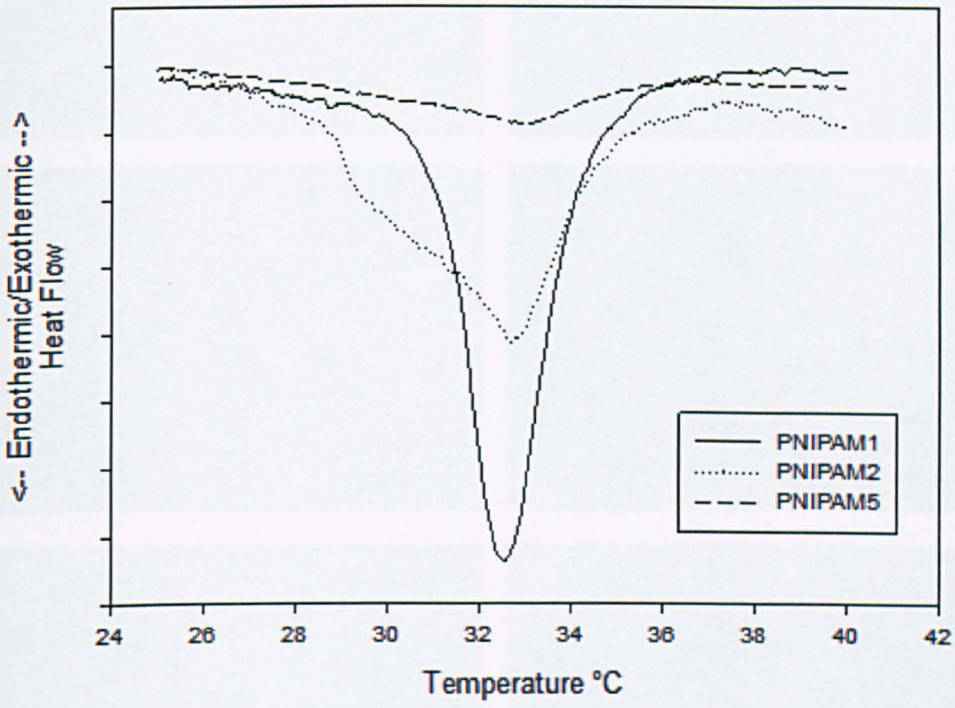

Figure 2-1– DSC thermograms for PNIPAM at different crosslinking densities

The volume change of porous PNIPAM below and above the LCST was reflected in the change of pore volume and pore size. This behaviour was observed by SEM imaging and further characterized by mercury intrusion porosimetry. The porous PNIPAM was put into water at room temperature for 15 minutes. The swollen PNIPAM was filtered. After wiping off water on the material surface, the swollen sample was rapidly frozen in liquid nitrogen. It was then freeze dried to represent the pore structure of PNIPAM below the LCST. As comparison, the glass vial containing the swollen PNIPAM in water was heated to 45 °C for 5 minutes to make sure the temperature was above LCST. The water was taken out from PNIPAM while the vial was still in the heated water

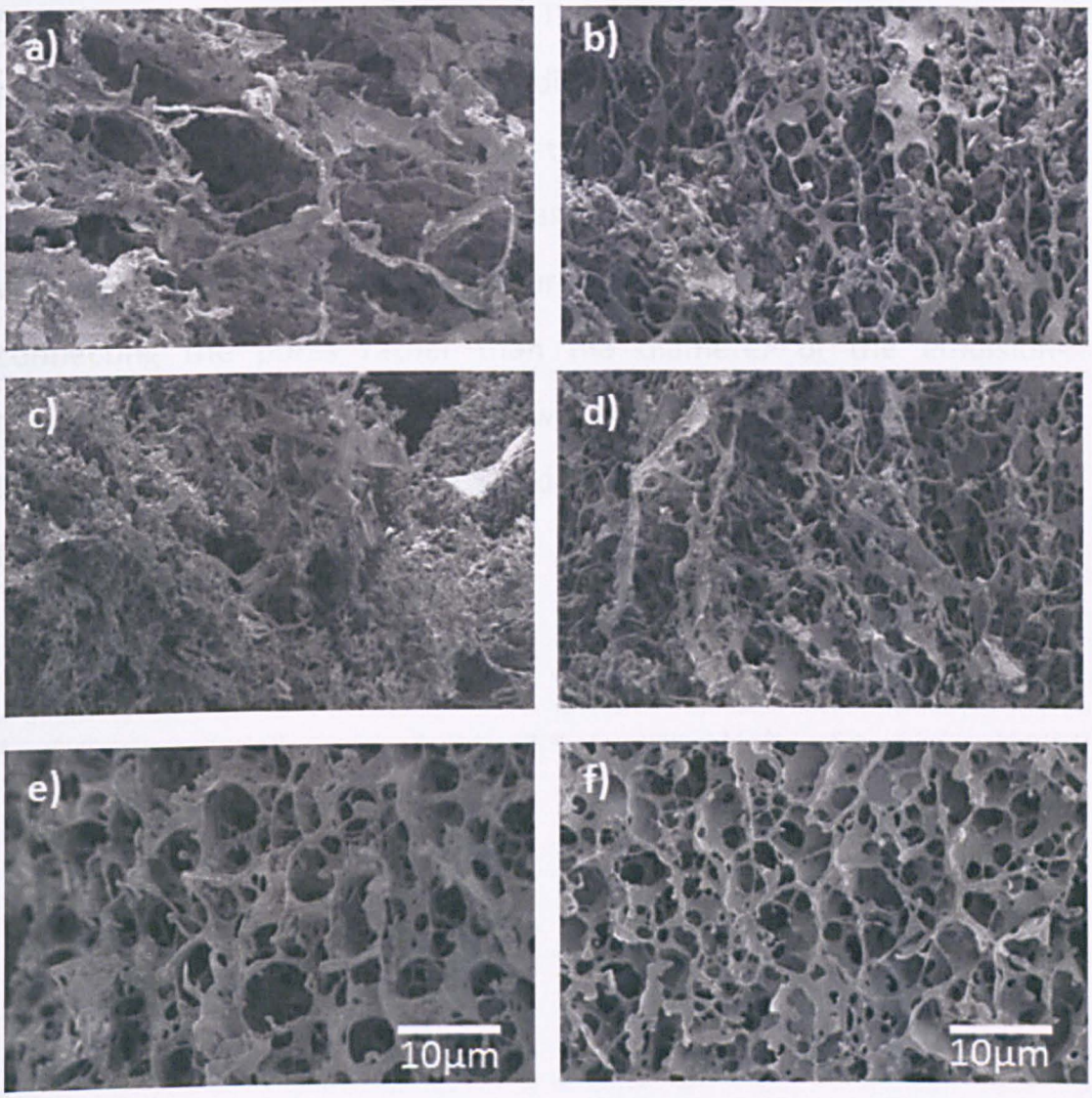

Figure2-2 - SEM images of PNIPAM with 1% crosslinker, below (a) and above (b), 2% crosslinker below (c) and above (d)and 5% below € and above (f) the LCST

bath. It was important to freeze the warm PNIPAM with little surface water rapidly in liquid nitrogen in order to represent the pore structure of PNIPAM above the LCST. Figure 2b shows the SEM image of 5% crosslinked PNIPAM above the LCST. The decrease in pore size was observed although this was not very obvious due to its highly interconnected pore structure. However, the decrease in pore size and pore volume could be clearly seen from the Hg intrusion data. As shown in table 2 and figure 3c, the pore size distribution was around 10 µm for

5 % crosslinked PNIPAM below LCST. For the sample above LCST, the pore sizes were decreased with a distribution around 4.8 μm (Figure 3c). For mercury intrusion porosimetry, the pore sizes were measured and calculated when mercury was penetrated into the pores at different pressure. Therefore, the pore sizes are relative to the windows connecting the pores rather than the diameter of the emulsion-templated pores. The pore volume was reduced from 5.8 cm^3/g (below LCST) to 3.5 cm^3/g (above LCST) due to the contraction of porous PNIPAM upon heating.

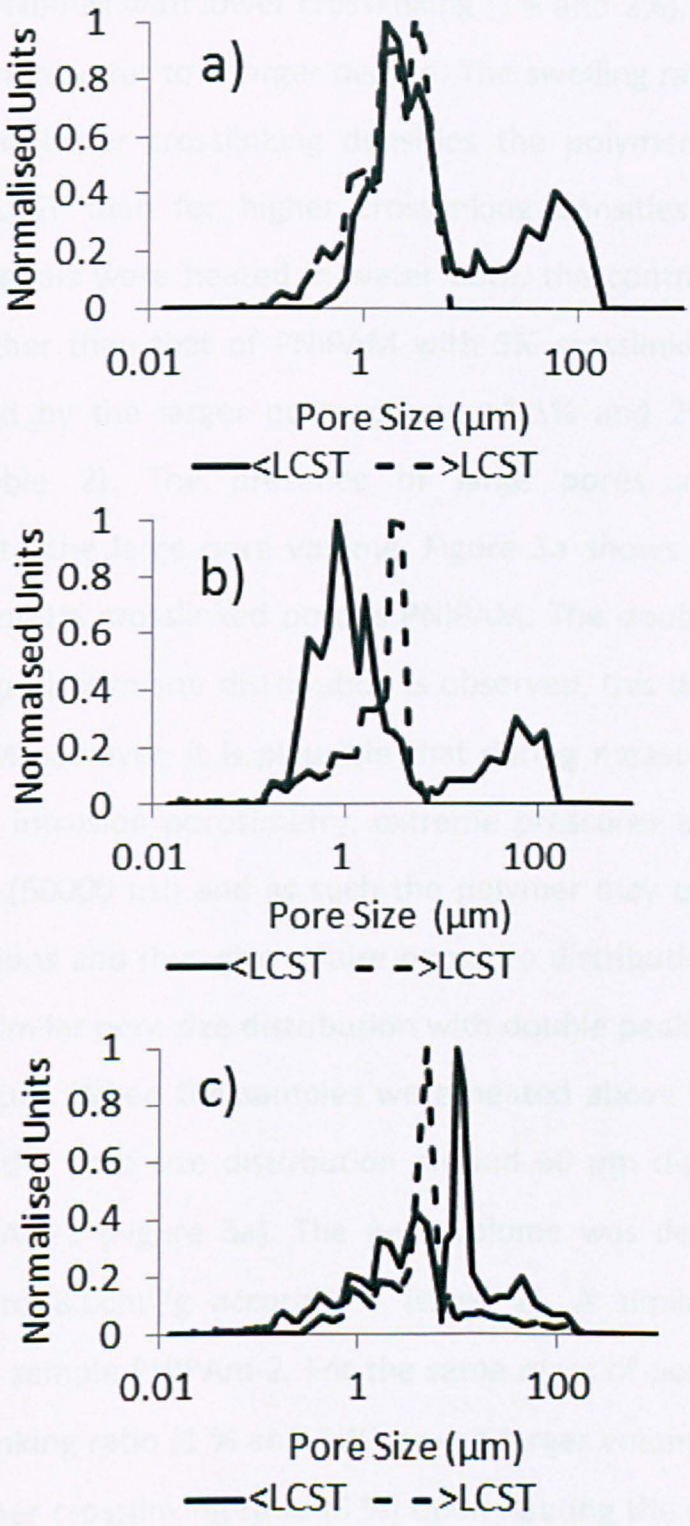

Figure 2-3 – Pore size distributions by Mercury intrusion porosimetry of PNIPAM of crosslinking densities 1% (a) 2% (b) and 5% (c)

For porous PNIPAM with lower crosslinking (1% and 2%), the materials were swollen in water to a larger degree. The swelling ratios in table 2 show how at lower crosslinking densities the polymer swells more below the LCST than for higher crosslinking densities. When the swollen materials were heated in water bath, the contraction degree was also higher than that of PNIPAM with 5% crosslinking ratio. This was reflected by the larger pore volume of 1% and 2% crosslinked PNIPAM (table 2). The presence of large pores around 60μm contributed to the large pore volume. Figure 3a shows the pore size distribution of 1% crosslinked porous PNIPAM. The double peak (60.4 μm and 1.6 μm) pore size distribution is observed, this does not agree with the SEM however, it is plausible that during measurements with the mercury intrusion porosimetry, extreme pressures are applied to the polymer (60000 psi) and as such the polymer may collapse under these conditions and thus give a false pore size distribution. PNIPAm-2 exhibited a similar pore size distribution with double peaks around 60.5 μm and 0.8 μm. When the samples were heated above LCST in 45 °C water bath, the pore size distribution around 60 μm disappeared for sample PNIPAm-1 (Figure 3a). The pore volume was decreased from 12.3 cm^3/g to 8.0cm^3/g accordingly (table 2). A similar trend was observed for sample PNIPAm-2. For the same mass of porous PNIPAM, lower crosslinking ratio (1 % and 2 %) gave a larger volume contraction than the higher crosslinking ratio (5 %) upon heating the sample above LCST, this observation can be explained by there being less crosslinked areas in the polymer therefore allowing for more flexibility within the chains of the PNIPAM, which then have the ability to contract more than if the crosslinking density was higher and thus more rigid. With

regard to the swelling and contraction properties in water, porous PNIPAM with 1 % and 2 % crosslinked ratios behaved in a similar way.

2.4.2 Uploading and release of Colloids

PS colloids were stained with Rhodamine B (RhB) primarily for the easy observation and monitoring by UV of their uploading and release. The porous PNIPAM was white. After soaking in RhB-PS colloidal suspension and being dried, the polymer turned red, indicating the loading of PS colloids. To prove that all the RhB molecules were attached to the PS colloids not freely available in the aqueous phase of the suspension the RhB-stained colloidal suspension was centrifuged at rpm 5000 for 20 minutes. All the red PS colloids were precipitated. The supernatant water phase was colourless. This water phase was also analysed by UV, showing no absorption peak at 420 nm. This confirmed that it was the loading of RhB-PS colloids rather than free RhB which turned the PNIPAM red. The UV monitoring at 420 nm truly reflected the concentration of PS colloids in water.

The dry PNIPAM with loaded PS colloids was cross-sectioned and exhibited the uniform distribution of red colour throughout the sample (figure 4b). The samples were then placed in water for temperature-triggered release of PS colloids. **Scheme 1** illustrates how PS colloids are loaded into and then released from porous PNIPAM using the surrounding temperature as trigger. After loading PS colloids into PNIPAM (steps 1 & 2), the sample was swollen in water with no PS colloids being released (<LCST, stored in a fridge with temperature around 4 °C, figure 4c). Indeed, we did not observe the solution turning red for at least 2 hours indicating no release or very little release of RhB-stained PS colloids, arising from the hydrophilicity of NIPAM below

the LCST (figure 4c). When the soaked sample in the vial was heated in a 45 °C water bath, it was clearly observed that the polymer started to contract and the red cloud being diffused out of the sample (as illustrated in steps 3 & 4, and figure 3d). As a result of RhB-stained PS colloids released and suspended directly in water, the water phase turned red.

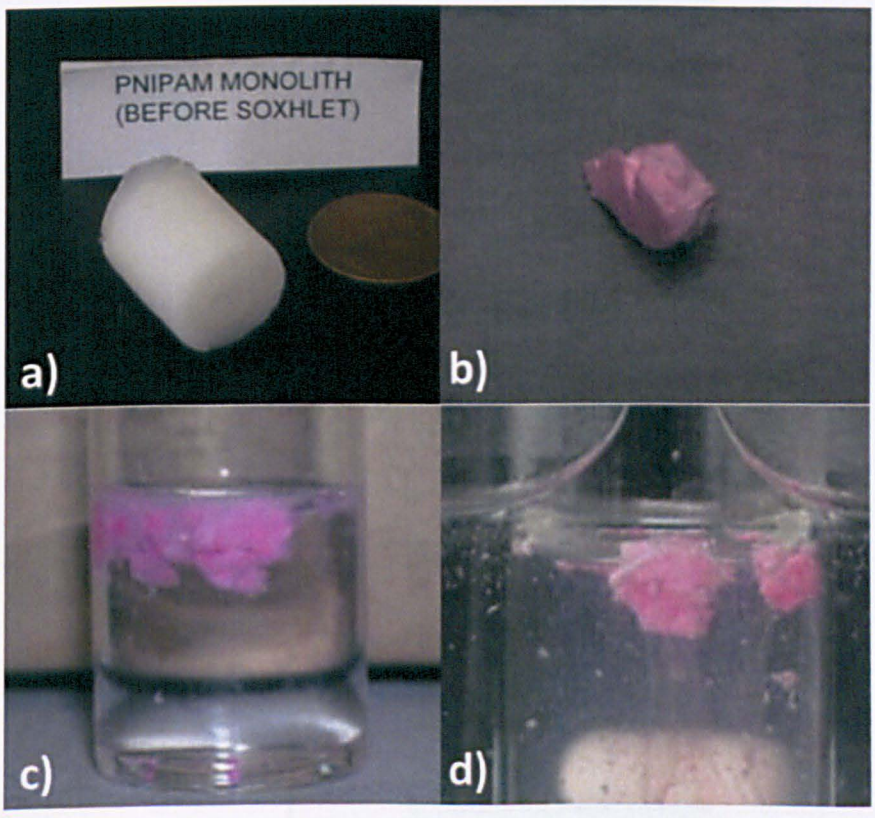

Figure 2-4 – Photographs of the prepared monolith before soxhlet extraction (a) a portion of the polymer after swelling in the PS-RhB solution (b). The polymer was then placed into water (c) were little PS-RhB was seen to be released before heating in a water bath to release the colloids (d)

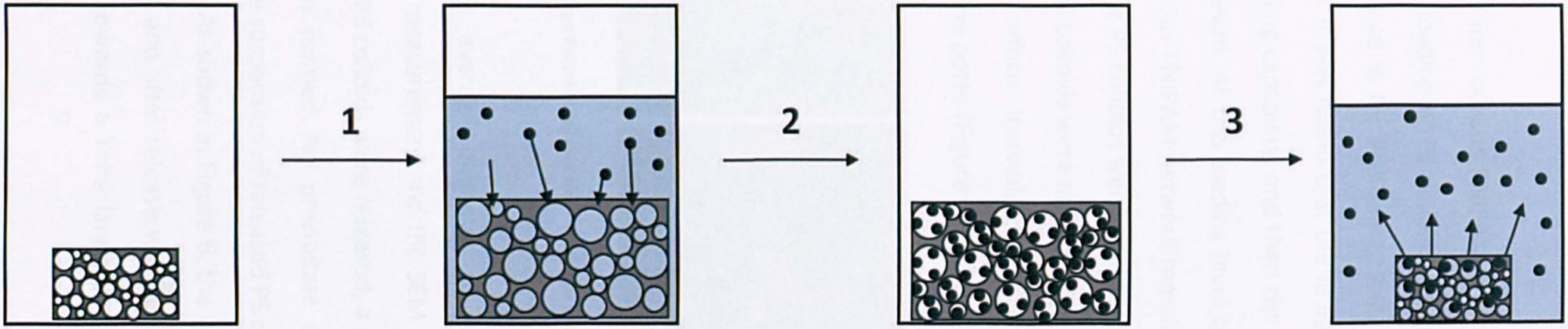

Scheme 1 - Schematic Representation for the Upload and release of polymeric colloids. In (1) the porous pNIPAM was allowed to swell in a aqueous suspension of PS colloids then filtered and dried (2). The swollen polymer was then placed in fresh water and heated above the LCST (3) to release the colloids.

The loading of PS colloids into porous PNIPAM was repeated at least three times. The average loading of PS colloids based on the mass of PNIPAM were obtained: 6.40 % for PNIPAm-1, 2.65 % for PNIPAm-2, and 0.83 % for PNIPAm-5. It was found that the lower the crosslinking ratio, the higher the swelling capability, and then the higher loading of PS colloids could be achieved. At this loading level of PS colloids, the highly interconnected porous PNIPAM network remained, as confirmed by the SEM (Figure 5a). The PS colloids were observed on the surface of the pores. However, the PS colloids were not seen distributing evenly or forming a layer on the surface. Instead, the PS colloids tended to aggregate on the edge of the pores (Figure 5b).

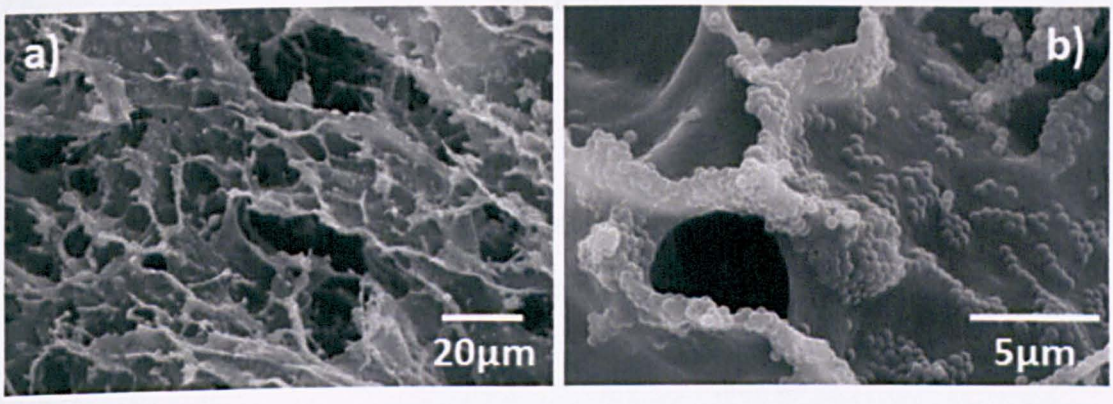

Figure 2-5 - SEM images of the swollen PNIPAM (a) and the PS colloids absorbed into the pores of the polymer monolith (b)

The PS colloids had an average diameter of 460± 10 nm, as characterized by the DLS measurement and the SEM imaging (Figure 6 and the inset). When the PS colloids were released, a stable suspension like the original one was formed. No precipitate of aggregated PS colloids was observed. The suspension of released PS colloids into water was characterized by DLS. As shown in Figure 6, the size distribution of PS colloids before loading and after release was very similar although the colloids size shifted towards a little larger (470 ± 10 nm). This

demonstrated that there was no aggregation of PS colloids occurring during the process of loading into and release from thermoresponsive porous PNIPAM.

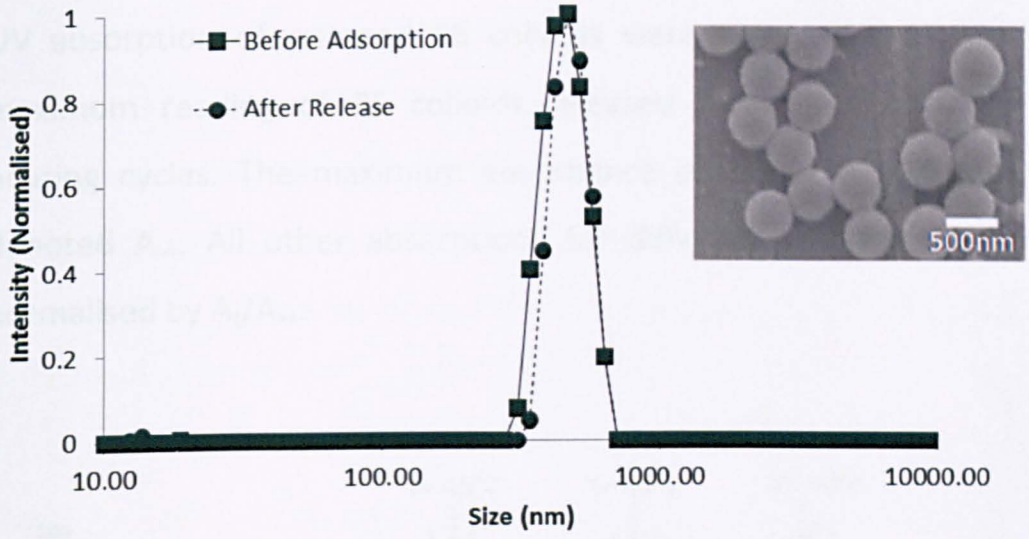

Figure 2-6 - DLS of the colloids before and after adsorption and SEM image of the colloids after release cycles (insert)

The release profiles of PS colloids below and above the LCST are shown in Figure 7 for porous PNIPAM with crosslinking ratios of 1, 2 and 5 %. The release was monitored by UV using a 96-well plate reader. A calibration curve of the PS colloids was performed and the absorption for RhB at 420 nm was used to assess the amount of released PS colloids. The same mass of PNIPAM samples was soaked in the same volume of PS colloidal suspensions with the same concentrations. It was found that 1 % crosslinked PNIPAM showed the highest PS colloids loading. The mass loading was the average data from three soaking experiments for PNIPAm-1, PNIPAm-2 and PNIPAm-5. Three cycles of release were performed for a temperature profile of the uptake and release of colloids from storing the samples in the fridge at 4 °C to heating the samples in a 45 °C water bath (see details in the experiment

section). Sample PNIPAm-1 exhibited the highest release of PS colloids according to the UV absorption peaks, up to 67% colloids release that were uploaded. In order to compare the loading capacity and releasing behaviour of PS colloids for PNIPAM at different crosslinking ratio, the UV absorption of released PS colloids were normalized against the maximum reading of PS colloids released from PNIPAm-1 after 3 heating cycles. The maximum absorbance observed at 420 nm was denoted A_∞. All other absorptions for different sampling (A_t) were normalised by A_t/A_∞.

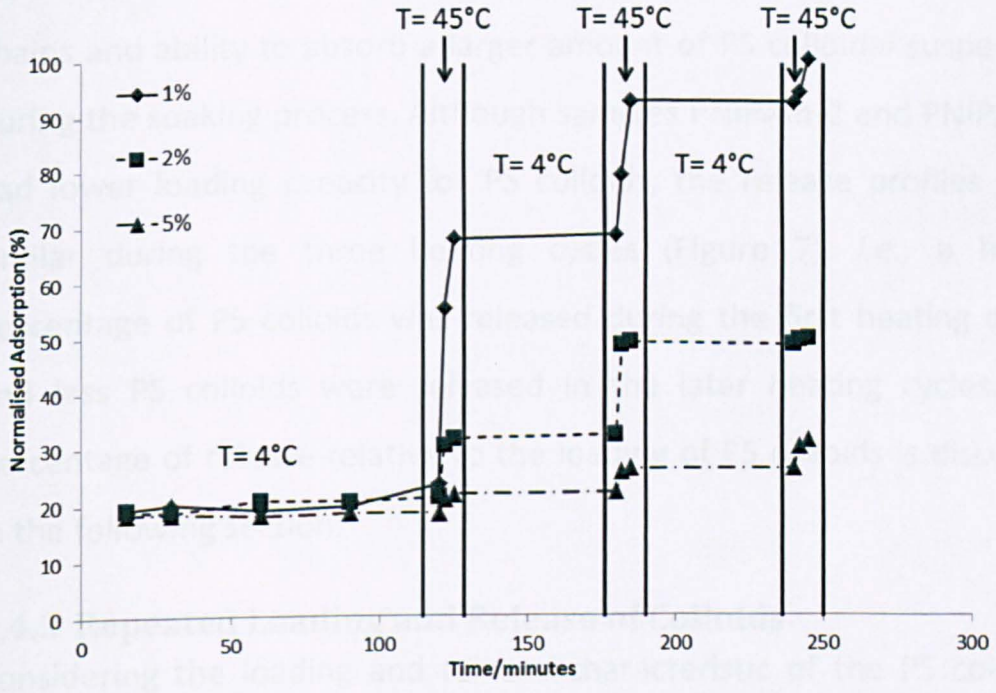

Figure 2-7 - UV release profiles of the colloids from PNIPAM at different crosslinking densities

A step release profile was observed for each sample (Figure 7). When the PNIPAM loaded with PS colloids were placed in water at 4 °C, an 18 % release was observed by the first measurement at the 15th minute. A similar release was observed for all three samples. This is reasoned that the PS colloids on or close to the surface of the materials were

suspended in water immediately. There was no more release of PS colloids from the PNIPAM for 2 hours while the samples were placed in water at 4°C. When these samples were heated in a 45 °C water bath, a burst release of PS colloids was seen and confirmed by the UV absorption. The samples were then stored in the fridge and two more heating cycles were performed. For sample PNIPAm-1, 50 % of PS colloids were released during the first heating cycle. Less PS colloids were released during the later heating cycles. It was quantified that 25 % and 7 % of PS colloids were further released during the second and third heating cycles respectively. Sample PNIPAm-1 had a higher loading capability of PS colloids, which resulted from its more flexible polymer chains and ability to absorb a larger amount of PS colloidal suspension during the soaking process. Although samples PNIPAm-2 and PNIPAm-5 had lower loading capacity for PS colloids, the release profiles were similar during the three heating cycles (Figure 7), *i.e.,* a higher percentage of PS colloids was released during the first heating cycles and less PS colloids were released in the later heating cycles. The percentage of release relative to the loading of PS colloids is discussed in the following section.

2.4.3 Repeated Loading and Release of Colloids

Considering the loading and release characteristic of the PS colloids, these porous PNIPAM might be referred as a pump to absorb and release the polymeric colloids in the presence of water simply by changing the surrounding temperature. However, to act like a pump, the porous materials should be able to perform many cycles of absorption and release. In this study, an initial effort was taken to

demonstrate the repeated loading and release of PS colloids by porous PNIPAM.

The profile of the mass loading and release with respect to the polymer weight is shown in Figure 8a. The loading of PS colloids was around 6.4 wt % for PNIPAm-1. Lower colloids loading were found for PNIPAM with higher crosslinking ratio (2.6 wt % for PNIPAm-2 and up to 1 wt % for PNIPAm-5). Around half or more loaded PS colloids were released during the heating cycle. The uptake of PS colloids by PNIPAM after one cycle of release was about 10% lower but kept constant for the next three loading cycles. It should be noted that not all the colloids loaded were released from the polymer during the heating cycle. There were three possible reasons to explain this: (1) when the polymer contracts, some small pores could "close over" thus trapping colloids from being released from the polymer; (2) the volume contraction ratio was limited and not all the colloids could be squeezed out; (3) the colloids could remain adsorbed on the surface of the pores because the interaction between hydrophobic PS colloids and the isopropyl group on the PNIPAM chains. The remaining PS colloids in PNIPAM could affect the further loading of PS colloids during the later soaking process. Our data showed that there was a slight reduction in PS colloid loading level for the 3 more cycles of uptake. However, the similar release profiles were observed for the PNIPAM samples under the test conditions.

The data in Fig. 8a were recalculated to show the percentage release of PS colloids in relation to the PS loading for each sample. The original mass of the dried polymer before any uploading had occurred was regarded as 0% with the first upload being 100 %. The release profiles

of the repeated loading and release of PS colloids for PNIPAM samples are shown in Figure 8b. By comparing the mass loss of PS colloids during the release process, one could see a true picture of how the PNIPAM with different crosslinking ratio were able to release the loaded colloids. The sample PNIPAm-1 showed up to 60% release of the total mass of colloids absorbed per cycle. The re-loadings of the PS colloids were up to 90 % of the original mass uptake. PNIPAm-2 gave a lower release of colloids with generally releasing up to 50 % per cycle of the loaded colloids. The reabsorption of colloids reached approximately 90% of the initial uptake. Sample PNIPAm-5 had the lowest colloid release with approximately 40 % of the total colloids being released per cycle. Polymers with a lower crosslinking density showed a higher swelling/contraction ratio and hence were able to release a higher percentage of loaded colloids. For polymer with a higher crosslinking density, the porous structure was rigid and a lower swelling/contraction ratio was observed. This led to a lower releasing capability for the loaded PS colloids. However, the re-loading of PS colloids could reach 90 % of the first loading for all the three samples. This suggested that the repeated loading and release was still effective even for the relatively highly crosslinked polymers.

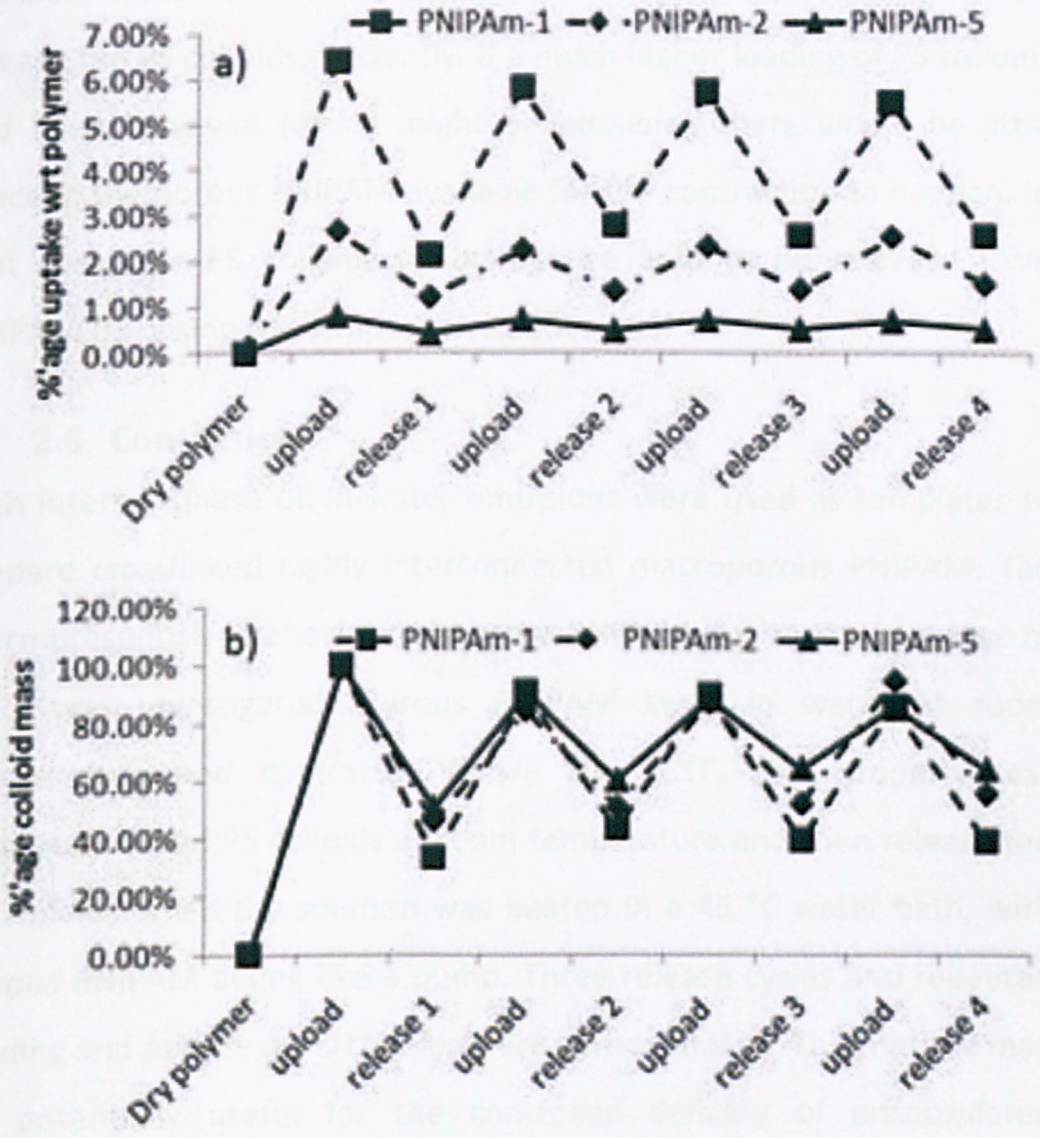

Figure 2-8 - Reproducible uploading and release of PS colloids: (a) shows the % uptake with respect to the polymer weight and (b) with respect to % colloid uptake

The highest mass loading of PS colloids (6.4 wt%) was found during the first soaking process for sample PNIPAm-1. This loading was still quite low considering the high pore volume available in porous PNIPAM. However, this was essential for the release of PS colloids via the mechanism of polymer swelling and contraction. As seen from the SEM image (Fig. 5), the PS colloids were only covering the pore surface but not occupying or blocking the pores. Therefore a lot of voids were still

available in the PNIPAM and the polymer could contract sufficiently and release the PS colloids efficiently. If a much higher loading of PS colloids had been achieved (which might be possible), there would be little space in the porous PNIPAM available for the contraction to happen. In that case, the PS colloids would not be able to be released from PNIPAM by raising the temperature above LCST.

2.5 Conclusions

High internal phase oil-in-water emulsions were used as templates to prepare crosslinked highly interconnected macroporous PNIPAM. The thermoresponsive behaviour of porous PNIPAM due to the presence of LCST was investigated. Porous PNIPAM swell in water at room temperature and contracted above the LCST. This property was explored to load PS colloids at room temperature and then release the PS colloids when the solution was heated in a 45 °C water bath, with porous PNIPAM acting like a pump. Three release cycles and repeated loading and release of PS colloids were demonstrated. This method may be potentially useful for the controlled delivery of encapsulated microspheres in a number of applications.

2.6 References

1. Huebsch, N.; Mooney, D. J. *Nature* **2009**, *462*, 426-432.
2. Peppas, N. A.; Hilt, J. Z.; Khademhosseini, A.; Langer, R. *Advanced Materials* **2006**, *18*, 1345-1360.
3. Cameron, N. R.; Sherrington, D. C.; Albiston, L.; Gregory, D. P. *Colloid Polym. Sci.* **1996**, *274*, 592-595.
4. Zhang, H.; Cooper, A. I. *Soft Matter* **2005**, *1*, 107-113.
5. Su, F.; Bray, C. L.; Tan, B.; Cooper, A. I. *Advanced Materials* **2008**, *20*, 2663-2666.
6. Christenson, E. M.; Soofi, W.; Holm, J. L.; Cameron, N. R.; Mikos, A. G. *Biomacromolecules* **2007**, *8*, 3806-3814.

7. Kovacic, S.; Krajnc, P. *J. Poly. Sci., A: Polym. Chem* **2009**, *47*, 6726-6734.
8. Zhao, C.; Danish, E.; Cameron, N. R.; Kataky, R. *J. Mater. Chem.* **2007**, *17*, 2446-2453.
9. Cameron, N. R. *Polymer* **2005**, *2005*, 1439-1449.
10. Kulygin, O.; Silverstein, M. S. *Soft Matter* **2007**, *3*, 1525-1529.
11. Williams, J. M.; Wrobleski, D. A. *Langmuir* **1988**, *4*, 656-662.
12. Krajnc, P.; Stefanec, D.; Pulko, I. *Macromol. Rapid Commun.* **2005**, *26*, 1289-1293.
13. Zhang, H.; Cooper, A. I. *Chem. Mater.* **2002**, *14*, 4017-4020.
14. Silverstein, M. S.; Tai, H.; Sergienko, A.; Lumelsky, Y.; Pavlovsky, S. *Polymer* **2005**, *46*, 6682-6694.
15. Busby, W.; Cameron, N. R.; Jahoda, C. A. B. *Biomacromolecules* **2001**, *2*, 154-164.
16. Lumelsky, Y.; Silverstein, M. S. *Macromolecules* **2009**, *42*, 1627-1633.
17. Menner, A.; Verdejo, R.; Shaffer, M.; Bismarck, A. *Langmuir* **2007**, *23*, 2398-2403.
18. Zhang, H.; Hardy, G. C.; Rosseinsky, M. J.; Cooper, A. I. *Advanced Materials* **2003**, *15*, 78-81.
19. Ikem, V. O.; Menner, A.; Bismarck, A. *Angew. Chem., Int. Ed.* **2008**, *47*, 8277-8278.
20. Menner, A.; Ikem, V. O.; Salgueiro, M.; Shaffer, M.; Bismarck, A. *Chem. Comm.* **2007**, 4274-4276.
21. Zhang, S.; Chen, J. *Chem. Comm.* **2009**, 2217-2219.
22. Safinia, L.; Wilson, K.; Mantalaris, A.; Bismarck, A. *Macromol. Biosci.* **2007**, *7*, 315-327.
23. Cummins, D.; Duxbury, C. J.; Quaedflieg, P. J. L. M.; Magusin, P. C. M. M.; Koning, C. E.; Heise, A. *Soft Matter* **2009**, *5*, 804-811.
24. Gil, E. S.; Hudson, S. A. *Prog. Polym. Sci* **2004**, *29*, 1173-1222.
25. Schild, H. G. *Prog. Polym. Sci* **1992**, *17*, 163-249.
26. Klouda, L.; Hacker, M. C.; Kretlow, J. D.; Mikos, A. G. *Biomacromolecules* **2009**, *30*, 4558-4566.
27. Yavuz, M. S.; Cheng, Y.; Chen, J.; Cobley, C. M.; Zhang, Q.; Rycenga, M.; Xie, J.; Kim, C.; Song, K. H.; Schartz, A. G.; Wang, L. V.; Xia, Y. *Nat. Mater.* **2009**, *8*, 935-939.

28. Mano, J. F. *Adv. Eng. Mater.* **2008**, *10*, 515-527.
29. Peppas, N. A.; Khare, A. R. *Adv. Drug Delivery Rev.* **1993**, *11*, 1-35.
30. Zhang, H.; Cooper, A. I. *Advanced Materials* **2007**, *19*, 2439-2444.
31. Freitas, S.; Merkle, H. P.; Ganer, B. *J. Controlled Release* **2005**, *102*, 313-332.

3 EMULSION TEMPLATING AS ROUTES TO THE PRODUCTION OF ORGANIC NANODISPERSIONS

3.1 Chapter Overview

Emulsion templated poly (vinyl alcohol) (PVA) monoliths were produced via freeze-drying. Indomethacin was used as a model drug and the preparation of its nanoparticles in-situ within the porous materials were observed. The nanodispersions could be prepared by simple dissolution of the composite materials into water.

3.2 Introduction

Chapter 1 discusses in great detail the process explored for the formulation of water insoluble drugs. One aspect that is explored is that of Nanosuspensions are thermodynamically unstable and as such needs to be stabilised to retain particle size against aggregation. A choice of stabiliser is selected to promote such a particle size reduction and a physically stable formulation. A wide range of organic materials are poorly soluble in water. Typical examples are poorly water-soluble drugs. Lipinski reported that 31.2% of a group of 2246 compounds synthesized in academic laboratories between 1987 and 1994 had solubility equal to or less than 20 μg/ml.[1] The low bioavailability resulting from low water solubility is a great concern in the pharmaceutical research industry. Overcoming the problem of drug solubility is thus of great interest. Various efforts have been made to address this problem by delivery in nanocarriers and by nanoparticles engineering.[2-5] A wide range of carriers such as polymer capsules and micelles, cyclodextrin complexations and lipid-based formulations have

been investigated in an effort to enhance the inherent solubility of the drugs.[6-7] In the method of nanoparticles engineering, poorly water-soluble drugs are micronized to produce small particles at the level of micrometres and nanometres.[8-10] According to the Nernst–Brunner/Noyes–Whitney equation (1), the dissolution rate of an organic compound is proportional to the surface area available for dissolution.[10] Therefore, the dissolution rate of poorly water-soluble drugs could be increased substantially via reducing particle size to nanometer range. Based on the calculation by the Stokes equation, nanoparticles with sizes <300 nm will not settle for a density of particles of 1.15 and η of 1, which is essential for many potential applications.[11]

$$\frac{dX}{dt} = \left(\frac{AD}{h}\right)\left(\frac{C_S - X_d}{V}\right) \qquad (1)$$

The Nernst-Brunner/Noyes-Whitney equation where, dX/dt is the dissolution rate, D is the diffusion coefficient, A is the particle surface area, h is the effective boundary layer thickness, C_s is the saturated solubility and Xd is the amount dissolved and V is the volume of fluid available for dissolution..

Drug nanoparticles can be prepared by means of high pressure homogenization, milling, or microfluidization.[12-14] Drug nanoparticles can also be formed from molecules in a solution or in an emulsion. Emulsion evaporation, solvent displacement, solvent diffusion and rapid freezing have been widely used to prepare drug nanoparticles.[15-19] As a type of green and sustainable solvents, supercritical fluids (particularly supercritical carbon dioxide) has been explored to produce drug particles in the processes of rapid expansion, rapid expansion to

aqueous solutions, and anti-solvent effect on organic drug solutions.[8, 19-21]

Freeze drying is a process where a solution is frozen in contact with a cold liquid or in a cold environment, and the frozen sample is then placed in a freeze dryer to remove the frozen solvent under vacuum. Water-based solutions are usually processed by freeze drying to produce drug or protein particles. The freeze-drying technique has been developed recently to construct advanced porous materials.[22-23] A spray freezing of solutions and emulsions into cold liquid has been developed to prepare microparticles with significantly enhanced water solubility[24-25]. The rapid freezing technique with emphasis on thin film freezing has also been employed to produce drug nanoparticles.[26] However, the pore structure of the scaffold and its influence on drug particles has not been investigated. We developed a new method to prepare porous organic nanocomposites by freeze-drying emulsions.[27] In this method, an organic compound (an organic dye) was dissolved in an organic solvent which was then emulsified into an aqueous polymer solution to form an oil-in-water emulsion. Freeze-drying of the emulsion led to the formation of organic nanoparticles inside the porous polymer. The porous materials could be rapidly dissolved in water to release the organic nanoparticles to form a stable aqueous nanodispersion. Aqueous triclosan nanoparticle dispersions were formed this way and an enhanced biocidal activity was demonstrated compared to triclosan aqueous ethanol solution.

For the commonly-used water-in-oil emulsion approach, the drug nanoparticles are normally formed in the water phase by emulsion solvent diffusion,[18] emulsion dilution,[28] or the extraction of organic

solvent from the emulsions for example by supercritical fluids.[21] However, for the purpose of storage, characterization or some applications, the recovery of the nanoparticles via the removal of solvent is required and is still a challenge. Common techniques include spray drying, freeze drying and ultrafiltration which are energy intensive or with limited yields. A salt flocculation method was recently proposed to recover amorphous nanoparticles.[29] It was noticed that although drug nanoparticle engineering techniques were successful for enhancing the dissolution properties of poorly water-soluble drugs, there were limitations such as particle aggregation and poor wettability. Hot-melt extrusion of micronized itraconazole particles with hydrophilic polymers was demonstrated to overcome some of the limitations.[30]

In this chapter, we extended the approach of freeze-drying emulsions to produce poorly water-soluble drug nanoparticles. Indomethacin (IMC), a poorly water-soluble non-steroidal drug for the treatment of inflammation and pain, was used as a model drug and processed to prepare IMC nanoparticles within *porous* hydrophilic poly(vinyl alcohol) (PVA). The IMC nanoparticles could be released into water instantly to form aqueous nanoparticle dispersions via the dissolution of PVA. The effects of PVA concentration, surfactant concentration and IMC concentration on the size and surface charge of IMC nanoparticles were investigated in detail. In this method, all the drug molecules were turned into nanoparticles and entrapped within the dissolvable porous polymers. In principle, there is no need to recover the nanoparticles and the nanoparticles may be formulated when required by dissolving into water or other suitable solvent. Also because the nanoparticles were formed in the porous polymer, the aggregation of IMC nanoparticles

could be avoided. The materials were formed in the format of a monolith rather than powders and thus easy to be handled, stored, and transported

3.3 Experimental

3.3.1 Materials

Indomethacin (IMC), poly (vinyl alcohol) (PVA, Mw 9K), sodium dodecylsulphate (SDS), and o-xylene were purchased from Sigma-Aldrich and used as received. Distilled water was used in all cases.

3.3.2 Preparation of IMC nanoparticles within the porous polymer.

IMC was dissolved in o-xylene at the concentration of 0.05, 0.1, 0.5 wt %. PVA was dissolved in water to make aqueous solutions at the concentration of 1, 2 and 5 wt %. SDS was used as a surfactant and dissolved in aqueous PVA solutions at the concentrations of 1 wt %, 5 wt % and 10 wt %. To form an oil-in-water emulsion, the IMC solution was added into the aqueous PVA-SDS solution dropwise while stirring at 500 rpm using a lab stirrer for 15 minutes. The volume ratio of oil phase to aqueous phase in the emulsions was varied at 50:50, 75:25 and 80:20.

The formed emulsion in a glass beaker was rapidly frozen in liquid nitrogen and then transferred to a freeze dryer (VirTis AdVantage) with a shelf temperature of – 30 °C. The freeze-drying process was carried out for 48 hours to remove both water and o-xylene. The IMC nanoparticles were formed directly in the porous polymers

Table 1 Preparation conditions for the emulsions and characterization data for the formed IMC nanoparticles and porous materials

Entry	PVA (wt%)	SDS (wt%)	IMC (wt%)	Oil Volume (%)	Surface Tension (dyne/cm^3)	Droplet Size[1] (μm)	Particles Size[2] (nm)	Zeta Potential[3] (mV)	Pore Volume[4] (mL/g)	Mean Pore Size[4] (μm)
S1	5	5	0.1	50	42.15	27 ± 12.8	151 ± 22	-15.5 ± 11.70	11.73 ± 0.6	6.89 ± 0.7
S2	5	5	0.1	75	nm[b]	8 ± 4.6	188 ± 35	-21.1 ± 7.15	20.21 ± 1.0	20.12 ± 2.0
S3	5	5	0.1	80	nm[b]	10 ± 4.5	230 ± 28	-16.9 ± 7.73	24.46 ± 1.3	28.41 ± 2.8
S4	5	0	0.1	50	46.58	102 ± 53.9	227 ± 28	-14.6 ± 4.43	27.56 ± 1.4	33.16 ± 3.3
S5	5	1	0.1	50	42.93	85 ± 48.0	244 ± 45	-13.5 ± 4.72	18.02 ± 0.9	18.65 ± 1.9
S6	5	10	0.1	50	26.64	11 ± 5.3	195 ± 28	-24.5 ± 7.09	10.65 ± 0.5	5.92 ± 0.6
S7	2	5	0.1	50	26.90	65 ± 36.2	185 ± 23	-16.1 ± 6.34	17.6 ± 0.9	17.67 ± 1.8
S8	1	5	0.1	50	35.48	101 ± 50.0	169 ± 27	-25.2 ± 4.83	24.91 ± 0.7	21.12 ± 2.1
S9	5	5	0.05	50	nm[b]	nm[a]	137 ± 33	-26.9 ± 8.96	nm[a]	nm[a]
S10	5	5	0.5	50	nm[b]	nm[a]	286 ± 54	-13.6 ± 5.11	nm[a]	nm[a]

Note: The average values for droplet size, particles size and zeta potential calculated by the relevant instrument software are listed in this table.

nm[a] Droplet sizes were not measured for samples S9 and S10 because it was believed that the change of IMC concentration would not affect the size of droplets.

nm[b] Surface tension measurements for these samples are already measured for the corresponding surfactant concentrations (S1)

1 – measured by laser scattering

2 – measured by DLS

3 – measured by electrophoresis

4 – measured by mercury porosimetry

during the freeze-drying process. All the freeze-dried samples were kept in a dessicator. Table 1 summarises the preparation conditions and characterization data for the formed IMC nanoparticles.

3.3.3 Characterisation

The droplets sizes of the formed emulsions were measured using a Malvern Mastersizer 2000 with a Hydro 2000 SM dispersion unit. The emulsion (3 drops) was added to the dispersion unit containing approximately 100 mL water with a stirring rate of 1200 rpm.

Surface tension measurements where performed using a Kibron Delta-8 surface tensiometer. Aqueous solutions of PVA/SDS with differing concentrations were prepared. 50µl of each sample was pipetted into a 96-well plate. To show the influence of polymer concentration, the surfactant concentrations where kept constant (0, 1, 5 and 10 wt %) and the polymer concentration was varied by 0.5 wt % from 1 wt % to 5 wt %. To assess the influence of surfactant concentration, the polymer concentration was kept constant (1, 2 and 5 wt %) and the surfactant concentration was varied from 0 to 10 wt % in 1 wt % increments. The surface tension measurements were analysed by Delta manager 2.73 software. Each data point is an average of 8 values.

The dried materials were sectioned to reveal the internal porous structures. The samples were adhered to an aluminium stub using a silver colloidal suspension and allowed to dry. A sputter coater (EMITECH K550X) was used to coat the samples with gold at 40mA for 3 minutes. A Hitachi S-4800 field emission SEM was used to reveal the pore structure at 3 KV. The pore sizes and pore volumes of the dried materials were examined using a Micromeritics Autopore IV 9500

porosimeter. Samples were subjected to a pressure cycle starting at approx 0.5 psi, increasing to 60000 psi in predefined steps.

The IMC nanoparticle-loaded porous polymer was dissolved in water at the concentration of 0.5 wt%. The IMC nanoparticles were released and an aqueous IMC nanoparticle dispersion was formed. The IMC nanodispersions were analysed at 25 ^{0}C using a Malvern Zetasizer equipped with a zeta-potential detector with a backscattering detection at 173°. The scattering intensity signal for the detector is passed through a correlator where this data is analysed by the software to give a size distribution. The size and zeta potential of the hydrated IMC nanoparticles in water were obtained. Each measurement was repeated at least 3 times and the average data were used to plot the figures. 10μl of a diluted IMC nanodispersion was dropped onto holey carbon filmed copper grids (400 mesh) and allowed to dry overnight. A scanning transmission microscopic (STEM) detector attached to the Hitachi S-4800 SEM was used to observe the dry IMC nanoparticles at 30 KV.

3.4 Results and Discussion

0.1 wt % IMC solution was firstly emulsified into an aqueous solution containing 5 % PVA and 5 % SDS with an oil:water volume ratio= 50:50. The formed emulsion could be frozen and freeze-dried to produce a porous material[22,23] while the IMC nanoparticles could be formed *in situ* within the macropores.[20] Due to its highly interconnected porosity, the material could be rapidly dissolved in water and a clear solution containing IMC particles was produced. The DLS measurement showed that the size of IMC nanoparticles in water was around 130 nm. This

was further confirmed by observing dry IMC particles with a STEM monitor. As shown in Figure 1, the sizes of dry IMC nanoparticles were in the range of 100 – 200 nm.

An emulsion is a mixture of two immiscible phases, with one phase dispersed in another. In this study, an organic solution was emulsified in an aqueous phase to form an oil-in-water emulsion. PVA was dissolved in the continuous aqueous phase while IMC was dissolved in the droplet organic phase. The emulsion could be frozen to lock in the structure.

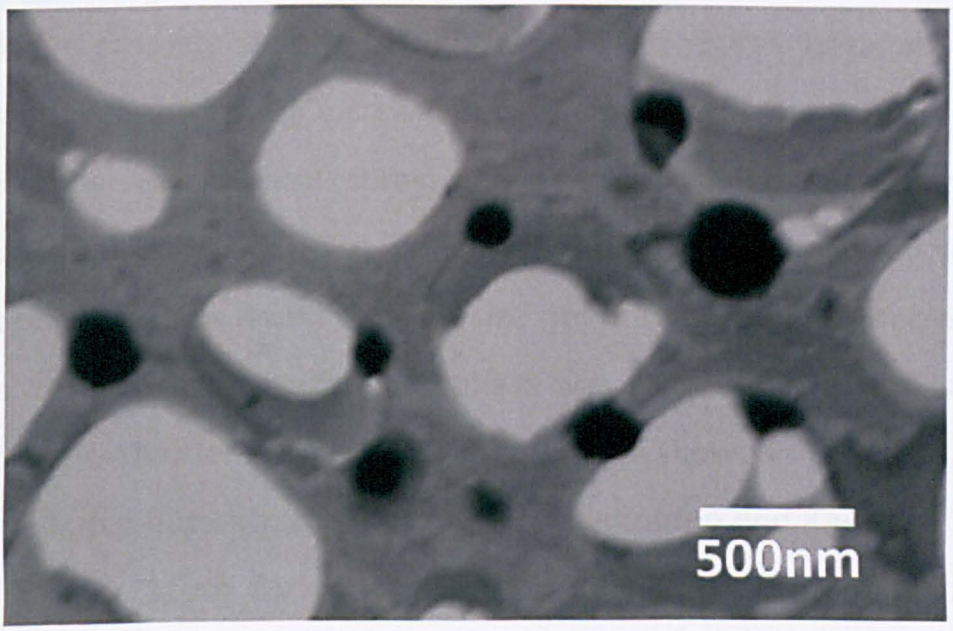

Figure 3-1 STEM image of IMC nanoparticles (black) on holey carbon TEM grids (grey)

The formation of emulsions was the key to produce IMC nanoparticles within porous PVA during the freeze-drying process. Emulsions with different formulations were formed and then freeze dried. Their effects on IMC nanoparticles were further investigated.

3.4.1 Ratio of oil to water in the emulsions

When forming emulsions, the ratio of oil to water could be systematically varied. This could affect the porosity of the materials[27] and the loading of the formed nanoparticles. The ratios of oil:water at

50:50, 75:25 and 80:20 were investigated. With a higher percentage of oil phases in the emulsion, a higher porosity of the materials and a higher loading of IMC nanoparticles were expected after the freeze-drying process. Figure 2a-c shows the porous structure of the materials formed from emulsions containing 50 %, 75 % and 80 % oil phase. For the material made from the emulsion containing 50 % oil phase, the emulsion-templated spherical pores were observed dispersing in the ice-templated porous matrix. There were some very large emulsion-templated pores, which could be due to the coalescence of the emulsion droplets before being frozen. The pores became more interconnected with the increase in oil phase volume percentage, with the number of spherical pores increased and the size of the pores decreased (Figure 2a-c). The formed emulsions were analysed using a Mastersizer. It was found that the size of emulsion droplets decreased when a higher percentage of oil phase was present in the emulsions. The size distributions of emulsion droplets are shown in Figure 2d. The peak size decreased from 27 μm for 50 % emulsion and 8 μm for 75 % emulsion to 7 μm for 80 % emulsion (Table 1). This tendency of decrease of emulsion droplets was consistent with change of pore size in dry porous materials as observed by SEM.

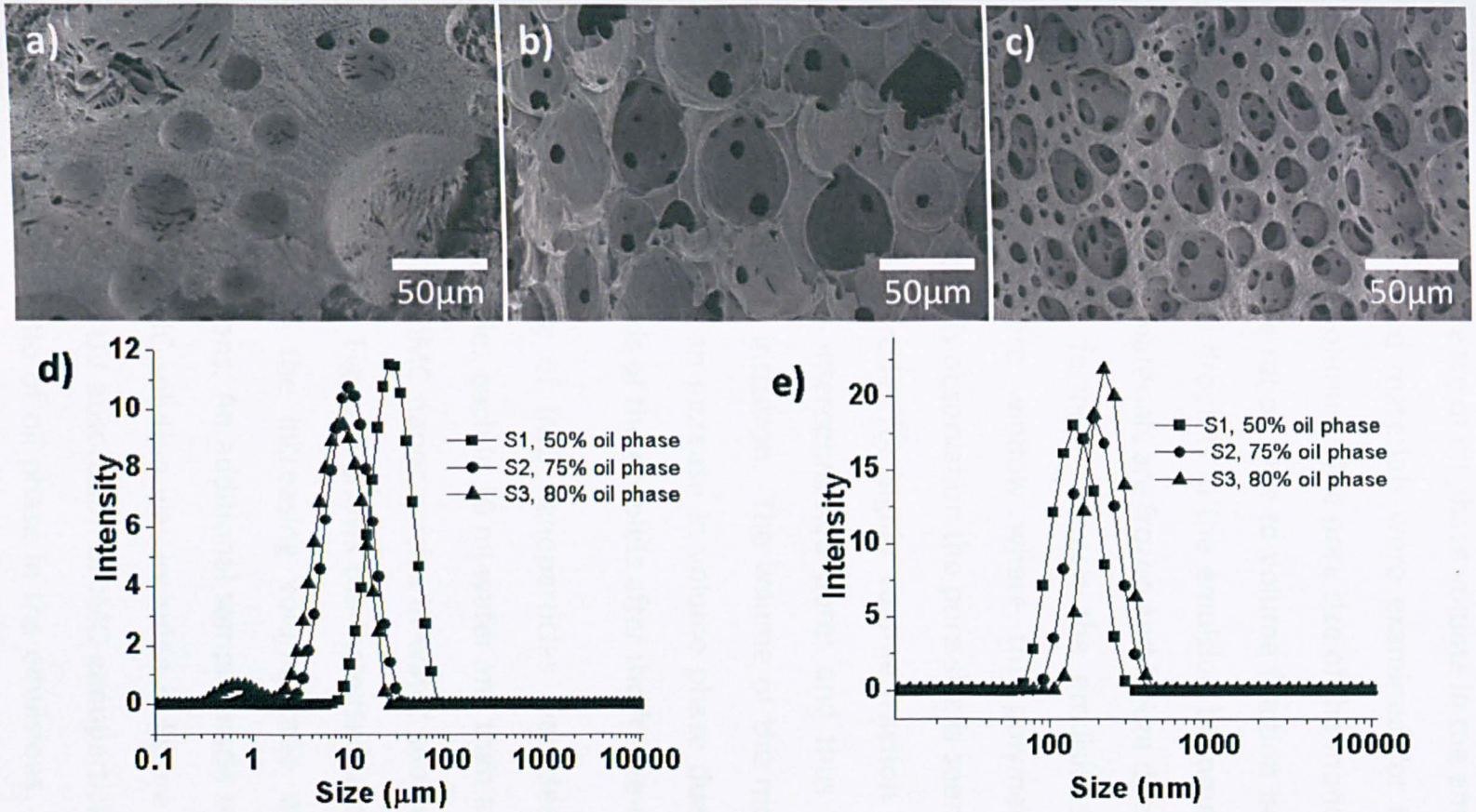

Figure 3-2 SEM images of porous PVA with IMC nanoparticles prepared from the emulsions containing (a) 50%, (b) 75% and (c) 80% oil phase. (d) The droplet size distributions of the emulsions containing different volume percentage of oil phase. (e) The size of IMC nanoparticles in water as measured by DLS. Note: IMC particles will not be seen in the pores of the material due to the difference in contrast between the organic nanoparticle and the polymer

The IMC nanoparticle dispersions formed from these materials were analysed by DLS. It was observed that the size of nanoparticles increased with the increase of oil phase volume in the emulsions (Figure 2e). The freeze dried materials were examined for their pore size distribution and pore volumes. The pore size of the monoliths increases with increasing volume ratio. Due to volume fraction being above the threshold of 0.74ø the droplets in the emulsion become close packed. Due to this when the materials are frozen and freeze dried a thin film of polymer that can be formed between the emulsions droplets can rupture leaving a pore window where the polymer would have existed.[31] Owing to this observation the pore size is seen to increase as when the mercury intrudes for higher volume fraction monoliths, the mercury intrudes into interconnected pores and thus this is what is measured by mercury intrusion. The volume of the monoliths is also seen to increase with an increase in volume phase due to more area being left from the voids of the droplets after the freeze-drying process.

The increased loading of IMC nanoparticles was demonstrated by dissolving 0.05 g samples each in 10 ml water and then analysed by UV-vis spectroscopy. The IMC nanoparticles in water showed a maximum absorption at 320 nm. Figure 3 shows the increased absorption at 320 nm corresponding to the increasing volume ratio of IMC organic solution in the emulsions. An additional sample made of the emulsion containing 66 v/v% IMC solution was included in Figure 3. In the inset figure in Figure 3, the UV absorption of IMC nanoparticles was plotted against the volume ratio of oil phase in the emulsions. This suggested that the loading of IMC nanoparticles roughly followed a linear relation to the oil phase volume percentage in the originally formed emulsions.

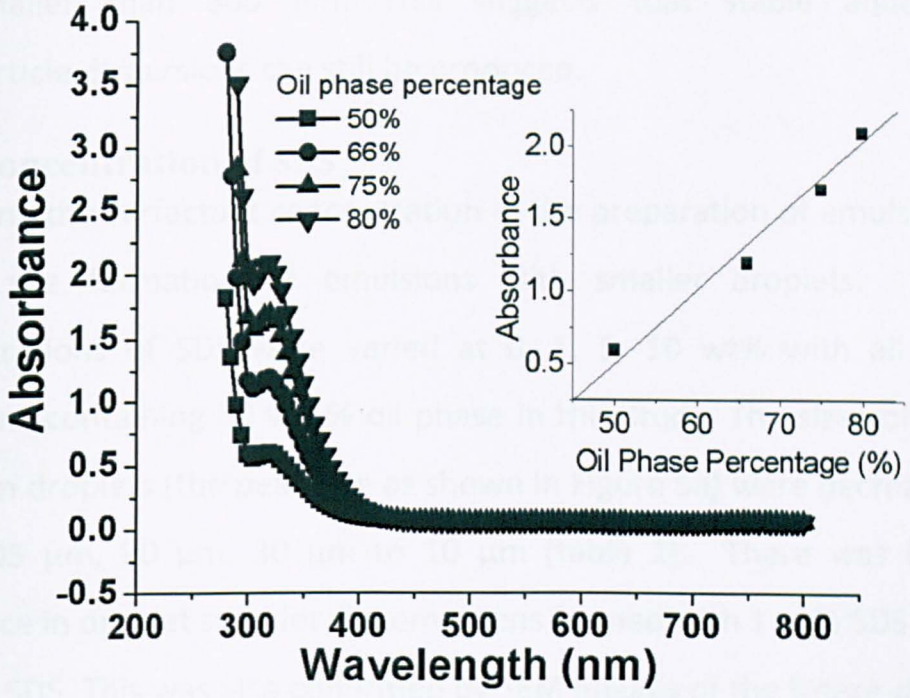

Figure 3-3 UV spectra of porous PVA/IMC nanoparticles composites dissolved in water. The materials were made from the emulsions containing different percentage of oil phase. The inset shows the UV absorbance versus oil phase percentage.

For an emulsion, the volume percentage of the droplet phase can be varied in a wide range e.g. 10 % ~ 95 %. The change in the volume percentage of internal phase for an emulsion can produce the porous materials with tuneable pore morphology and pore volume[19] and also the loading of IMC nanoparticles. The loading of IMC nanoparticles is increased 3 times when the used emulsion contains 75 v/v oil phase (water: oil = 1:3), compared to the sample made from the emulsion containing 50 v/v % oil phase (water:oil = 1:1). This is confirmed by the UV study in Figure 3. When the internal phase percentage was increased from 50 v/v% to 80 v/v% in this study, a trend of size increase was observed (Figure 2). However, the IMC nanoparticles produced are

still smaller than 300 nm. This suggests that stable aqueous nanoparticle dispersions can still be produced.

3.4.2 Concentration of SDS

Increasing the surfactant concentration in the preparation of emulsions led to the formation of emulsions with smaller droplets. The concentrations of SDS were varied at 0, 1, 5, 10 wt% with all the emulsions containing 50 v/v % oil phase in this study. The sizes of the emulsion droplets (the peak size as shown in Figure 5a) were decreased from 105 μm, 90 μm, 30 μm to 10 μm (table 1). There was little difference in droplet sizes for the emulsions formed with 1 wt% SDS and without SDS. This was also confirmed by SEM images of the freeze-dried porous materials. As shown in Figure 5b, very large spherical pores resulted from the oil drops in the emulsion containing no SDS were observed. When the SDS was added in the emulsion at the concentration of 1 wt%, a similar porous structure was observed. When the concentration of SDS was further increased to 5 wt% and 10 wt%, the sizes of the spherical pores were decreased and the pore size distributions were more uniform (Figure 2a and Figure 5c) .

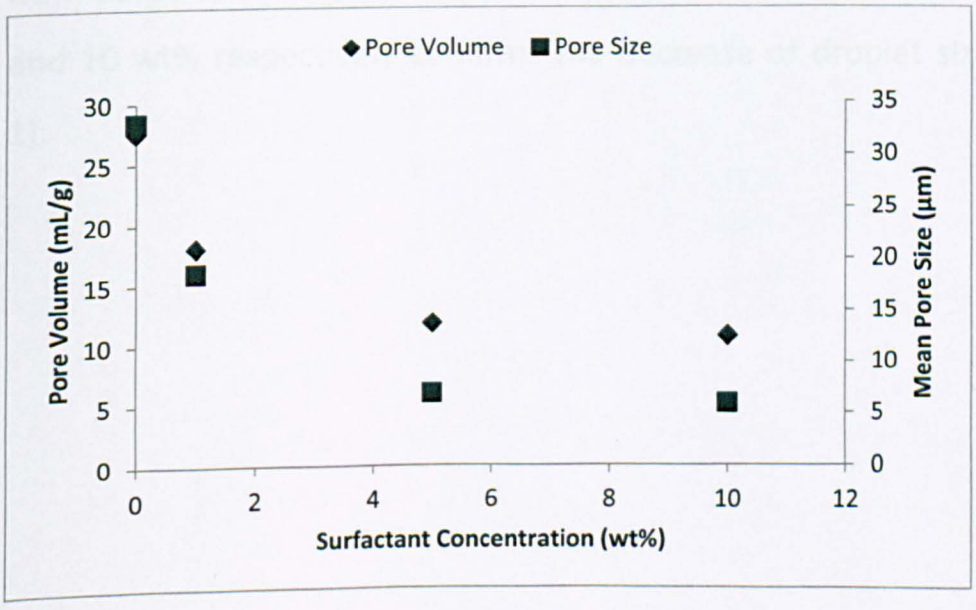

Figure 3-4 Pore Size and Pore Volume measurements for changing surfactant concentration. The PVA concentration was kept constant at 5 wt%

The pore size and volumes of the dried materials were examined. Table 1 shows the changes in pore size and volumes of the materials. Figure 4 summarises the pore volumes and the pore sizes. For sample S4, with a surfactant concentration of 0 wt% the pore volume is 27.56 mL/g. On increasing the surfactant concentration, the pore volume decrease to 18.02, 11.73 and 10.65 mL/g for surfactant concentrations of 1, 5 and 10 wt% respectively (table 1). With the surfactants having the emulsifying effect, by increasing the surfactant concentration allows for the surfactant to stabilise the droplets, the covering of the surfactant around the droplets increases and thus the individual droplet sizes decreased (as seen from the droplet size measurements). Due to the decrease of the droplets sizes, when freeze-dried, the voids left behind from the removal of the droplets are smaller. The pore volume decreases as the pores become closed (see figure 2a) as a result, mercury cannot intrude into the pores of the material and therefore the pore volume is recorded as decreasing. The drop in mean pore sizes from 33.16 to 18.65 μm, 6.89 and 5.92 μm for concentrations of 0, 1 5 and 10 wt% respectively confirms the decrease of droplet sizes (table 1).

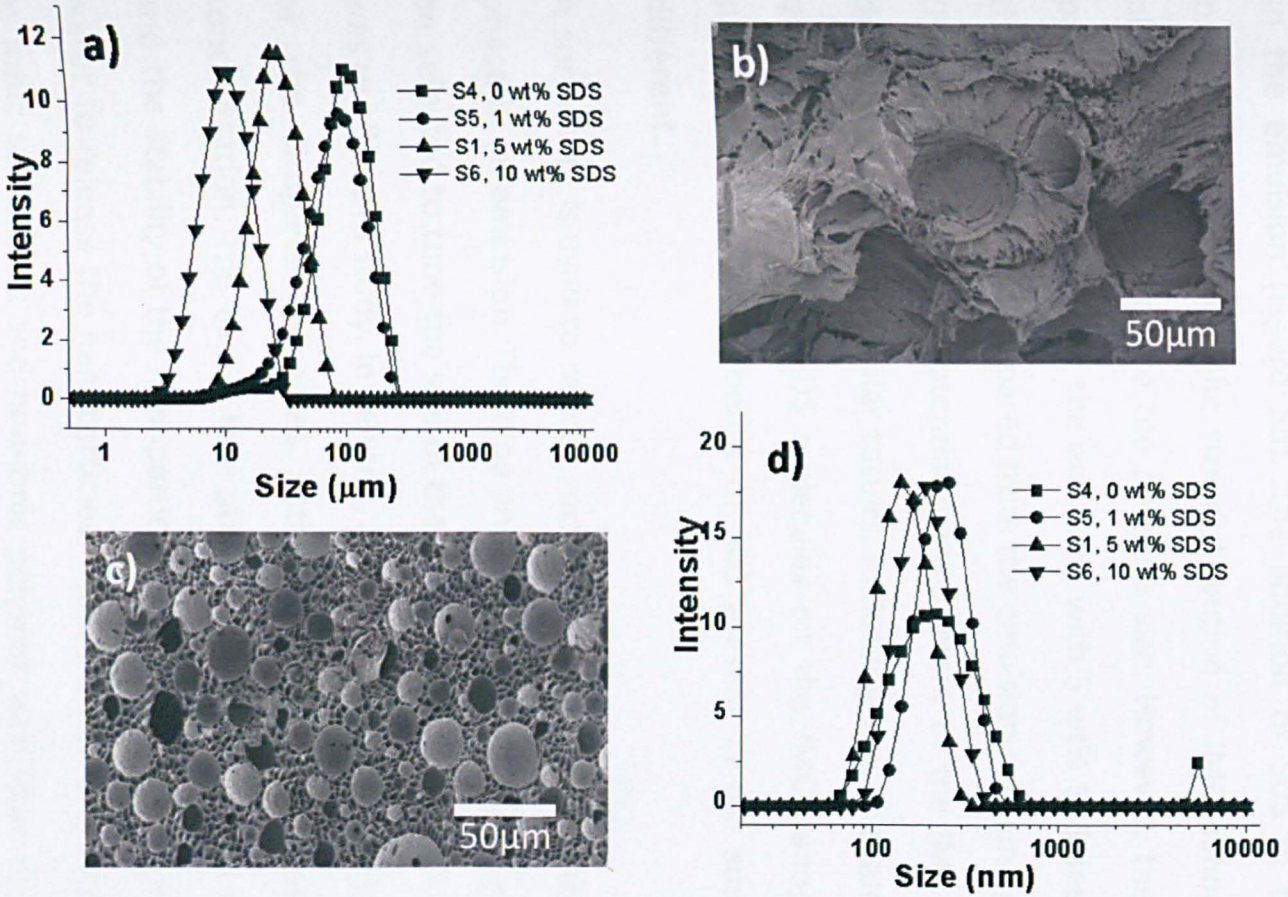

Figure 3-5 Emulsions were prepared with 50% oil phase but various SDS concentrations at 0 wt%, 1 wt%, 5 wt%, and 10 wt%. (a) The droplet size distributions of the emulsions. (b) The porous structure of the material made from the emulsion containing no SDS. (c) The porous structure of the material made from the emulsion containing 10 wt% SDS. (d) The size of IMC nanoparticles in water.

The porous composite materials formed after freeze-drying were dissolved in water to produce aqueous IMC nanoparticle dispersions. The DLS measurement showed that IMC particles with a broad size range (70 nm – 600 nm, peak size at 200 nm) were formed without SDS in the emulsion (Figure 5d). The addition of SDS in the emulsion preparation narrowed the size distribution of IMC nanoparticles and also appeared to reduce the particles size. However, the size of IMC particles prepared from the emulsion with 5 wt% SDS seemed smaller than those particles prepared from the emulsion containing 10 wt% SDS (Figure 5d). The zeta potential measurement of the IMC nanoparticle dispersions showed similar results, indicating that the surface charges or the adsorption of SDS molecules on the IMC nanoparticles was similar although the amount of SDS present in the suspension was different.

A surfactant is used to reduce surface tension and stabilize the droplet phase in an emulsion. The type and concentration of the surfactant can be selected to tune the size of the droplets. SDS, an anionic surfactant, was used in this study. In general, and as observed in this study, the size of the droplets decreases with the increase of the surfactant concentration. This can in turn affect the size of formed nanoparticles and the stability of the nanoparticles when the material is dissolved in water to release the nanoparticles. Different types of surfactants such as ionic surfactants and non-ionic polymer surfactant can be used to stabilize oil-in-water emulsions. For pharmaceutical applications, biocompatibility and toxicity of the surfactant is a concern. A bio-surfactant such as phospholipids may be selected for use in this preparation process.

The surface tension effect of the SDS concentration was performed by keeping the concentration of the polymer constant and varying the concentration of the surfactant. Figure 6 shows the effect of the varying the amount of surfactant and polymer in PVA/SDS mixtures.

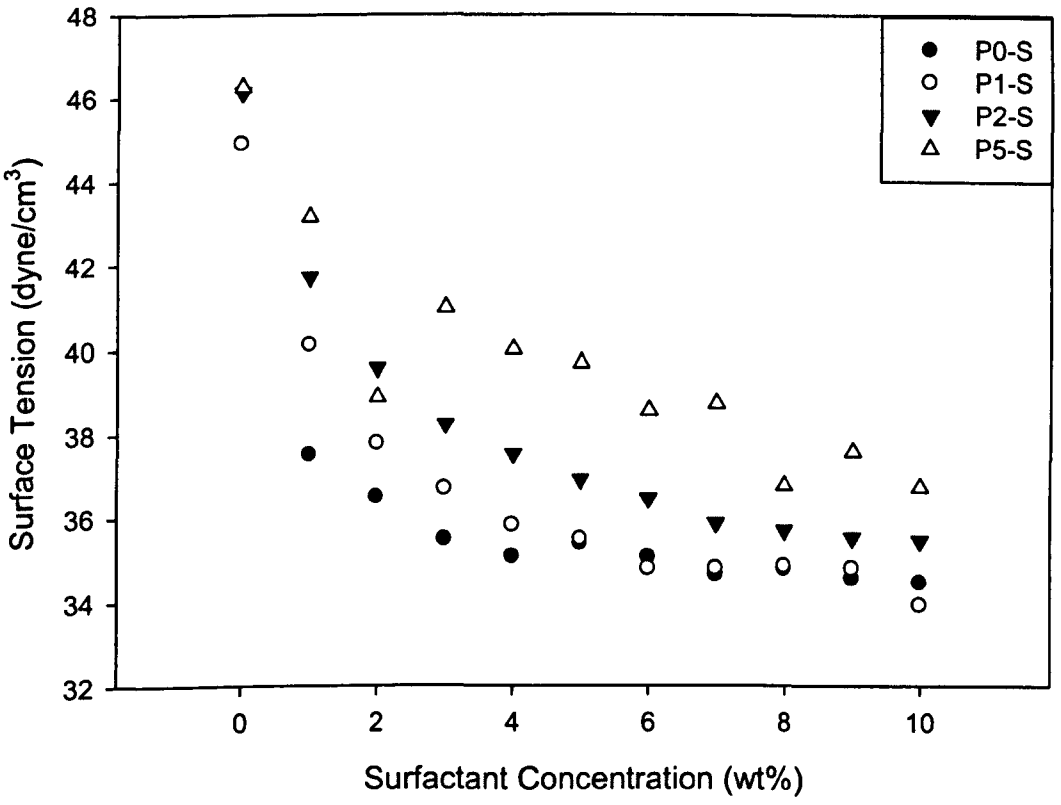

Figure 3-6 Surface tension measurements for PVA/SDS mixtures by varying surfactant concentration. PVA concentrations were kept constant at 0, 1, 2 and 5 wt% (as denoted by Px) and the surfactant concentration was varied from 0-10 wt% in 1 wt% increments.

In comparison to the surface tension of water (72.8 dynes/cm^3 at 20 °C) the surface tension is reduced significantly upon addition of the surfactant SDS. Even with low concentrations of SDS used (1 wt%) the surface tension is reduced sufficiently to stabilise the emulsion formed. Upon increasing the surfactant concentration the surface tension, as is expected, reduces.

3.4.3 Concentration of PVA

PVA was dissolved in the continuous aqueous phase of the emulsion. After freeze drying, PVA could provide a material matrix to support the formed IMC nanoparticles. It was also well known that PVA could act like a co-surfactant to stabilize the emulsions. The concentrations of PVA were varied at 1 wt%, 2 wt%, and 5 wt% in this study. As can be observed in Figure 7a, the sizes of emulsion droplets are increased with the decrease of PVA concentration. After freeze-drying, the produced porous materials showed similar pore structures although the pore volume of the material increased with the decrease of PVA concentration.[21] Figure 8 exemplifies the observation of the decrease in pore size and pore volume of the monoliths with increasing concentration of polymer. As the polymer concentration increases the emulsion droplet decreases from 101 μm to 27 μm for samples S8 and S1 respectfully (table 1). The polymer concentration evidently has an effect on the size of the droplets and therefore the morphology of the freeze-dried monoliths. The pore volume and size increase respectively from 11.73 ml/g and 6.89 μm for sample S1 to 24.91 ml/g and 21.12 μm for sample S8 (table 1).

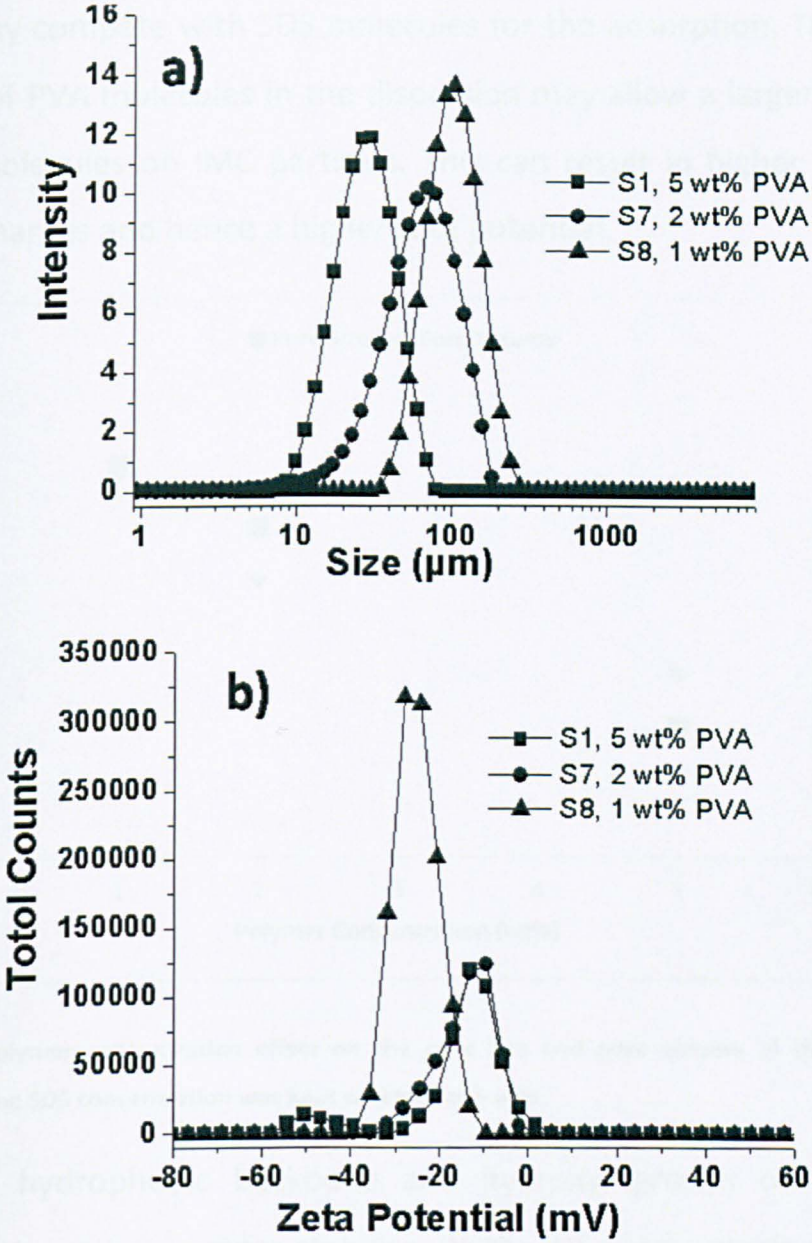

Figure 3-7(a) The droplet size distributions of the emulsions containing PVA at the concentration of 1 wt%, 2 wt%, and 5 wt%. (b) The zeta potential of the IMC nanoparticles produced from these emulsions. The concentration of SDS is 5 wt%.

From the DLS measurement of the IMC nanoparticle dispersions, it appeared that the size of IMC nanoparticles did not change with the variation of PVA concentration. However, the zeta potential of the IMC nanoparticles shifted to a larger negative value (Figure 7b). In the aqueous dispersion, PVA also adsorb to the surface of IMC particles

which may compete with SDS molecules for the adsorption. The fewer amount of PVA molecules in the dispersion may allow a larger number of SDS molecules on IMC particles. This can result in higher negative surface charges and hence a higher zeta potential.

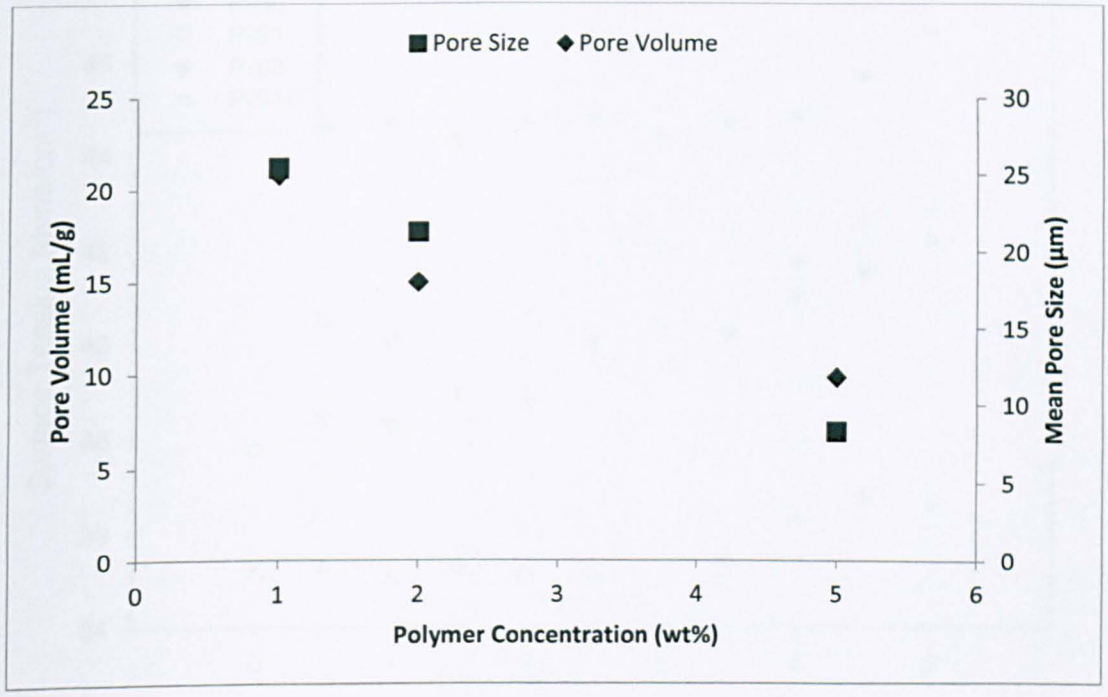

Figure 3-8 Polymer concentration effect on the pore size and pore volume of the prepared monoliths. The SDS concentration was kept constant at 5 wt%.

With the hydrophobic backbone and hydroxyl groups on polymer chains, PVA can be an extra stabiliser at the oil-water interface. Thus, by decreasing the concentration of PVA, the emulsification capability is reduced leading to larger droplet sizes. With the main purpose of PVA here is to form a porous scaffold to support the formation of nanoparticles, the choice of polymers can be very flexible. In principle, any water-soluble hydrophilic polymer depending on the requirement for specific applications can be used in this method. For example, widely used polymer additives in drug formulations such as

hydroxypropyl methyl cellulose, poly(ethylene glycol), and polyvinylpyrrolidone may be used in this process.

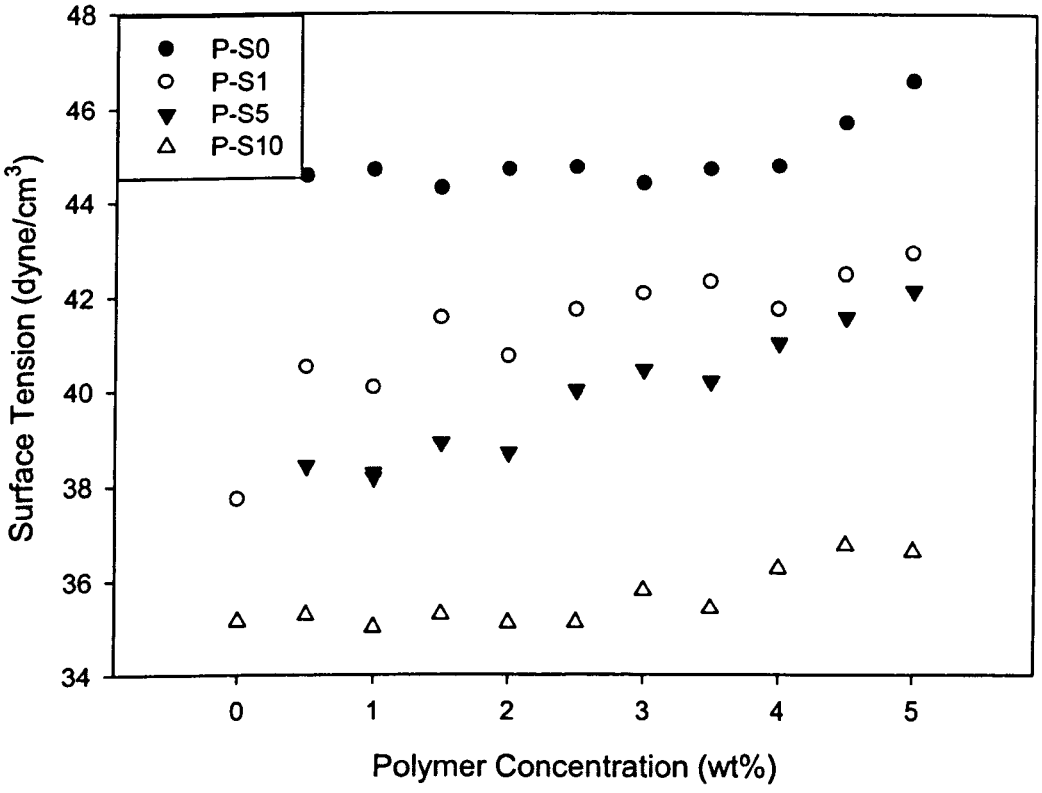

Figure 3-9 Surface tension measurements for increasing polymer concentrations. The SDS concentrations were kept constant at 0, 1, 5 and 10 wt% and the PVA concentrations were varied from 0 to 5 wt% in 0.5 wt% increments (except 0% wt PVA and 0% wt SDS, i.e. surface tension of water)

The surface tension measurements for increasing the polymer concentration are shown in Figure 9. Increasing the polymer concentration can alter the concentration at which surfactant micelles can occur. The presence of polymer chains induces the formation of micelles below the critical micelle concentration (CMC). Rather than reaching the CMC a critical aggregation concentration can be reached (CAC) were the surface tension is higher. As more surfactant is added the polymer can become saturated with surfactant micelles and the

surfactant monomer concentration increases once more until the normal CMC is reached.

3.4.4 Concentration of IMC

IMC nanoparticles were formed from the sublimation of the solvent in the droplet phase of a frozen emulsion during a freeze-drying process. The concentrations of IMC solution, which was used to form an emulsion as droplet phase, were varied at 0.05 wt%, 0.1 wt%, and 0.5 wt %. As measured by DLS, the size of the nanoparticles changed with the change in IMC concentration (Figure 10a). The peak sizes of the IMC nanoparticles were around 250 nm, 150 nm, and 155 nm for the emulsions made from IMC solutions at 0.5 wt%, 0.1 wt%, and 0.05 wt% respectively. It should be noted that there were additional small peaks at around 25 nm and 6 nm for the IMC nanoparticles made from the emulsion containing 0.05 wt% IMC solutions (table 1). The zeta potential was similar for the IMC nanoparticles made from the emulsion containing 0.1 wt% and 0.5 wt% IMC solution. A larger negative zeta potential was observed for IMC nanoparticles prepared from the emulsion containing 0.05 wt% IMC solutions. This could be due to the amount of free SDS available in the measured aqueous media. As the concentration of the IMC decreases the amount of SDS needed to stabilise the drug decreases and therefore a net increase in the amount of free SDS in solution can lead to the increase in zeta potential.

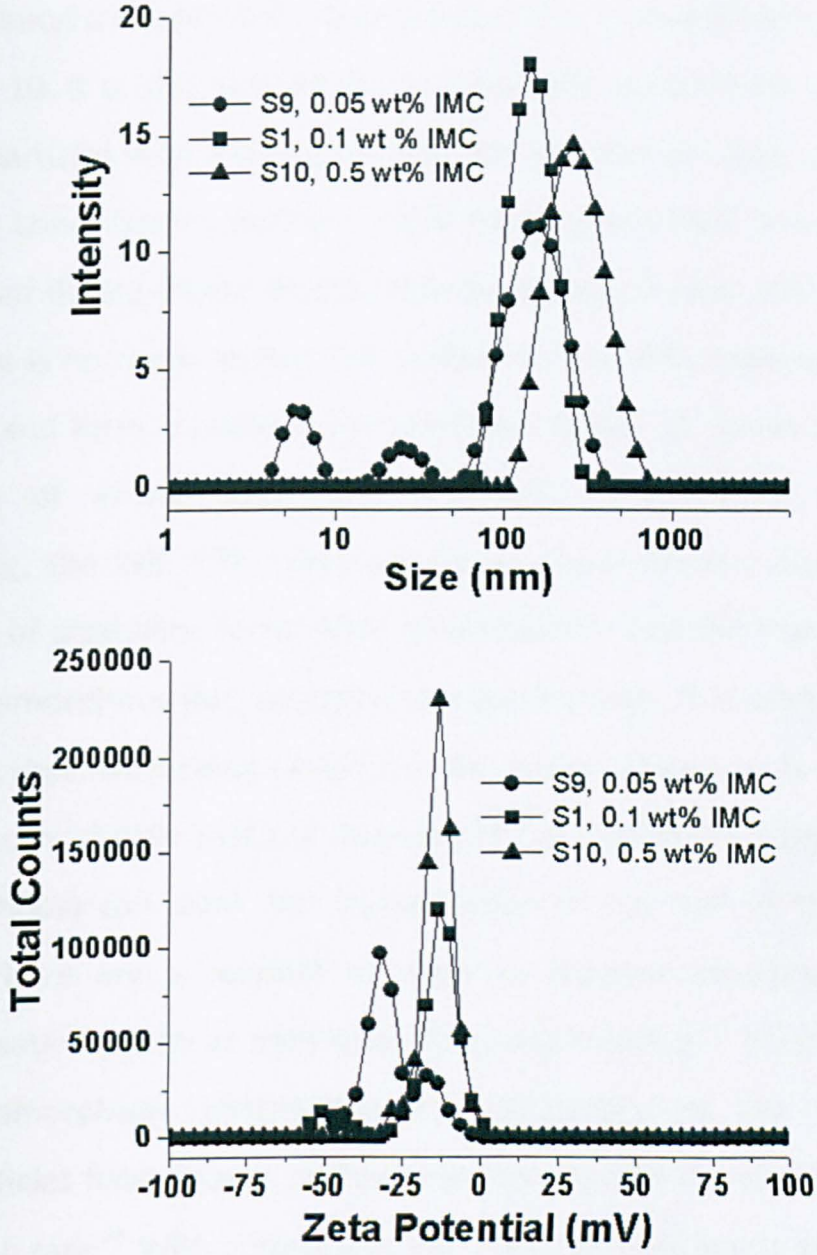

Figure 3-10 The emulsions with the IMC concentrations at 0.05 wt%, 0.1 wt%, and 0.5 wt % were processed to produce aqueous IMC nanoparticle dispersions. (a) The size of IMC nanoparticles. (b) The zeta potential of IMC nanoparticles.

During the freezing process, IMC concentrates in the droplets before the emulsion is completely frozen. The removal of water and the organic solvent during freeze drying produces the IMC nanoparticles within porous PVA. It is reasonable that a higher concentration of IMC and hence a larger number of IMC molecules in the droplets can lead to

the formation of larger IMC nanoparticles. This is clearly demonstrated in Figure 10. It is also noticed that a lower IMC concentration leads to smaller particles with a broad particle size distribution. Due to the fact that IMC concentrates during a rapid freezing and IMC nanoparticles are formed during freeze drying while being kept frozen, it is believed that there is no room on the PVA surface for the IMC molecules to re-organize and form crystalline nanoparticles. Figure 11 shows the PXRD spectrum of as-purchased IMC and IMC nanoparticles. Before processing, the IMC XRD spectrum shows sharp peaks indicating the presence of crystalline form. After emulsification and the freeze-drying process, amorphous IMC nanoparticles are formed. It is worth noting, however, that the loading of IMC on the porous composite is 4 wt%; it could be conceivable that the intensity of the PVA/SDS scaffold (which is amorphous) can mask the crystallization of the IMC (if this is the case). There are a number of ways to prepare amorphous solid pharmaceuticals such as melt quenching and freezing.[24] Poorly water-soluble amorphous pharmaceuticals particularly in the form of microparticles have shown improved wettability and increased intrinsic dissolution rate.[25] With amorphous IMC nanoparticles in this study, it is expected that the dissolution rate in water may be significantly improved.[32]

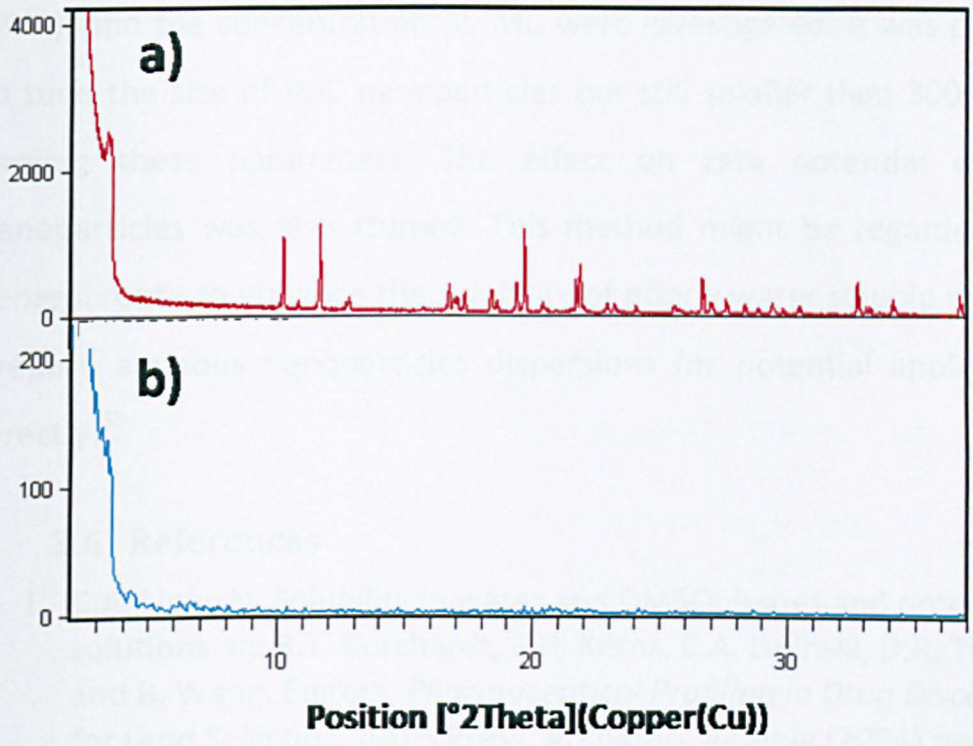

Figure 3-11 PXRD spectra of as-purchased IMC (a) and IMC nanoparticles (b) prepared in this study.

3.5 Conclusions

Aqueous nanoparticles dispersion of a poorly water-soluble drug Indomethacin (IMC) was prepared by freeze-drying emulsions and then rapidly dissolving in water. Oil-in-water emulsions with IMC dissolved in the organic droplet phase were frozen and freeze-dried. This process produced highly interconnected porous PVA with in situ formation of IMC nanoparticles (< 300 nm). The IMC nanoparticles were supported within the pores and thus a general issue of nanoparticles aggregation was avoided. The prepared materials could be rapidly dissolved in water and the IMC nanoparticles were released at the same time to form stable aqueous nanoparticle dispersions. The formulation of the emulsions was very important of the preparation of IMC nanoparticles. Effects of oil phase volume percentage in the emulsion, the concentration of the surfactant (SDS), the concentration of polymer

(PVA), and the concentration of IMC were investigated. It was possible to tune the size of IMC nanoparticles but still smaller than 300 nm by varying these parameters. The effect on zeta potential of IMC nanoparticles was also studied. This method might be regarded as a general route to enhance the solubility of poorly water soluble drugs or prepare aqueous nanoparticles dispersions for potential applications directly.[33]

3.6 References

1. C.A. Lipinski, Solubility in water and DMSO: issues and potential solutions. In: R.T. Borchardt, E.H. Kerns, C.A. Lipinski, D.R. Thakker and B. Wang, Editors, *Pharmaceutical Profiling in Drug Discovery for Lead Selection*, AAPS Press, Arlington, Virginia (2004) pp. 93–125.
2. K. Soppimeth, T. Aminabhavi, A. Kulkarni, W. Radzinski, J. Controlled Release, 2001, 70, 1-2, 1-20
3. M. Smola, T. Vandamme, A. Sokowlowski, Int. J. Nanomedicine, 2008, 3, 1, 1-19
4. Y. Liu, K. Li, B. Liu, Biomaterials, 2010, 31, 35, 9145-9155
5. J. Chan, J-W Rhee, L. Zhang, R. Langer, K. Yuet, Biomaterials, 2009, 30, 8, 1627-1634
6. A. Fahr and X. Liu, *Expert Opin. Drug Deliv.* **4** (2007), p. 403.
7. S.P. Rannard and A. Owen, *Nano Today* **4** (2009), p. 382.
8. A.A. Date and V.B. Patravale, *Current Opin. Colloid Interface Sci* **9** (2004), p. 222.
9. S. Kamiya, T. Kurita, A. Miyagishima and M. Arakawa, *Drug Dev. Ind. Pharm.* **35** (2009), p. 1022.
10. F. Kesisoglou, S. Panmai and Y. Wu, *Adv. Drug Deliv. Rev.* **59** (2007), p. 631.
11. B.E. Rabinow, *Nat. Rev. Drug Discovery* **3** (2004), p. 785.
12. S. Verma, R. Gokhale and D.J. Burgess, *Int. J. Pharm.* **380** (2009), p. 216.
13. B.V. Eerdenbrugh, G.V. Mooter and P. Augustijns, *Int. J. Pharm.* **364** (2008), p. 64.
14. S. Sepassi, D.J. Goodwin, A.F. Drake, S. Holland, G. Leonard, L. Martini and M.J. Lawrence, *J. Pharm. Sci.* **96** (2007), p. 2655

15. M.N.V.R. Kumar, U. Bakowsky and C.M. Lehr, *Biomaterials* **25** (2004), p. 1771.
16. X. Chen, J.M. Vaughn, M.J. Yacaman, R.O. Williams and K.P. Johnston, *J. Pharm. Sci.* **93** (2004), p. 1867.
17. K.A. Overhoff, J.D. Engstrom, B. Chen, B.D. Scherzer, T.E. Milner, K.P. Johnston and R.O. Williams, *Eur. J. Pharm. Biopharm.* **65** (2007), p. 57.
18. H. Murakami, M. Kobayashi, H. Takeuchi and Y. Kawashima, *Powder Technol* **107** (2000), p. 137.
19. P. Pathak, M. Meziani and Y. Sun, *Expert Opin. Drug Deliv.* **2** (2005), p. 747.
20. E. Reverchon, *Ind. Eng. Chem. Res.* **41** (2002), p. 2405.
21. Y. Shekunov, P. Chattopadhyay, J. Seitzinger and R. Huff, *Pharm. Res.* **23** (2006), p. 196.
22. M.C. Gutiérrez, M.L. Ferrer and F. del Monte, *Chem. Mater.* **20** (2008), p. 634.
23. H. Zhang, I. Hussain, M. Brust, M.F. Butler, S.P. Rannard and A.I. Cooper, *Nat. Mater.* **4** (2005), p. 787.
24. T.L. Rogers, J. Hu, Z. Yu, K.P. Johnston and R.O. Williams, *Int. J. Pharm.* **242** (2002), p. 93.
25. J. Hu, K.P. Johnston and R.O. Williams, *Int. J. Pharm.* **271** (2004), p. 145.
26. K.A. Overhoff, K.P. Johnston, J. Tam, J. Engstrom and R.O. Williams, *J. Drug Deliv. Sci. Technol.* **19** (2009), p. 89.
27. A. Menner, A. Bismarck, Macromolecular Symposia, 2006, 242, 19-24
28. H. Zhang, D. Wang, R. Butler, N.L. Campbell, J. Long, B. Tan, D.J. Duncalf, A.J. Foster, A. Hopkinson, D. Taylor, D. Angus, A.I. Cooper and S.P. Rannard, *Nat. Nanotechnol.* **3** (2008), p. 506.
29. M. Trotta, M. Gallarate, M.E. Carlotti and S. Morel, *Int. J. Pharm.* **254** (2003), p. 235.
30. M.E. Matteucci, J.C. Paguio, M.A. Miller, R.O. Williams and K.P. Johnston, *Pharm. Res.* **25** (2008), p. 2477.
31. D.A. Miller, J.T. McConville, W. Yang, R.O. Williams and J.W. McGinity, *J. Pharm. Sci.* **96** (2007), p. 361.
32. J. Hu, T.L. Rogers, J. Brown, T. Young, K.P. Johnston and R.O. Williams, *Pharm. Res.* **19** (2002), p. 1278.
33. D. Duncalf and S.P. Rannard, *Chem. Ind.* **2** (2010), p. 24.

4 PREPARATION OF POROUS CHITOSAN AND THE pH DEPENDENT RELEASE OF ORGANIC NANOPARTICLES

4.1 Chapter Overview

Porous chitosan can be prepared via emulsion templating and freeze-drying. The prepared monoliths were prepared using different molecular weights of chitosan. Oil Red nanoparticles, as an organic dye; and Indomethacin nanoparticles, as a model drug were prepared *in situ* during the emulsion-freezedrying process. The prepared organic nanoparticles can be released from the chitosan using different volume fractions of 50 % and 80 % oil phase in water phase at different pH . The structures of the chitosan monoliths, the release profiles of the dye and the drug and the particle characteristics are reported herein.

4.2 Introduction

Chitosan (a heteropolymer) is the N-deacetylated derivative of chitin. The structure of chitin (a) and chitosan (b) are show in figure 1:

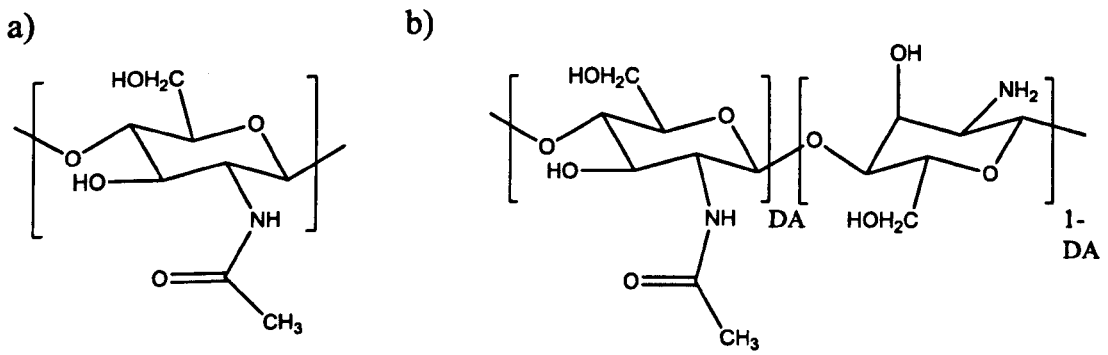

Figure 4-1 - Structures of Chitin (a) and chitosan (b). DA=Degree of acetylation

Chitin is easily obtained from crab and shrimp shells. Chitin can be processed in the presence of an alkali such as 40% Sodium Hydroxide to produce deacetylated chitosan (scheme 1).[1] The degree of deacetylation (DD) can be determined by NMR spectroscopy; the DD of commercial chitosan is typically 60-100%. The amine group in chitosan has a pKa in the region of 6.5. Due to this pKa value; in acidic media, the amino group can be easily protonated.

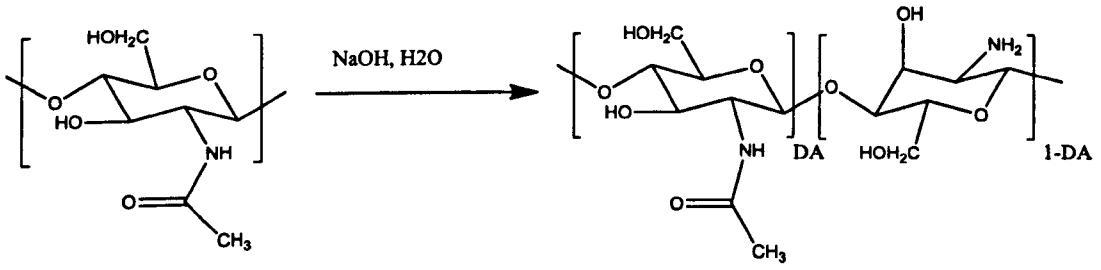

Scheme 1 - Preparation of chitosan from chitin

Chitosan and its derivatives can be used to prepare hydrogels,[2-3] films,[4] microparticles[5] and nanoparticles[5-6] for application of drug delivery.[2-7]

When the DD of chitosan is above 50 %[8] it is soluble in dilute acids such as acetic acid, formic acid etc. In dilute acids chitosan can be protonated at the free amino groups.[9-10] Once dissolved, chitosan can be gelled by increasing the pH.[11] Chitosan derivatives and blends have also been gelled via glutaraldehyde crosslinking[12] and UV irradiation.[13]

Emulsions have been used to template Chitosan in the literature[14]. Chitosan in the continuous water phase and 2-5-dimethoxy-2,5-dihydrofuran (DHF) as a temperature controlled crosslinking agent were used as tissue scaffolds. The emulsion was heated to 75 °C to crosslink the polymer. Ice templates can also be used to prepare hierarchally macroporous chitosan for tissue engineering[15].

Chitosan has been used as a delivery system for indomethacin. Specific examples include chitosan liposomes[16-17] and Chitosan microspheres.[18-19] No literature known to the author has been found for specific release of indomethacin from emulsion templated materials; therefore, herein we present a novel emulsion templated release system for indomethacin after first using Oil Red as an organic model.

4.3 Experimental

4.3.1 Materials

Chitosan (Low Mw, Medium Mw, High Mw), Triton X-405, Pluronics F-127, Oil Red (OR), Indomethacin (IMC), Cyclohexane (CH), O-xylene (XYL) were all purchased from Sigma-Aldrich and used as received. Acetic acid was of analytical grade. Distilled water was used in all cases. pH 2, 7 and 10 solutions were prepared by adjustment with aqueous hydrochloric and aqueous sodium hydroxide, measured with a calibrated pH probe.

4.3.2 Preparation of Emulsion templated Chitosan monoliths

Table 1 summarises the preparation conditions for the chitosan materials, composition of their emulsions.

Table 1 - Preparation conditions of the chitosan materials used

Entry	Chitosan Mw	Chitosan conc (wt%)	Surfactant	Surfactant amount	Volume Ratio (%)
1L-OR 50	LOW	1	Triton X-405	0.4 ml	50
1M-OR 50	MEDIUM	1	Triton X-405	0.4 ml	50
1H-OR 50	HIGH	1	Triton X-405	0.4 ml	50
1L-OR 80	LOW	1	Triton X-405	0.4 ml	80
1M-OR 80	MEDIUM	1	Triton X-405	0.4 ml	80
1H-OR 80	HIGH	1	Triton X-405	0.4 ml	80
1L-IMC 50	LOW	1	Pluronic F127	0.2 g	50
1M-IMC 50	MEDIUM	1	Pluronic F127	0.2 g	50
1H-IMC 50	HIGH	1	Pluronic F127	0.2 g	50
1L-IMC 80	LOW	1	Pluronic F127	0.2 g	80
1M-IMC 80	MEDIUM	1	Pluronic F127	0.2 g	80
1H-IMC 80	HIGH	1	Pluronic F127	0.2 g	80

4.3.2.1 Preparation Using OR-CH as internal phase

In a vial, using an overhead LabEgg stirrer with a paddle attachment OR-CH (0.025 wt%, 2 ml and 8 ml for 50 % and 80 % emulsion respectively) was added dropwise to a stirring solution (approx. 500 rpm) of triton x-405 (0.4 ml) in acetic acid (0.2 M, 2 ml);. After stirring for 10 minutes chitosan (low, medium or high molecular weight, 0.02 g) was added. The emulsion was continued to stir for approximately 15 minutes. A slight colour change was observed which indicated the dissolution of

chitosan to form the gel. It is worth noting that a gel can be prepared with no emulsion present.

4.3.2.2 Preparation using IMC-XYL as internal phase

In a vial, using an overhead LabEgg stirrer with a paddle attachment IMC-XYL (0.1 wt%) was added dropwise (2 ml and 8 ml for 50 % and 80 % emulsion respectively.) to a stirring solution (approx. 500 rpm) of Pluronics (0.2 g) in acetic acid (0.2 M, 2 ml); After stirring for 10 minutes, chitosan (low, medium or high molecular weight, 0.02 g) was added. The emulsion was continued to stir for approximately 15 minutes. A slight colour change was observed which indicated the dissolution of chitosan to form the gel

4.3.3 Release of Organic nanoparticles from Chitosan Monoliths

Chitosan monolith (0.05 ± 0.001 g) was weighed and placed into aqueous solutions of pH 2, pH 7 and pH 10 (5 ml). Over predefined time periods a sample of the aqueous media was removed (200 µl) and replaced with fresh stock solution. The removed aqueous media was monitored for UV absorption and release profiles were produced for each corresponding sample.

Monitoring the release was performed using a 96-well multiplate reader. 200 µl of the released aqueous suspension was pipetted into a well of a 96-well flat bottomed polypropylene plate. The absorption peak was monitored by scanning from 200 to 800 nm in 2 nm steps. The height of the peak was subtracted from the baseline to give the absorption reading of each sample. The data points were normalized using:

$$M = \frac{A_t}{A_\infty} \qquad (1)$$

Were M is the normalized unit, A_t is the absorption at time t and A_∞ is the highest final absorption reading of all the readings. The final release time for particles after 2 hours at pH 2 was taken. It was confirmed with a controlled experiment that the absorption does not changed after a further reading 18 hours after this time.

The release rates were calculated by using Higuchi Model for release of molecules from an insoluble matrix (equation 1)[20]:

$$M = \frac{A_t}{A_\infty} = kt^{½} \quad (2)$$

Where k is the rate constant and t is the time of the measurement. The regression function on Excel was used to calculate the R^2 for each release curve.

4.3.4 Characterisation

The droplet sizes of the formed chitosan emulsions were measured using a Malvern Mastersizer 2000 with a Hydro 2000 SM dispersion unit. The emulsion (3 drops) was added to the dispersion unit containing approximately 100 mL water with a stirring rate of 2000 rpm.

The dried chitosan materials were sectioned to reveal the internal porous structures. The samples were adhered to an aluminium stub using a silver colloidal suspension and allowed to dry. A sputter coater (EMITECH K550X) was used to coat the samples with gold at 40mA for 3 minutes. A Hitachi S-4800 field emission SEM was used to reveal the pore structure at 3 KV. The void sizes and pore volumes of the dried materials were examined using a Micromeritics Autopore IV 9500 porosimeter. Samples were subjected to a pressure cycle starting at approx 0.5 psi, increasing to 60000 psi in predefined steps.

The released organic nanoparticles were dialysed extensively using snakeskin dialysis tubing for several days. The OR nanoparticles were released and an aqueous OR nanoparticle dispersion was formed. The OR nanodispersions were centrifuged for 15 minutes at 13000 rpm using an Eppendorf Centrifuge 5415D and the supernatant liquid was filtered through a 1 μm syringe. These conditions were suitable enough to remove the polymer by centrifuge yet keep the nanoparticles suspended in solution which could be observed by a clear red dispersion in the case of OR. The nanodispersions were analysed at 25 ^{0}C using a Malvern Zetasizer equipped with a zeta-potential detector with a backscattering detection at 173°. The size and zeta potential of the hydrated organic nanoparticles in water were obtained. 10 μl of a diluted IMC nanodispersion was dropped onto holey carbon filmed copper grids (400 mesh) and allowed to dry overnight. A scanning transmission microscopic (STEM) detector attached to the Hitachi S-4800 SEM was used to observe the dry IMC nanoparticles at 30 KV.

Sample of freeze-dried non-emulsion templated chitosan and as purchased chitosan as reference was prepared for Solid-state NMR analysis. The ^{1}H-^{13}C cross polarisation (CP) MAS NMR experiments were carried out at 400.16 MHz for ^{1}H and 100.56 MHz for ^{13}C on a 4mm ^{1}H/X/Y probe. A ^{1}H $\pi/2$ pulse length of 3.40 μs was used at an MAS rate of 8.0 kHz. A recycle delay of 6.0 s and Hartmann-Hahn contact time of 2.0 ms were used. The chemical shifts were referenced using hexamethylbenzene (HMB).

4.4 Results and Discussion

4.4.1 Preparation of porous Chitosan

Cyclohexane or O-xylene can be used as the internal phase when preparing emulsion template chitosan. The organic molecule can be dissolved into the oil phase; the continuous phase is the chitosan 'gel' in acetic acid. Figure 2 (a-c) shows the droplet sizes of the emulsions prepared with Triton X-405 and cyclohexane. The droplet sizes are seen to be averaging about 70μm for emulsions with 50 % internal phase. Increasing the oil phase to 80 % decreases the average droplet size due to the emulsion volume phase is above the 0.74 volume ratio and the emulsion droplets become distorted and are observed to be smaller. Due to the close-packed nature of the droplets the size of these are seen to decrease to 20 μm on average.

Changing the internal oil phase to o-xylene and stabilizing with Pluronic surfactant as opposed to Triton used earlier; the average droplet size is approximately 12 μm for 50 % emulsions and decreases to 3 μm for 80 % emulsions. Figure 2 (d-f) shows the droplet size distributions for the emulsion prepared with o-xylene stabilized with Pluronic surfactants. Pluronics were used for the preparation of emulsion templated chitosan for release of IMC due to the fact that Triton X-405 has an absorption peak around 280 nm. As a result of this when IMC is released absorption of Triton masked the absorption of Indomethacin, therefore a true reflection on the release of IMC could not be followed by UV. As Pluronics exhibit no absorption, it became a more viable surfactant to use. The droplets for 50 % emulsion with Pluronics are lower than that for CH stabilized with Triton. The critical micelle concentration of Pluronic F127 has been shown to be in the region of 0.2 wt%[21]. The

concentration used in the preparation of the emulsions is above this micelle concentration and therefore the amount of micelles present to stabilize the droplets is higher. Pluronic F127 is a triblock copolymer which exhibits a PEO_x-PPO_y-PEO_x (x=100, y=65) chain where the PEO sections are hydrophilic and the PPO section of the polymeric surfactant is hydrophobic. When the micelle structure is formed the middle section of the Pluronic; the PPO chain exists in the internal 'hydrophobic' region of the micelle whereas the PEO end chains sit in the outer region. The internal micelle space can be smaller than that of the Triton micelle space, due to the cone angle of the triblock copolymer surfactant.

In unreported experiments, Pluronics surfactant was chosen as a surfactant template for oil-in-water emulsions using IMC as the drug molecule due to Triton X-405 incompatibility for UV for monitoring the release of the molecule. Triton X-405 has a strong absorption at 280 nm and therefore if used in conjunction with IMC (absorption at 320 nm) it is difficult to attribute the UV spectra to that of the indomethacin released from the chitosan. For the emulsions using the Pluronics surfactant, the size of the oil droplets is seen to be smaller than for the droplets observed using cyclohexane.

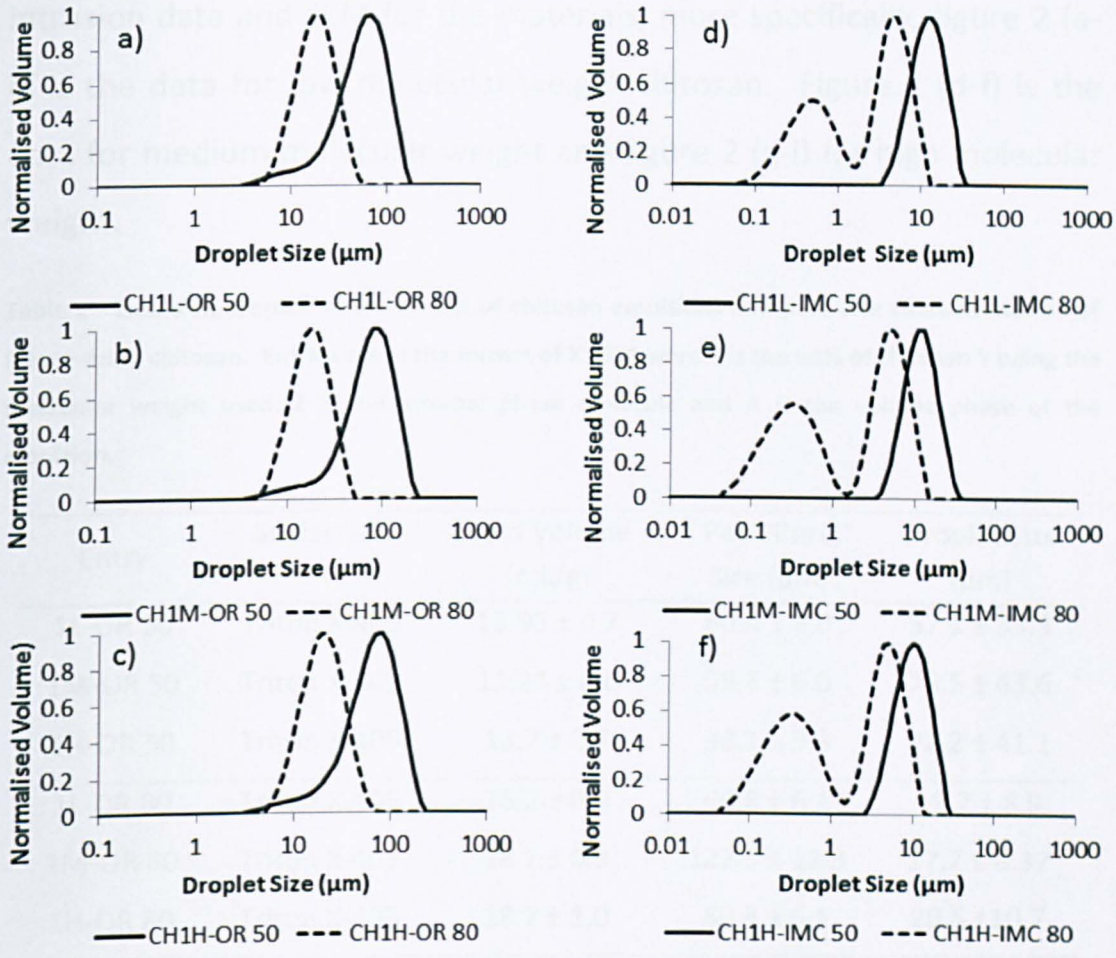

Figure 4-2 - Droplet size measurements for chitosan emulsions (low Mw to high Mw) prepared with surfactant-internal solvents of OR:Triton-cyclohexane (a-c) and IMC:Pluronics-o-xylene (d-f). The solid lines and the dashed lines represent 50% and 80% volume phase respectively

The emulsions can be frozen and freeze-dried to remove the solvents and yield a porous material. The organic nanoparticles could be formed in situ within the macropores as described in Chapter 3 for PVA systems. The emulsions are frozen to lock the morphology and keep the structure during drying. The frozen emulsion was freeze-dried to produce a porous structure with in-situ formation of organic nanoparticles.

4.4.2 Freeze-dried Chitosan Morphology

The freeze-dried macroporous monoliths can be sectioned and analysed for its pore shape, size and morphology. Table 2 shows the mercury

intrusion data and SEM for the materials, more specifically, figure 2 (a-c) is the data for low molecular weight chitosan. Figure 2 (d-f) is the data for medium molecular weight and figure 2 (g-l) for high molecular weight.

Table 2 - Emulsion droplet measurement of chitosan emulsions and pore size characterisation of freeze-dried chitosan. Entries are in the format of XY-Z A were X is the wt% of chitosan Y being the molecular weight used, Z is the internal phase molecule and A is the volume phase of the emulsion.

Entry	Surfactant	Void Volume (mL/g)	Peak Pore Size (μm)	Droplet Size (μm)
1L-OR 50	Triton X-405	13.95 ± 0.7	60.0 ± 6.0	57.1 ± 33.5
1M-OR 50	Triton X-405	11.24 ± 0.6	59.6 ± 6.0	75.5 ± 43.6
1H-OR 50	Triton X-405	13.7 ± 0.7	33.1 ± 3.3	72.2 ± 41.1
1L-OR 80	Triton X-405	18.2 ± 0.9	60.8 ± 6.1	19.7 ± 8.9
1M-OR 80	Triton X-405	18.1 ± 0.9	122.6 ± 12.3	17.7 ± 8.37
1H-OR 80	Triton X-405	18.7 ± 1.0	60.8 ± 6.1	20.5 ±10.7
1L-IMC 50	Pluronics F127	9.69 ± 0.5	17.2 ± 1.7	12.3 ± 5.7
1M-IMC 50	Pluronics F127	11.3 ± 0.6	11.3 ± 1.1	12.0 ± 5.6
1H-IMC 50	Pluronics F127	11.08 ± 0.6	11.3 ± 1.1	10.0 ± 4.8
1L-IMC 80	Pluronics F127	19.26 ± 0.9	122.3 ± 12.2	3.0 ± 2.0
1M-IMC 80	Pluronics F127	13.84 ± 0.7	33.0 ± 3.3	3.0 ± 2.3
1H-IMC 80	Pluronics F127	11.77 ± 0.6	33.0 ± 3.3	2.7 ± 2.1

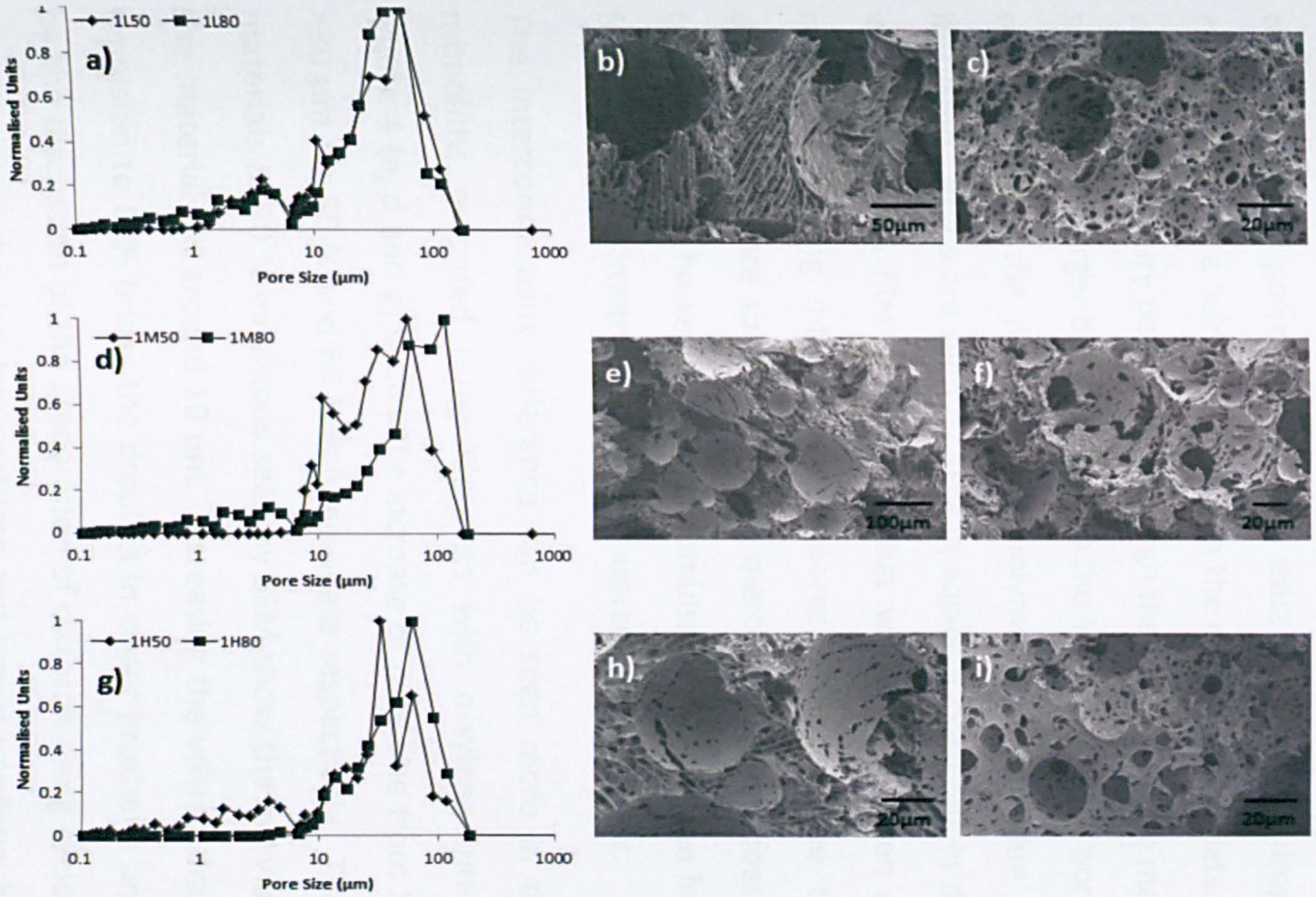

Figure 4-3 - Mercury porosimetry of freeze-dried chitosan emulsions prepared from Triton X-405 and cyclohexane and their corresponding SEM images. Low molecular weight (a-c) , medium molecular weight (d-f) and high molecular weight (g-i). The Hg intrusion data is given in figure a, d and g. SEM images for 50% volume phase are given in b, e and h and 80% volume phase given in c, f and i

The void sizes of the chitosan prepared from an internal phase of cyclohexane is approximately 30-50 μm (see figure 3 a,d,g). At 80 % templated emulsions, the emulsion droplets become smaller (50 μm to 20 μm) and are in close proximity and during the freeze-drying process, the thin film of polymer which can exist between the droplets can be ruptured giving a 'window' between the emulsion droplets. As a result of this, as mercury penetrates through the materials, the measured void size becomes larger due (>50 μm) to the interconnected pore size of the materials and the pressure the polymer is under due to mercury intrusion. Voids are seen by SEM in adjacent positions in the structure where the thin film of polymer that would have been present has ruptured leaving interconnected pores behind. Due to this, the difference in pore size observed by mercury intrusion does not appear to be different, however, for 80 % emulsions reading can be accounted for by the porosimetry readings for interconnected pores.

The interconnectivity difference can be seen more in the chitosan monoliths prepared using Pluronics with o-xylene internal phase. Figure 4 (a, d and g) shows the increase of pore size from 10-20 μm to >30 μm for 50 % and 80 % volume phase respectively. The templated materials at 50 % emulsions seen by SEM show the individual voids of the materials of around 10 μm. Increasing the volume fraction of the emulsion to 80% brings the droplets in closer proximity and as eluded by the discussion of the preparation of chitosan using cyclohexane, the film between the droplets ruptures and leaves windows between the voids. The average pore size increases from 10 μm to 50 μm in each case.

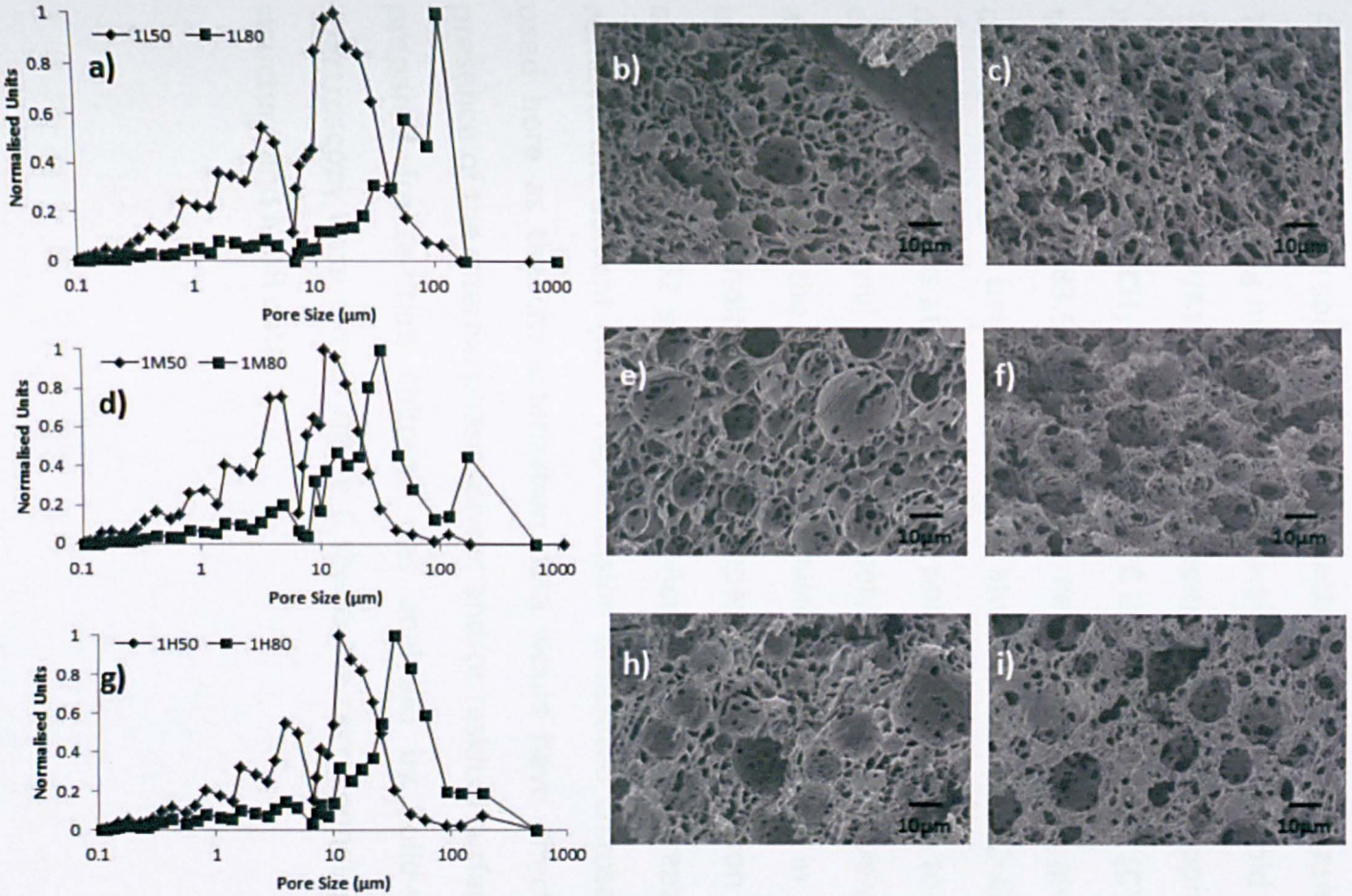

Figure 4-4 - Mercury porosimetry of freeze-dried chitosan emulsions prepared from Pluronics and o-xylene and their corresponding SEM images. Low molecular weight (a-c) , medium molecular weight (d-f) and high molecular weight (g-i)

Solid-State NMR was employed to characterize the freeze-dried materials. Figure 5 shows the NMR spectrum of as purchased chitosan and the freeze-dried chitosan (figure 6) from acetic acid.

Figure 5 gives the solid state-NMR spectrum for as purchased chitosan. The corresponding numbers for the peaks are given in bold in figure 5. ^{13}C NMR data (CP/MAS 8kHz): 23.9 ppm (CO-**C**H_3), 57.9 ppm (**C** in ring nearest –OH and **C**H_2-OH), 61.0 ppm (**C** in ring), 75.7 ppm (**C** in ring next to R-OH group), 83.6 ppm (**C** in ring next to -NHCO**C**H_3 group), 105.4 ppm (**C** in ring in between 2 Oxygen atoms), 174 ppm (**C**=O). The key data are the peaks at 23.9 and 174.1 ppm corresponding to the methyl carbon and carbonyl carbon of the acetyl group respectively. This is in agreement with the literature.[21] Chitosan was gelled in acetic acid under similar conditions to the preparation of emulsion templated chitosan. i.e. (0.02 g in 2 ml 0.2M Acetic Acid) and freeze dried to remove the solvent (NB. The emulsion templated chitosan was not used here as the characterization data would have affected by the presence of the internal phase solvent and/or residual surfactant). The prepared freeze-dried chitosan was analysed by Solid-state NMR spectroscopy once more. Figure 6 shows the corresponding proposed structure and NMR data.

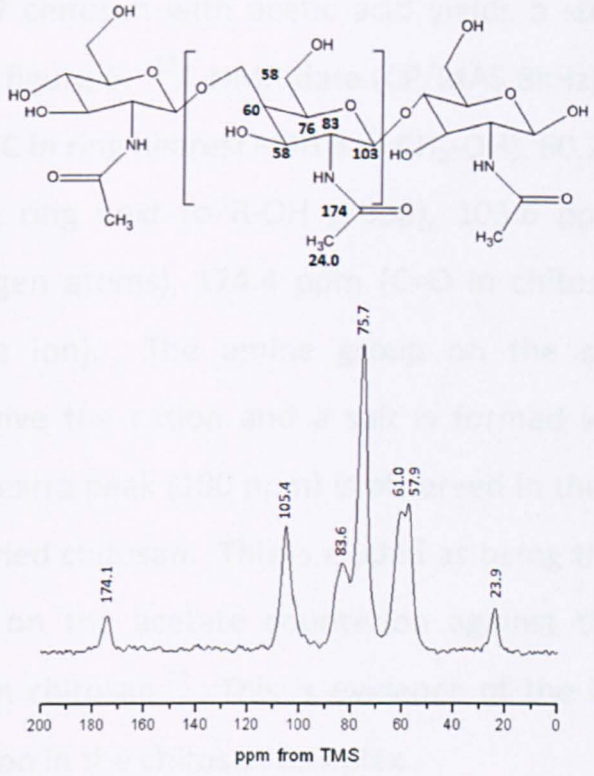

Figure 4-5 - Solid-state NMR: 1H-13C CP/MAS NMR spectrum of Chitosan at 8kHz

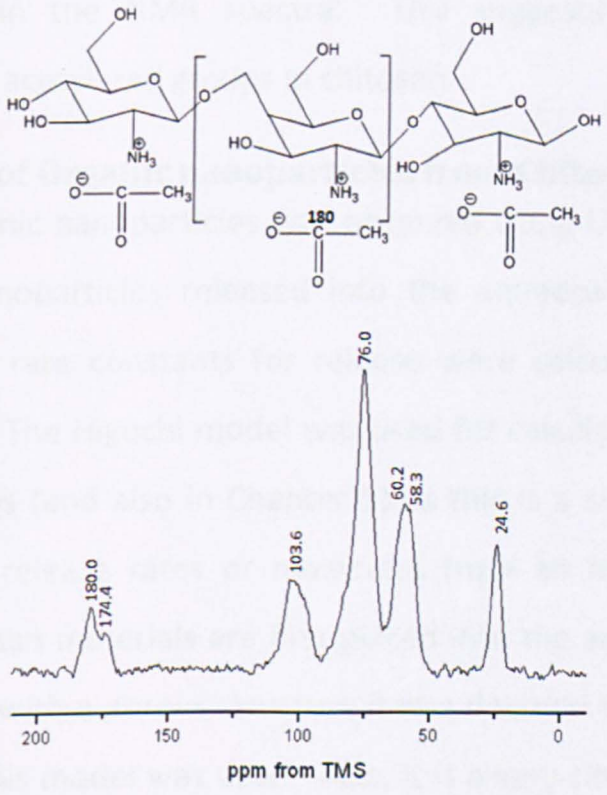

Figure 4-6 – Solid State NMR spectroscopy: 1H-13C CP/MAS NMR of freeze dried Chitosan with acetic acid at 8kHz

Freeze-drying of chitosan with acetic acid yields a structure which is hypothesized in figure 6. ^{13}C NMR data (CP/MAS 8kHz): 24.6 ppm (CO-**C**H_3), 58.3 ppm (**C** in ring nearest –OH and **C**H_2-OH), 60.2 ppm (**C** in ring), 76.0 ppm (**C** in ring next to R-OH group), 103.6 ppm (**C** in ring in between 2 Oxygen atoms), 174.4 ppm (**C**=O in chitosan), 180.0 ppm (**C**=O in acetate ion). The amine group on the chitosan can be protonated to give the cation and a salt is formed with the acetate counterion. An extra peak (180 ppm) is observed in the NMR spectrum for the freeze-dried chitosan. This is eluded as being the carbon of the carbonyl group on the acetate counterion against the deacetylated amine groups on chitosan.[21] This is evidence of the inclusion on the acetate counterion in the chitosan complex.

What is also observed is the fact that the peaks at 174 and 24 ppm are still observed in the NMR spectra. This suggests the continued presence of the acetylated groups in chitosan.

4.4.3 Release of Organic nanoparticles from Chitosan monoliths

Release of organic nanoparticles was observed using UV absorption of the organic nanoparticles released into the aqueous phase. When normalized the rate constants for release were calculated using the Higuchi model. The Higuchi model was used for calculating the release rates of particles (and also in Chapter 5) as this is a simple model for calculating the release rates or molecules from an insoluble matrix. When the chitosan materials are first placed into the aqueous media it is insoluble and with a porous structure it was deemed to have a matrix and therefore this model was used. Also, it is a very simplified method to quantify the release of the organic nanoparticles from chitosan materials. The release rates were calculated using the Higuchi model

(equation 2); the gradient of a plot of M_∞/M_t was plotted as the y-axis and the square root of time as the x-axis. The gradient of the plots were deemed as the rate constant k in the equation. The R^2 values are calculated through regression function in Excel.

4.4.3.1 Release of OR from Templated Chitosan

Oil Red can be released from freeze-dried emulsion templated chitosan. Below is an account of the observations for OR release. The corresponding particle sizes and zeta potentials for each data set are also given. The effects of pH, volume ratio and chitosan Mw are discussed.

Effect of pH

Table 3 - Table to show the summary of rate constants due to the effect of pH for sample C1-C6.

Sample	Sample Code	pH	Rate Constant ($min^{-½}$)	R^2
1L-OR 50	C1	2	0.1063 ± 0.002	0.9769
1L-OR 50	C2	7	0.0083 ± 0.007	0.8589
1L-OR 50	C3	10	0.081 ± 0.004	0.9504
1L-OR 80	C4	2	0.1535 ± 0.003	0.9835
1L-OR 80	C5	7	0.0385 ± 0.002	0.9323
1L-OR 80	C6	10	0.1109 ± 0.004	0.9562

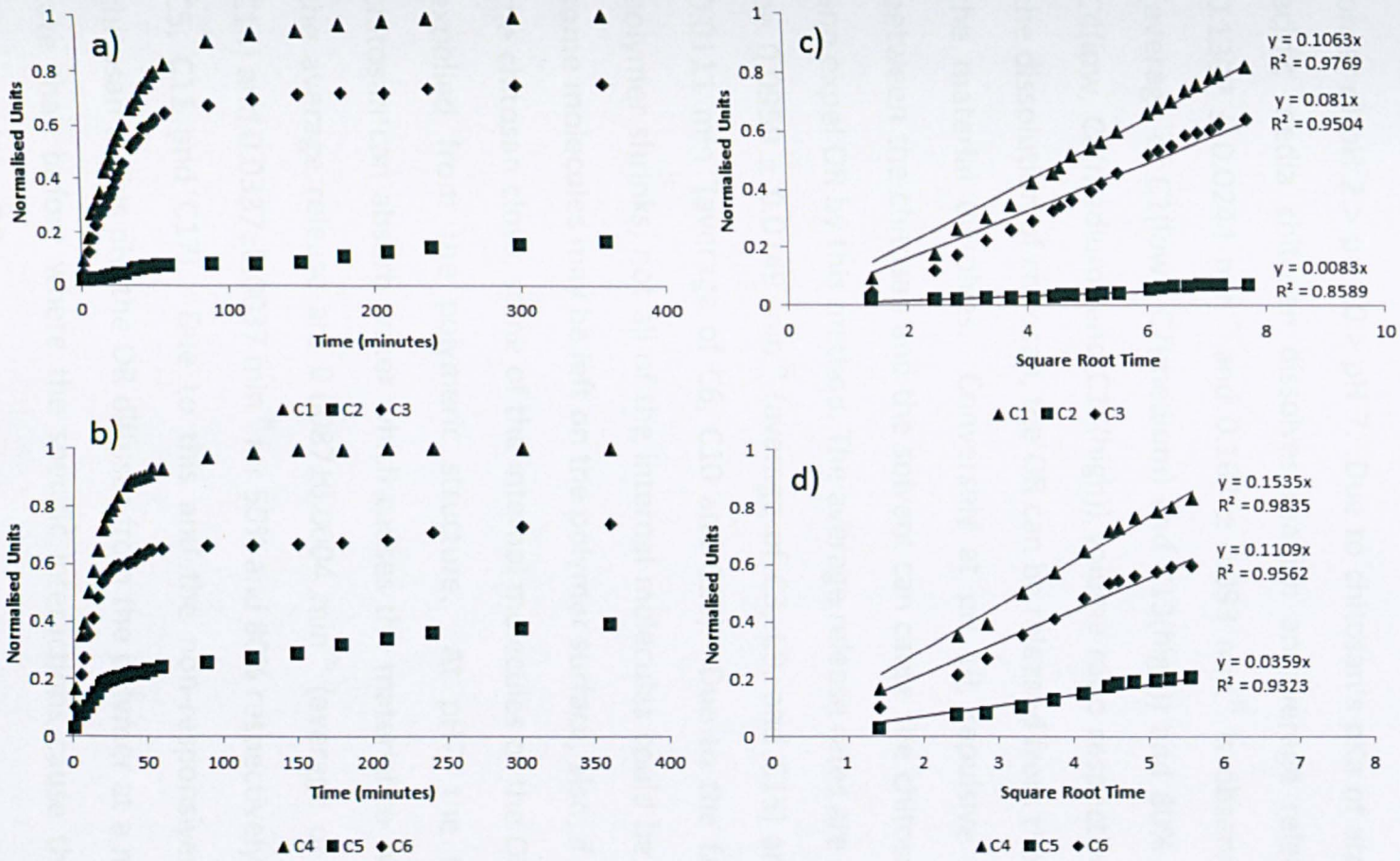

Figure 4-7 - Release profiles and corresponding release rates for samples C1-C6

Figure 7 shows the release kinetics of the OR from chitosan using samples C1-C6 as examples. One observation that is consistent through the observations is the fact that the rate of release of the OR is in the order of pH 2 > pH 10 > pH 7. Due to chitosan's pKa of around 6.5; in acidic media chitosan dissolves readily: an average release rate of 0.1307 ± 0.0244 $min^{-½}$ and 0.163 ± 0.093 $min^{-½}$ is observed for 50% (average of C1(low), C7(medium) and C13(high)) and 80% (average of C4(low, C8(medium) and C16(high)) volume ratio respectively. Due to the dissolution of chitosan, the OR can be released from the polymer as the material dissolves. Conversely at pH 10, repulsive interactions between the chitosan and the solvent can cause the chitosan to shrink and expel OR by this method. The average release rates are observed to be 0.0959 ± 0.0149 $min^{-½}$ (average of C3, C9, and C15) and 0.1012 ± 0.0111 $min^{-½}$(average of C6, C10 and C18). Due to the fact that the polymer shrinks, not all of the internal molecules could be released as some molecules may be left on the polymer surface, also, if the voids of the chitosan close, some of the internal molecules of the OR cannot be expelled from the polymeric structure. At pH7, the freeze-dried chitosan can absorb water which causes the material to swell slightly, the average release are 0.0087±0.0004 $min^{-½}$ (average of C2, C8 and C14) and 0.0337±0.0037 $min^{-½}$ for 50% and 80% respectively (average of C5, C11 and C17). Due to this and the non-responsiveness of the chitosan at this pH, the OR diffuses from the polymer at a much slower rate than before where the specific interactions cause the increases release of the OR.

Effect of Volume ratio

As already shown and discussed in chapter 3 and already published:[22] increasing the volume ratio increases the amount of drug (or organic molecule) per unit gram available within the materials. As a result of this, more molecules of OR are available to be released from the chitosan. This is observed in figure 8 which compares the release kinetics from C1 and C4, from 50% and 80% volume ratio respectively.

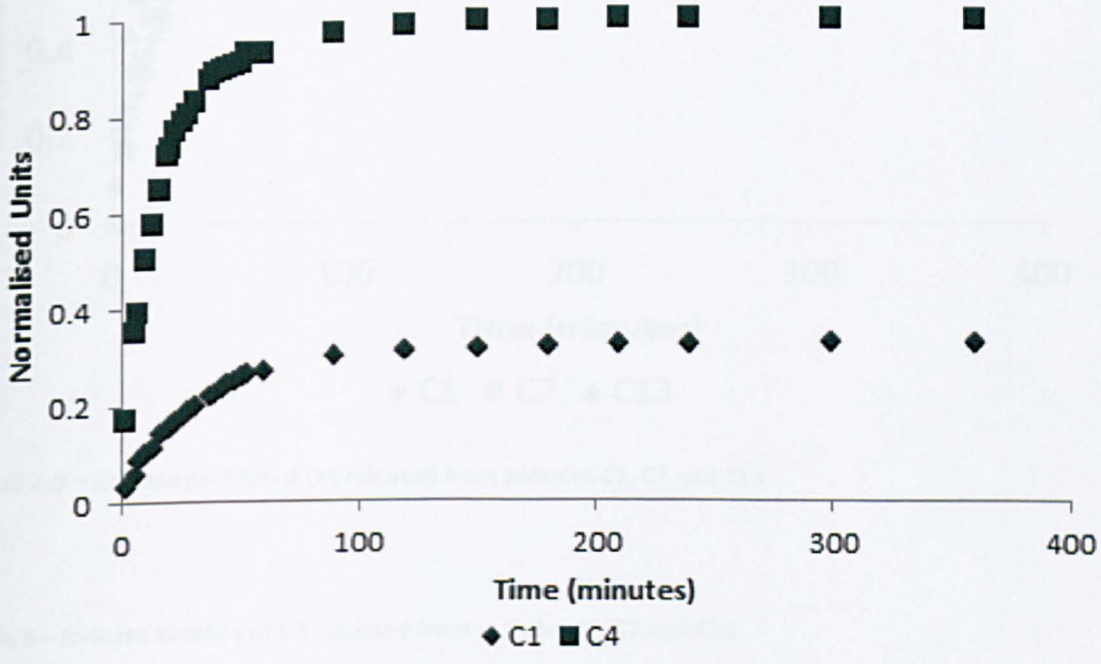

Figure 4-8 - effect of volume ratio on the release profiles of OR from emulsion templated chitosan, example shown is for sample C1 and C4

Table 4 - rate constant summary for changing the volume ratio samples C1 and C4 as examples

Sample	Sample Code	pH	Rate Constant ($min^{-½}$)	R^2
1L-OR 50	C1	2	0.1063 ± 0.002	0.9769
1L-OR 80	C4	2	0.1535 ± 0.003	0.9835

Due to the increased void volume and pore area observed by mercury intrusion and SEM, the material is more porous and therefore can allow more molecules to be released at a quicker rate; not only this, but with the increased loading at higher volume ratio of IMC, this is exemplified

by an increase in release rate from 0.1063 $min^{-½}$ for 50% to 0.1535 $min^{-½}$ for 80% volume ratio.

Effect of Chitosan Molecular Weight

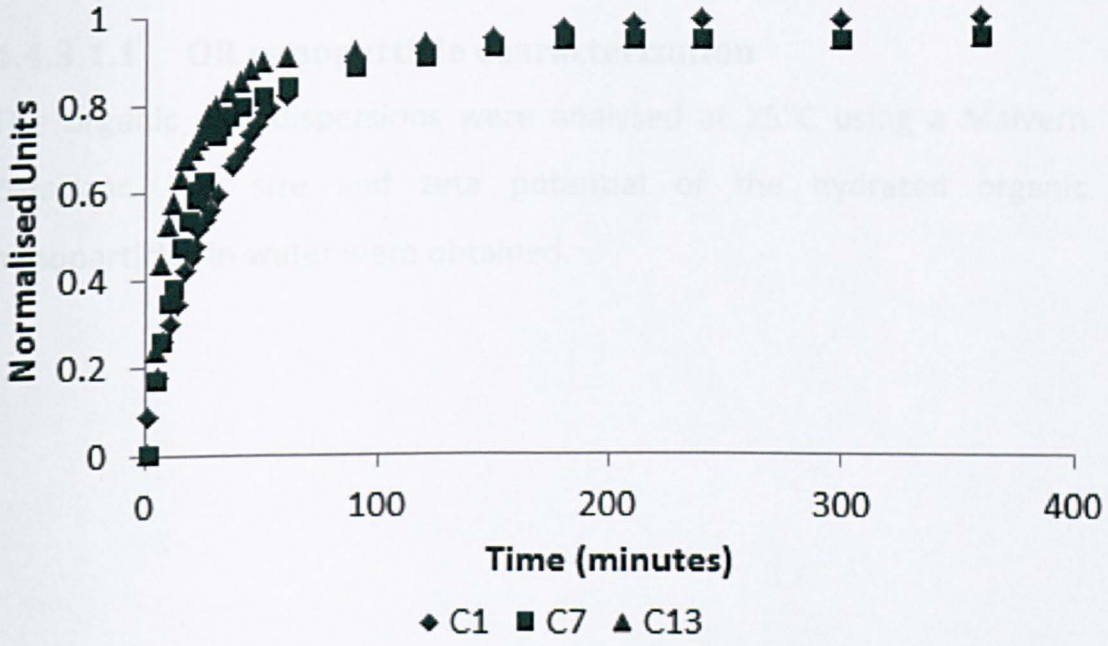

Figure 4-9 – Release profiles of OR released from samples C1, C7 and C13

Table 5 – Release Kinetics of OR released from samples C1, C7 and C13

Sample	Sample Code	pH	Rate Constant ($min^{-½}$)	R^2
1L-OR 50	C1	2	0.1063 ± 0.002	0.9769
1M-OR 50	C7	2	0.1305 ± 0.010	0.9271
1H-OR 50	C13	2	0.1553 ± 0.016	0.8971

Table 5 and Figure 9 show the release rates at pH 2 using 50% emulsion templated chitosan for differing molecular weights. This trend observed is not existent through other comparisons, however. Despite using a higher molecular weight of chitosan, the prepared emulsions exhibit similar droplet sizes; also when the materials are freeze-dried

they exhibit similar pore sizes (circa. 50 μm) and volumes (circa. 11-14 ml/g). Therefore when each corresponding material is placed into different pH media the release rates are seen to be in the same order of magnitude.

4.4.3.1.1 OR nanoparticle characterization

The organic nanodispersions were analysed at 25^{0}C using a Malvern Zetasizer. The size and zeta potential of the hydrated organic nanoparticles in water were obtained.

Effect of pH

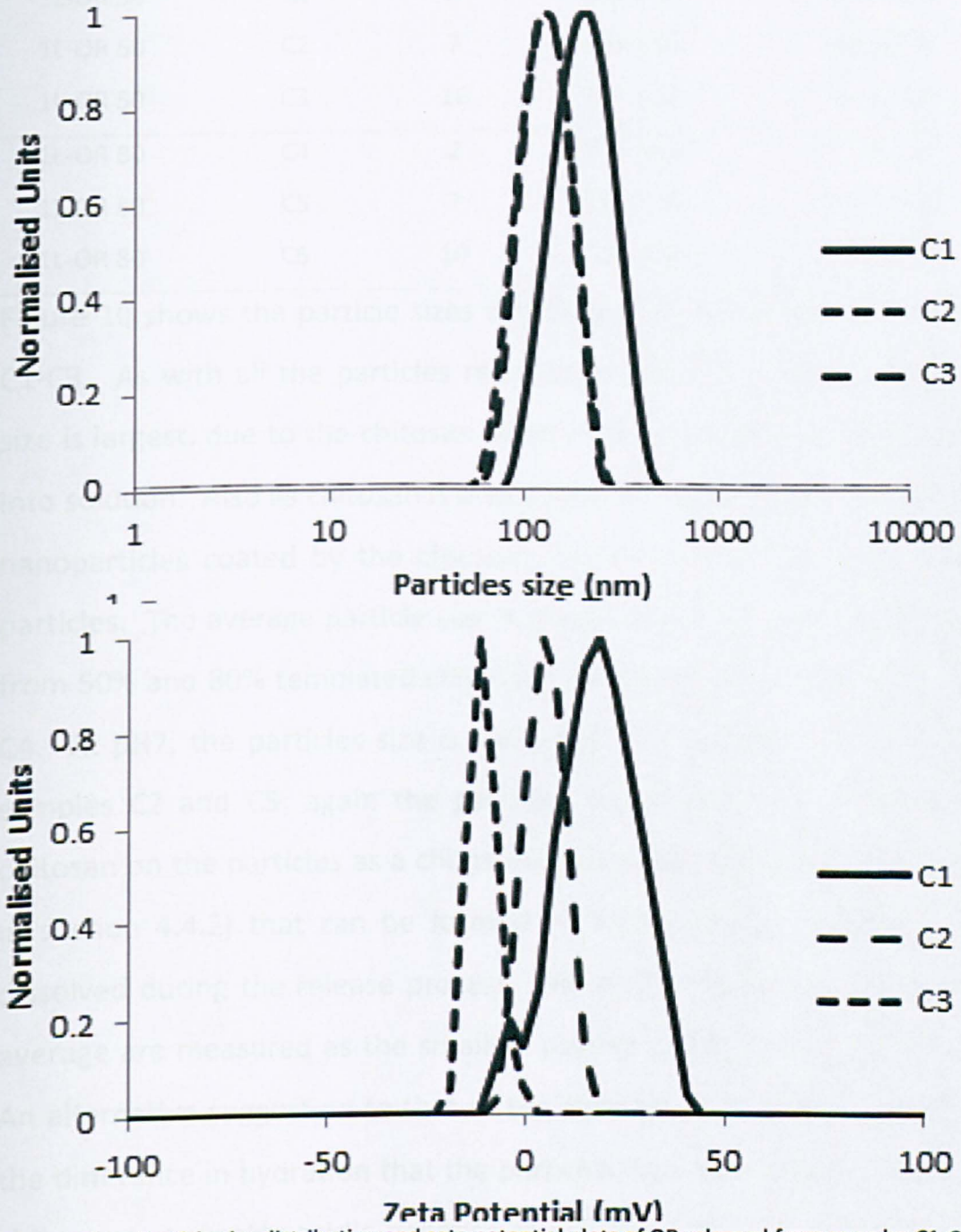

Figure 4-10 – Particle size distribution and zeta potential plots of OR released from samples C1-C3

Table 6 - Particle size and zeta potential measurements for samples C1-C3

Sample	Sample Code	pH	Particle Size (nm)	Zeta potential (mv)
1L-OR 50	C1	2	214 ± 85	42.7 ± 12.7
1L-OR 50	C2	7	134 ± 46	1.95 ± 2.4
1L-OR 50	C3	10	135 ± 43	-15.2 ± 1.4
1L-OR 80	C4	2	203 ± 68	53.3 ± 11.7
1L-OR 80	C5	7	174 ± 40	2.11 ± 2.6
1L-OR 80	C6	10	124 ± 32	-10.8 ± 1.6

Figure 10 shows the particle sizes and zeta potential plots for samples C1-C3. As with all the particles released at pH2, the average particle size is largest, due to the chitosan dissolution upon releasing of the OR into solution. Also as chitosan is a weakly acidic polymer the size of the nanoparticles coated by the chitosan could influence the size of the particles. The average particle size is measured at 214 nm and 203 nm from 50% and 80% templated chitosan respectively for samples C1 and C4. At pH7, the particles size is measured 134 nm and 174.4 nm for samples C2 and C5; again the particles could have some coating of chitosan on the particles as a chitosonium acetate salt (see explanation in section 4.4.2) that can be formed on freeze drying which can be dissolved during the release process. At pH10, the particles sizes, on average are measured as the smallest particles 134.7 nm and 124 nm. An alternative suggestion to that of the chitosan coating the particle is the difference in hydration that the particles have at each pH. Again as chitosan is a weakly acidic polymer at pH 7 and pH 10 the forces are repulsive with the aqueous media and therefore the hydrodynamic radius could be affected. At pH10 also as the chitosonium acetate salt may not be seen to dissolve and coat the particles the particle size of

124 nm could truly represent the hydrodynamic particle size of the OR stabilised by surfactant.

The zeta potential measured for the particles can be affected by the pH of the media. At pH2 the average zeta potential measured for particles are: 47.2 mV and 52.3 mV for samples C1 and C4 at pH2. At pH7 the zeta potentials are 1.95 mV and 2.11 mV for samples C2 and C5 and at pH10 the potentials are -15.2 mV and -10.8 mV.

Effect on volume ratio

Figure 11 shows the particle size and zeta potential comparison of samples C1 and C4 where the particles are released at pH2:

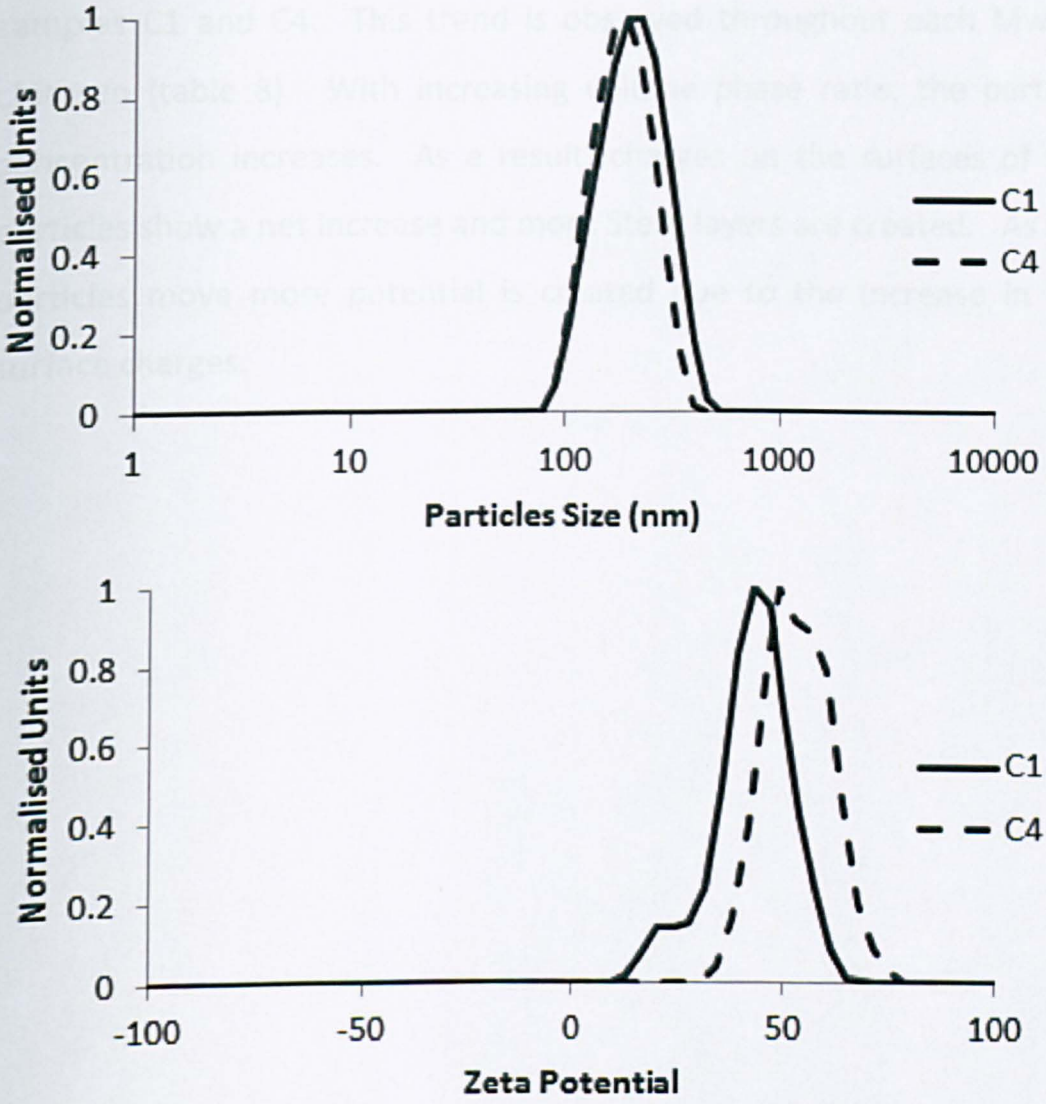

Figure 4-11 – Particle size distribution and zeta potential plots of samples C1 and C4

Table 7 shows the particle size and zeta potential for samples C1 and C4. In general, the particle sizes are not affected by volume ratio, no trend is observed. The nucleation and precipitation of the OR on the surface of the chitosan may be affected little by the volume phase of the chitosan monoliths. When the volume ratios are changed, the

particle sizes deviate but only by a small error with respect to each Mw of chitosan (table 8).

The zeta potential measurements at pH 2 are 42.7 and 53.3 mV for samples C1 and C4. This trend is observed throughout each Mw of chitosan (table 8). With increasing volume phase ratio, the particle concentration increases. As a result, charges on the surfaces of the particles show a net increase and more Stern layers are created. As the particles move more potential is created due to the increase in the surface charges.

Effect of Chitosan molecular weight

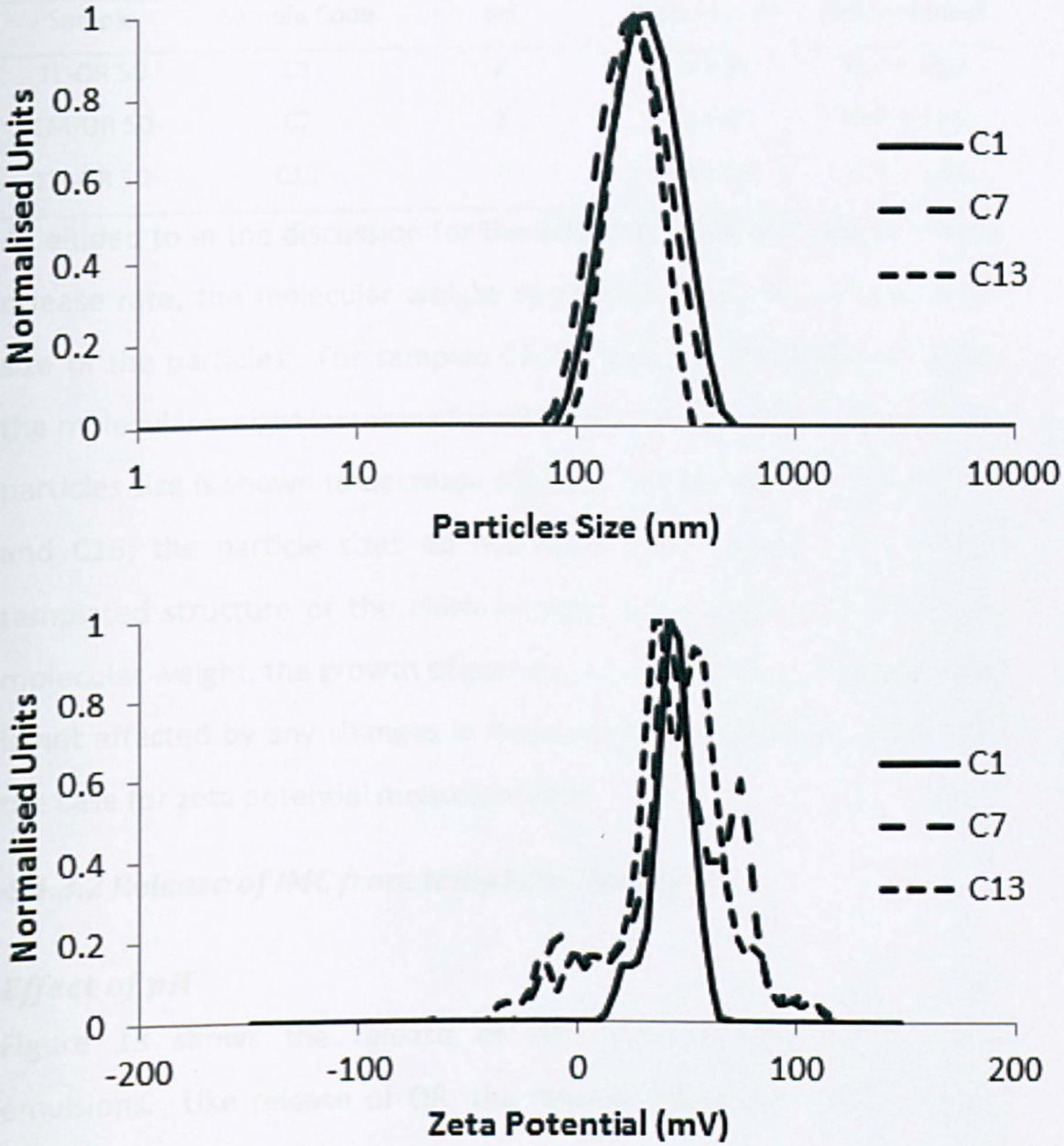

Figure 4-12 – Particle size and zeta potential plots of OR released for samples C1, C7 and C13

Table 8 - Particle size and zeta potential measurements for samples C1, C7 and C13

Sample	Sample Code	pH	Particle Size	Zeta potential
1L-OR 50	C1	2	214 ± 85	42.7 ± 12.7
1M-OR 50	C7	2	191 ± 77	44.8 ± 14.6
1H-OR 50	C13	2	188 ± 53	42.6 ± 12.6

As eluded to in the discussion for the effect of molecular weight on the release rate, the molecular weight of chitosan does not influence the size of the particles. For samples C1, C7 and C13, for example where the molecular weight increases for 50 % templated samples in pH 2; the particles size is shown to decrease slightly. Conversely samples C4, C10 and C16; the particle sizes do not follow the same trend. As the templated structure of the chitosan does not change significantly by molecular weight, the growth of particles on the surface of the chitosan is not affected by any changes in the material morphology; this is also the case for zeta potential measurements.

4.4.3.2 Release of IMC from template Chitosan

Effect of pH

Figure 13 shows the release of IMC from freeze-dried chitosan emulsions. Like release of OR, the release rate of the IMC is in the order of pH 2>pH 10>pH 7.

Table 9 – Release kinetics of IMC released from samples C19-C24

Sample	Sample Code	pH	Rate Constant ($min^{-½}$)	R^2
CH1L-IMC 50	C19	2	0.1287 ± 0.004	0.9633
CH1L-IMC 50	C20	7	0.0501 ± 0.001	0.9719
CH1L-IMC 50	C21	10	0.081 ± 0.003	0.959
CH1L-IMC 80	C22	2	0.1425 ± 0.007	0.933
CH1L-IMC 80	C23	7	0.0335 ± 0.003	0.912
CH1L-IMC 80	C24	10	0.0678 ± 0.001	0.9798

With the ability of chitosan to dissolve at low pH due to its pKa the release rate of the IMC is shown to be higher (for example, C19). For release of IMC at pH 10 the release is less than that for pH 2. At pH 7 the release of IMC is slowest for this set of data, however in contrast to release of OR from templated chitosan, the rate of release observed is higher: for example: Sample C20 in comparison to C2 shows an increase in the rate from 0.0083 $min^{-½}$ to 0.0501 $min^{-½}$. The structure of the chitosan templated by the Pluronics which is shown in figure 4 is possibly accountable for the observed higher release rates. Chitosan templated by Pluronics shows a more interconnected structure than in comparison templated by Triton. With this increase in connectivity the amount of space available in the structure increases and therefore diffusion of the particles throughout the structure is increased

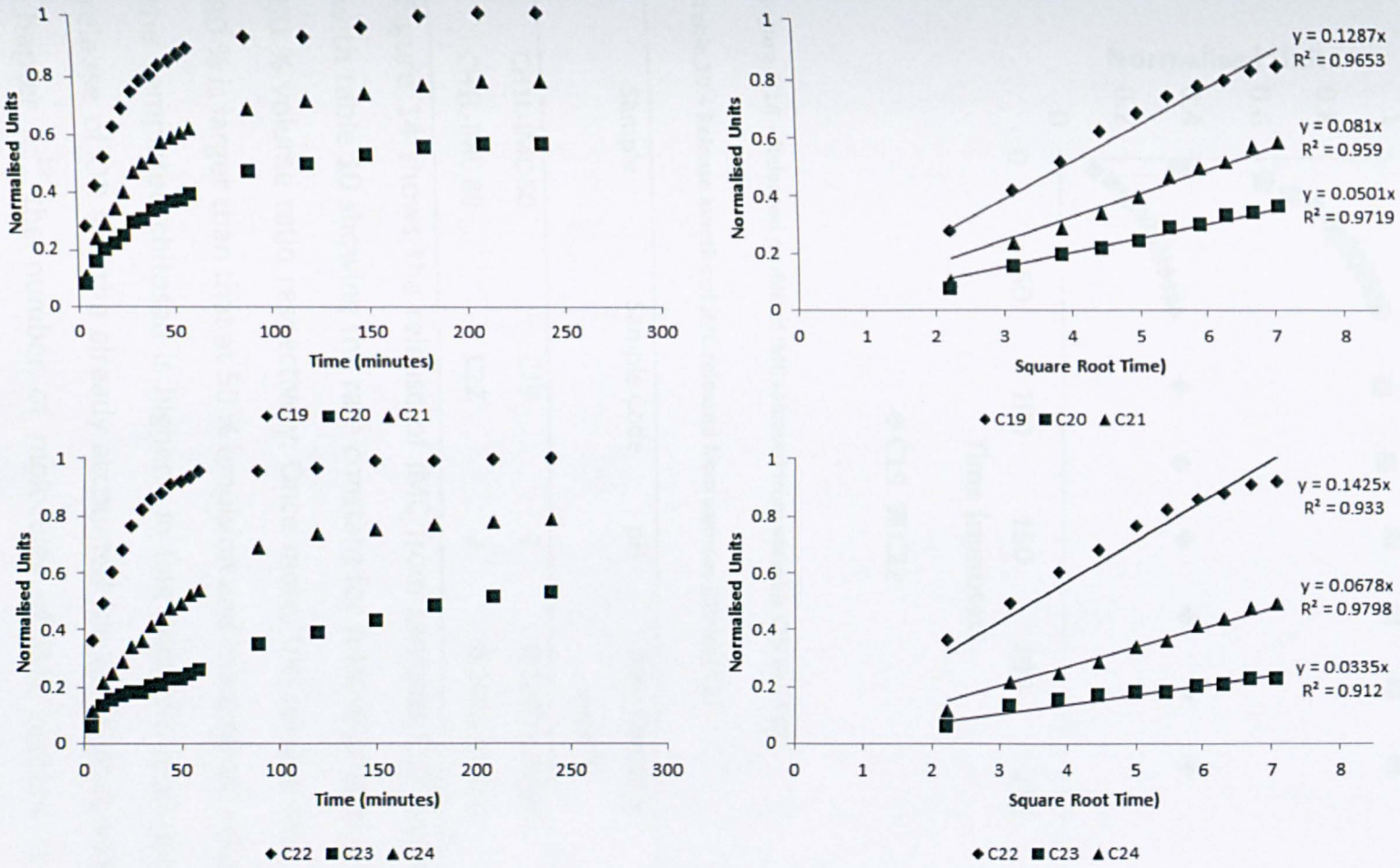

Figure 4-13 – Release profiles of IMC released from samples C19-C24

.Effect of volume ratio

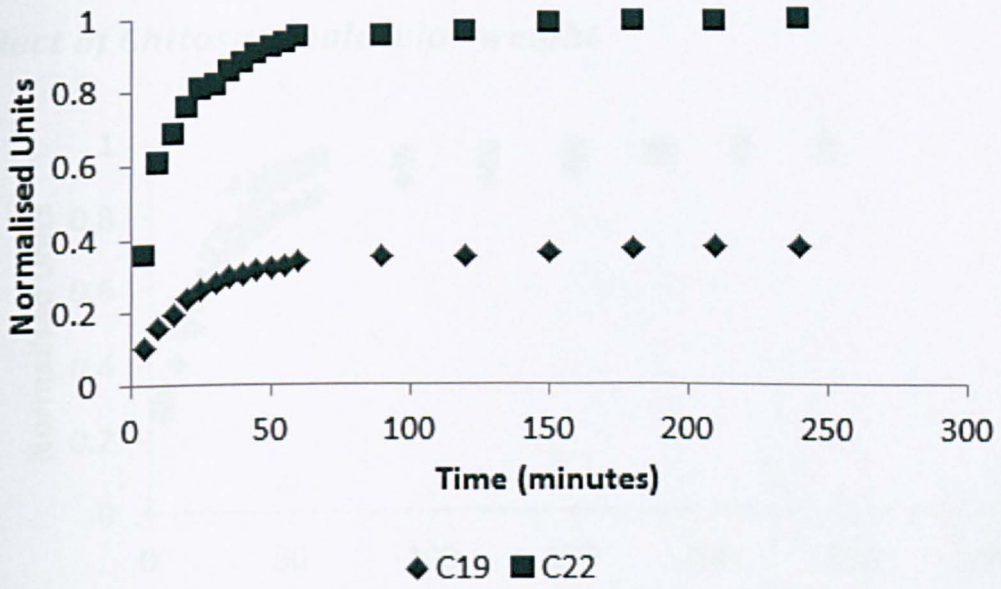

Figure 4-14 – Released profile of IMC released from samples C19 and C22

Table 10 – Release kinetics of IMC released from samples C19 and C22

Sample	Sample Code	pH	Rate Constant ($min^{-½}$)	R^2
CH1L-IMC 50	C19	2	0.1287 ± 0.004	0.9633
CH1L-IMC 80	C22	2	0.1425 ± 0.007	0.933

Figure 14 shows the release of IMC from samples C19 and C22 along with table 10 showing the rate constant for release of IMC at 50 % and 80 % volume ratio respectively. Once more, the release rate of IMC at 80 % is larger than that at 50 % emulsion and the amount released from the templated chitosan is higher. In line with the discussion for the release of OR and the already accounted for in the observations from chapter 3;[22] the number of molecules of IMC present in the 80% templated chitosan is much higher than that in 50% emulsions. Due to the increased number of molecules and also the higher

interconnectivity observed the release rate of the IMC from templated chitosan increases.

Effect of Chitosan molecular weight

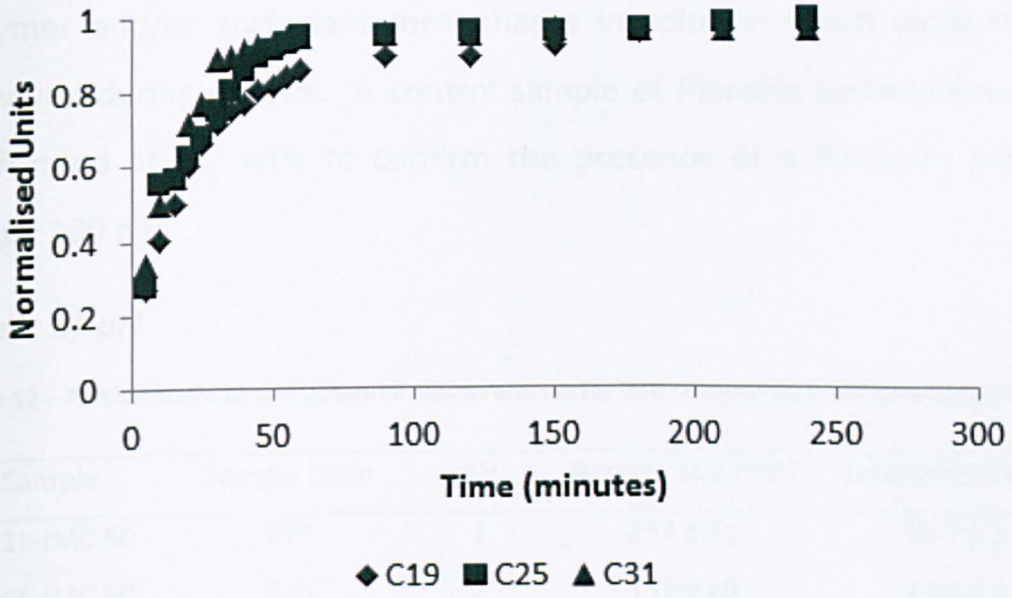

Figure 4-15 – Release plots of IMC from samples C19, C25 and C31

Table 11 – Release kinetics of IMC released from C19, C25, and C31

Sample	Sample Code	pH	Rate Constant ($min^{-½}$)	R^2
CH1L-IMC 50	C19	2	0.1287 ± 0.004	0.9633
CH1M-IMC 50	C25	2	0.1358 ± 0.002	0.9868
CH1H-IMC 50	C31	2	0.1454 ± 0.003	0.9786

As already discussed for the release of OR from porous chitosan, the molecular weight of the chitosan bares little effect on the release rates of IMC. As the materials pore volume barely fluctuates the amount of molecules of IMC per unit gram of chitosan remains the same and therefore the release rates from the porous material changes very little.

4.4.3.2.1 Particle Characterisation

Before continuing with the observations for the IMC particles released from the chitosan it is important to inform the reader that from herein any peak observed which are less than 100 nm are accounted for as polymer and/or surfactant mesophases in solution which were not removed during dialysis. A control sample of Pluronic surfactant was performed at 0.2 wt% to confirm the presence of a Pluronics peak below 100 nm.

Effect of pH

Table 12 – Particle size and zeta potential measurements for IMC released from samples C19-C21

Sample	Sample Code	pH	Particle Size (nm)	Zeta potential (mV)
CH1L-IMC 50	C19	2	253 ± 71	13.7 ± 5.4
CH1L-IMC 50	C20	7	152 ± 69	2.54 ± 3.0
CH1L-IMC 50	C21	10	202 ± 58	-10.8 ± 4.1
CH1L-IMC 80	C22	2	277 ± 99	24.7 ± 8.4
CH1L-IMC 80	C23	7	203 ± 63	3.39 ± 3.1
CH1L-IMC 80	C24	10	241 ± 63	-3.85 ± 2.6

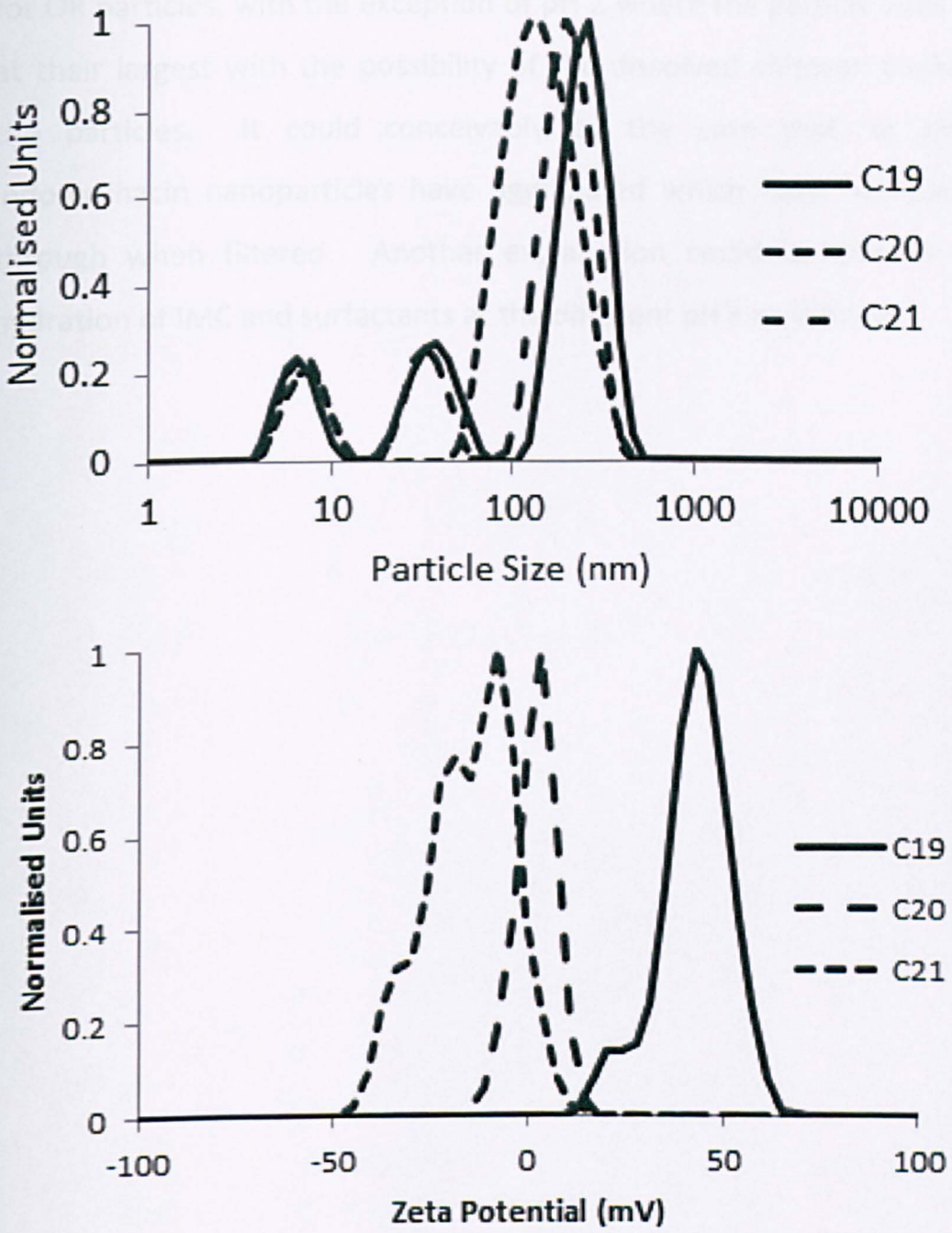

Figure 4-16 – Particle size distribution and zeta potential plots for IMC from samples C19-C21

Figure 16 shows the particle sizes for samples C19-C21. In general the particle size is seen as largest for pH 2 samples. The particle sizes for pH 2 samples are 252.8 nm and 276.9 nm for C19 and C22 respectively. This decreases at pH 7 from 151.9 nm to 203.4 nm for samples C20 and C23 and at pH10 the particle size increases to 202.4 nm and 241.1 nm for samples C21 and C24. This observation is different to that observed

for OR particles, with the exception of pH 2 where the particle sizes are at their largest with the possibility of the dissolved chitosan covering the particles. It could conceivably be the case that, at pH 7 indomethacin nanoparticles have aggregated which have not passed through when filtered. Another explanation could be due to the hydration of IMC and surfactants at the different pH's be different.

Effect of Volume Ratio

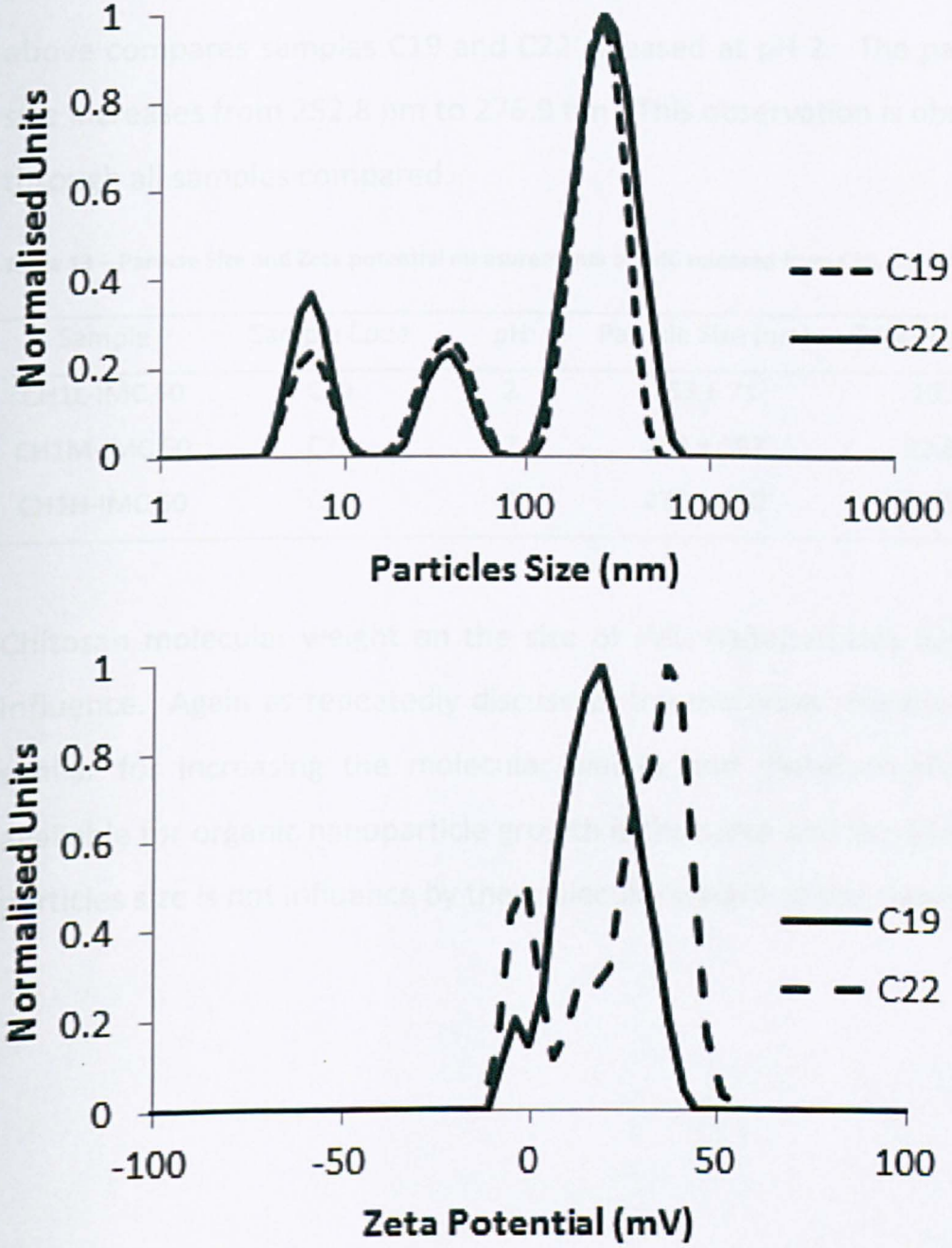

Figure 4-17 – Particle size distributions and zeta potential plots for IMC released from sample C19 and C22

With the increase in volume ratio comes an increase in the particle size. Due to the pore size and increasing volume, the amount of area

available for the organic nanoparticle to grow on the surface increase, and therefore the size of the nanoparticles can increase. The example above compares samples C19 and C22 released at pH 2. The particles size increases from 252.8 nm to 276.9 nm. This observation is observed through all samples compared.

Table 13 – Particle Size and Zeta potential measurements of IMC released from C19, C25 and C31

Sample	Sample Code	pH	Particle Size (nm)	Zeta potential (mV)
CH1L-IMC 50	C19	2	253 ± 71	13.7 ± 5.4
CH1M-IMC 50	C25	2	254 ± 152	22.8 ± 10.2
CH1H-IMC 50	C31	2	273 ± 110	23.5 ± 10.7

Chitosan molecular weight on the size of IMC nanoparticles has little influence. Again as repeatedly discussed, the materials morphology is similar for increasing the molecular weight and therefore the area available for organic nanoparticle growth is the same and therefore the particles size is not influence by the molecular weight of the chitosan

Effect of Chitosan Molecular weight

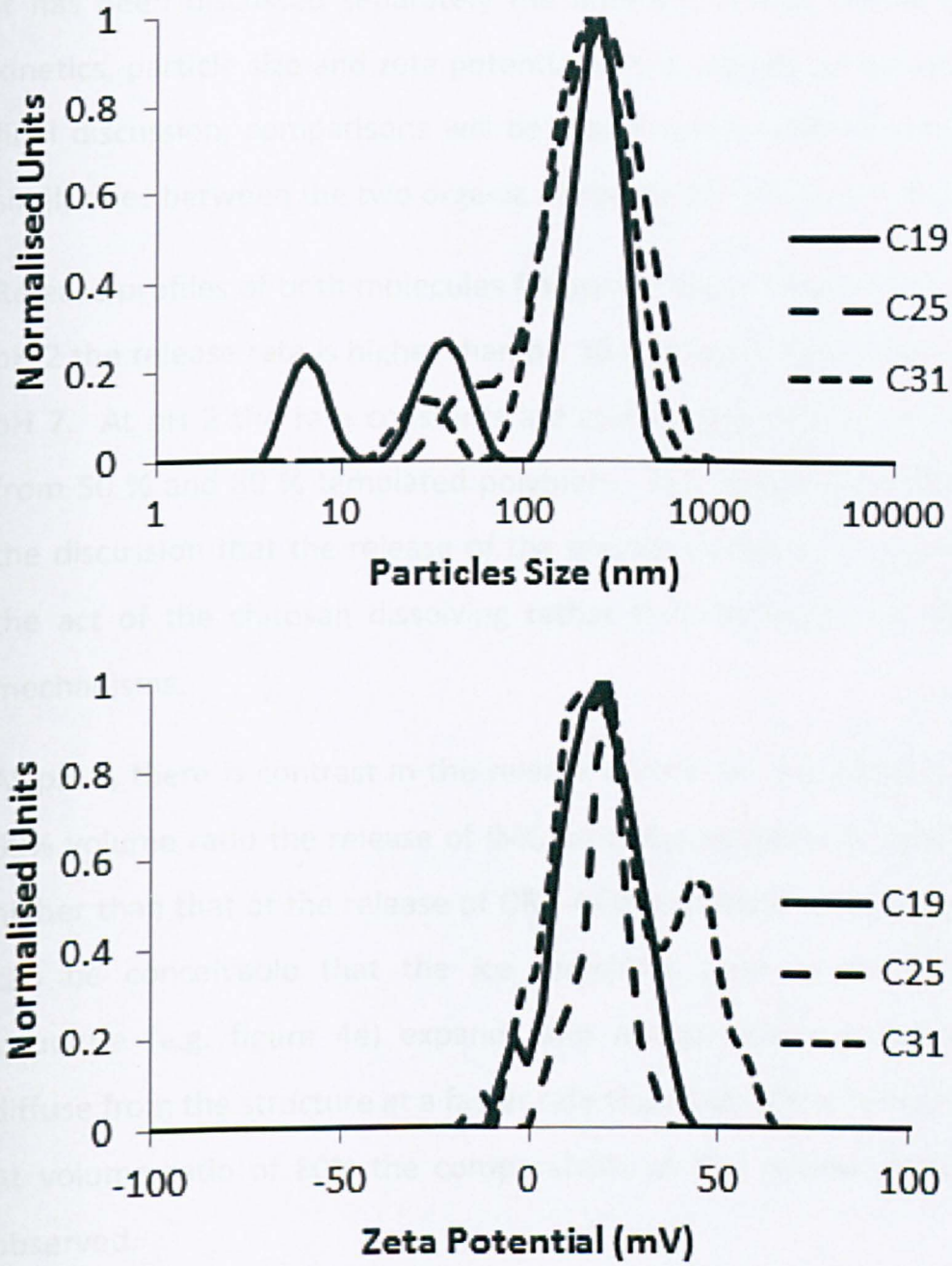

Figure 4-18 – Particle size distributions and zeta potential plots of IMC released from C19, C25 and C31

Comments on the choice of organic molecule

It has been discussed separately the different effects on the release kinetics, particle size and zeta potential of the organic molecules. As a final discussion, comparisons will be drawn on the differences and/or similarities between the two organic nanoparticles of OR and IMC.

Release profiles of both molecules follow the same trend in so far as at pH 2 the release rate is higher than pH 10 and again higher than that at pH 7. At pH 2 the rate constants are comparable throughout release from 50 % and 80 % templated polymers. This observation reinforces the discussion that the release of the organic molecule is governed by the act of the chitosan dissolving rather than by means of diffusion mechanisms.

At pH 7, there is contrast in the release constants. For polymers with 50% volume ratio the release of IMC from the polymers is significantly higher than that of the release of OR. As the material swells at pH 7, it can be conceivable that the ice templates seen in the CHIT-IMC structure (e.g. figure 4e) expands and allows molecules of IMC to diffuse from the structure at a faster rate than that of the release of OR. At volume ratio of 80% the comparability of the release profiles are observed.

Finally at pH 10, the release of IMC is comparatively slower than that for the release of OR. When the chitosan polymer contracts, due to the IMC particles being larger, the particles could diffuse slower due to lower Brownian motion of larger particles (unlikely) or as the windows of the IMC@CHIT monoliths are measured to be smaller, upon contraction, the pores may become smaller and thus not allowing

particles to move as freely through the polymer as the diffusion through the OR@CHIT monoliths.

Particles sizes of the IMC are larger than that of the OR particles released. One observation is that the size of the particles released at pH 2 is larger than that at any other pH. As discussed in the previous sections, the dissolution of chitosan onto the surface of the particles could be the influencing factor for the observations of the particles being larger in this case. When IMC nanoparticles are prepared, the surfactant is a polymeric one with a Mw of 12500 Da. In comparison the Mw of Triton X-405 is around 2000 Da. When the particles are released with surfactant and chitosan attached, these large differences in particle sizes could be explained also by the increased Mw of the Pluronic surfactant coating the IMC particles.

Zeta potential measurements of the IMC particles are lower in magnitude than the OR particles, yet exhibit the same trends. Due to the larger particle size of the IMC, the tendency of the particles to flocculate could be higher which is observed by the decreasing zeta potential measurements

Figure 19 shows the TEM images of OR and IMC released from Chitosan. The dry nanoparticles are in the range of 100-200 nm. It is also clearly shown the surfactant micelles that are formed and observed by DLS.

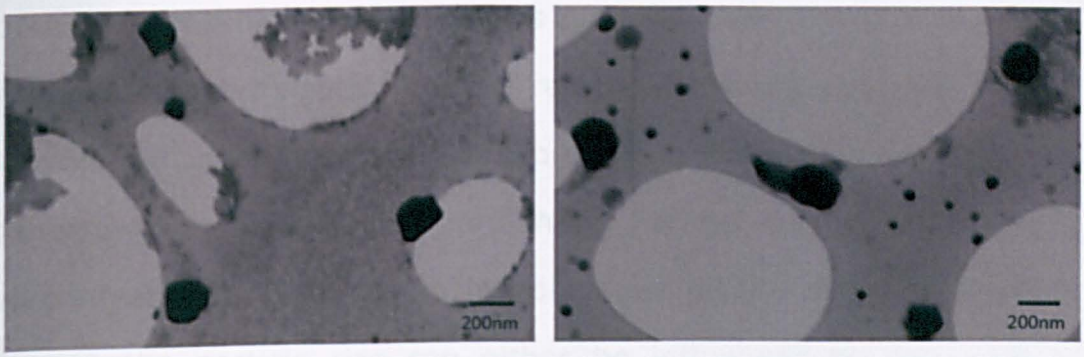

Figure 19 TEM of prepared OR and IMC nanoparticles released from Chitosan

4.5 Conclusions

Due to the capacities of chitosan to form a polyelectrolyte gel in weak acid, an emulsion template chitosan was prepared by forming a "gelled emulsion" and freeze-drying was employed to prepare the porous composites. Oil Red was first used to demonstrate the concept and Indomethacin was used as a model drug to show the release kinetics of the organic molecules from the porous chitosan at different pH's. The organic nanoparticles were formed in-situ in the freeze-drying step to prepare the porous composites via a step similar to emulsification-evaporation. The pore size of the materials where analysed, the molecular weight and the volume phase of the original emulsion ware changed to observe the change in morphology of the structures. The effects of pH, molecular weight and volume ratio where all investigated to observe the changes in release of the organic molecules. Generally, the organic molecules released at a higher rate at pH2 owing to chitosan's dissolution in acidic media and therefore complete release of the organic molecules. The rate was observed to be lower at pH10, due to the contraction of the polymer from repulsive forces in basic media causing the materials to shrink and expel its contents. The lowest rate observed was at neutral pH (7). At this pH, no attractive or repulsive

forces are present and the materials can swell. Due to the interactions of Chitosan with its guest host the release of the organic molecule can be hindered and release could be more due to diffusion of the materials rather than forces acting on its behalf. Particle sizes of OR and IMC were measured. Due to the morphologies of the chitosan for each system, the particle size can either be influenced (in the case of IMC@chit) or not (in the case of OR@chit). The zeta potential of the particles was measured for each sample which are influenced by the pH of the media.

4.6 References

1. Hansh Prashanth, K. V.; Kittur, F.S.; Tharancthan R. N. *Carbohydrate Polymer* **2002**, *50, 1,* 27-33.
2. Rani, M; Aganval, A.; Negi, Y. S. *Bioresources* **2010**, *5, 4,* 1-43.
3. Sun, J.; Jiang, G.; Qui, T.; Wang, Y.; Zhang, K.; Ding, F. *Journal of Biomedical Materials Research – Part A* **2010**, *95, 4,* 1019-1027.
4. Wang, L. C.; Chen, X. G.; Zhang, D. Y.; Xu, Q. C. *Journal of materials science: Materials in Medicine* **2007**, *18, 6,* 1125-1133
5. Agnihotri, S. A.; Mallikarjuna, N. N.; Aminabhavi, T. M. *Journal of Controlled Release* **2004**, *100, 1,* 1-27
6. Ravi Kumar, M. N. V. *Reactive and Functional Polymers* **2000**, *46, 1,* 1-27
7. Prabaharan, M. *Journal of Biomaterials applications* **2008**, *23, 1,* 5-36
8. Rinaudo, M. *Progress in Polymer Science* **2006**, 31, 603-632
9. Lee, K. Y.; Mooney D. J. *Chemical Reviews* **2001**, *101,* 1869-1877
10. Francis Suh, J. K.; Matthes, H. W. T. *Biomaterials* **2000**, *21,* 2589-2598

11. Cherite, A.; Chaput D.; Wang, C.; Combes, C.; Buschmann, M. D.; Hoemann, C. D.; Leroux, J. C.; Atkinson, B. L.; Binette, F.; Selmann, A. *Biomaterials* **2000**, *21*, 2155-2161
12. Mi, F. W.; Kuan, C. Y.; Shiu, S. S.; Lee, S. T.; Chang, S. F. *Carbohydrate Polymers* **2000**, *41*, 3890398
13. Ono, K.; Saito, Y.; Yura, H.; Ishikawa, K.; Kurita, A.; Akalke, T.; Ishikawa, M. *Jounal of Biomedical Materials Research* **2000**, *49*, 289-295
14. Franks, G. V.; Moss, B.; Phelan, D. *Journal of Biomaterials Sciences Polymer Edition* **2006**, *17, 12,* 1439-1450
15. Ko Y.G.; Kawazoe, N.; Tateishi,T; Chen, G *Journal of Biomedical Materials Research Part B: Applied Biomaterials* **2010**, *93B, 2,* 341-350
16. Liang, X.; Wang, H.; Jiang, X.; Chang, J. *Journal of Nanoparticle Research* **2010**, *12, 5,* 1723-1732
17. Cheng, H.; Huang, Y. C.; Yeh, H. Y.; Yeh, S. Y.; Huang, Y. Y. *Biomedical engineering applications basis and communications* **2009**, *21, 2,* 107-114
18. Aggarwai, A.; Kaur, A. K.; Tiwary, A. K.; Gupta, S. *Journal of Microencapsulation* **2001**, *18, 6,* 819-823
19. Bayomi, M. A. *Drug Development and industrial pharmacy* **2004**, *30, 4,* 329-339
20. Haguchi, T. *Journal of Pharmaceutical Sciences* **1963**, *52,* 1145-1149
21. Nunthanid, J. et. al. *Drug Development and Industrial Pharmacy* **2001**, 27, 2, 143-157
22. Grant, N.; Zhang, H. F. *Journal of Colloid and interfacial Science* **2011**, *356, 2,* 573-578

5 DISULPHIDE CROSSLINKED EMULSION TEMPLATED POLYMERS AND THE REDOX CONTROLLED RELEASE OF ORGANIC NANOPARTICLES

5.1 Chapter Overview

Emulsion templated PAM hydrogels were produced by crosslinking with a disulphide crosslinker, bis(acryloyl) cystamine. The hydrogels were prepared at crosslinking densities of 20:1 and 40:1 with respect to monomer:crosslinker at internal phase volume fractions of 50 and 75%. The materials prepared were characterized and used for the release of a poorly water soluble dye, Oil Red, into aqueous solutions using the reductive agents Dithiothreitol (DTT) and Triscarboxyethylphosphine (TCEP) to break the disulphide bonds.

5.2 Introduction

Biodegradable polymers and hydrogels are used in a variety of applications including tissue engineering[1] and drug release.[2-4] Hydrogels are insoluble in water but swell. Polymeric carriers have been investigated for their applications in sustained drug delivery and delivery of water soluble drugs.[5,6]

Disulphide crosslinkers have been commonly used for degradable polymers in the literature.[7-10] Disulphide bonded matrices play a role in pharmaceutical applications due to their stability under oxidizing conditions and degrading in reducing conditions.[11-13] The disulphide link (-S-S-) can be cleaved in aqueous media by using a variety of reducing agents such as Dithiothreitol (DTT), glutathione and Tris(2-

carboxyethyl)phosphine (TCEP).[11-14] Other reducing agents can include nucleophiles, electrophiles[15] or photochemistry.[16]

Here we use two methods for the reduction of disulphide bonds. Firstly DTT was used and secondly by using TCEP. DTT[17] reacts in two steps with disulphides intramolecularly and forms a stable cyclic disulphide (2), as in the reaction below:

$$XS^- + RSSR \rightarrow RSSX + RS^- \quad (1)$$

$$XS^- + RSSX \rightarrow XSSX + RS^- \quad (2)$$

DTT is not stable in the reduced form for long periods of time and DTT oxidation can occur through the presence of metal ions such as Fe^{2+} and Ni^{2+}.[18] TCEP, synthesized by Burns et. al. has been available since 1992.[19] In aqueous solutions TCEP is significantly more stable than DTT at pH values above 7.5 and is a much more useful reductant over a much wider range of pH (1.5-8.5) than DTT,[20] reacting with disulphide bonds according to the reaction below:[21]

$$(CH_3CH_2COOH)_3P: + RSSR + H_20 \rightarrow (CH_3CH_2COOH)_3P{=}O + 2RSH \quad (3)$$

Here, we report the preparation and characterization of degradable PAM emulsion templated polymers which can be degraded by cleaving with a reducing agent. The effects of crosslinker concentration, emulsion volume fraction and the reducing agent concentration where all studied.

5.3 Experimental

5.3.1 Materials

Acrylamide (AM, 99%), Triton X-405 (70% in water), Oil Red (OR), Cystamine dihydrochloride (96%), acryloyl chloride (97%), were all purchased from Sigma Aldrich and used as received. Chloroform, ethyl acetate, heptane, acetonitrile and sodium hydroxide were all of analytical grade and used as received. Distilled water was used in each case.

5.3.2 Preparation of the bisacryloylcystamine (BAC) crosslinker:

N,N'-bis-acrylcystamine was synthesized following the method:[22] Briefly 8 g of cystamine dihydrochloride was dissolved in 80 ml of 3.12 M NaOH solution, and then 9.6 g of acryloyl chloride in 20 ml of acetonitrile was added dropwise to the solution under vigorous stirring at 50 °C for 15 minutes or until effervescence ceased. The reaction product was extracted with hot chloroform at 50 °C. The extract was washed with 0.1 M HCl and saturated sodium chloride and dried on sodium sulphate for 1 day. After removal of the solvent under vacuum, the residue was recystallised using ethyl acetate:heptane (2:1) and identified by ^{1}H NMR, elemental analysis and mass spectrometry.

5.3.3 Preparation of emulsion template AM:BAC polymers

Table 1 summarises the preparation conditions for emulsion templated acrylamide. Emulsion templated poly (AM:BAC) was carried out at AM/BAC molar ratios of 20:1 and 40:1 in 10% w/v monomer solution. The crosslinker has low water solubility.[23] The crosslinker was dissolved in the monomer solution by sonication until dissolved. 10%w/v Ammonium persulphate (APS, 0.3 ml) was added to the solution

followed by Triton X-405 (0.4ml). A solution of Oil Red in Cyclohexane (OR-CH, 0.02 %wt/v) with N,N,N',N' Tetramethylethylenediamine (TMEDA, 30µl) was added dropwise to the aqueous phase whilst stirring using a lab egg stirrer. The formed emulsion was left to stir for 5 minutes before transferring to an oven at 60 °C overnight. For emulsions with an internal phase volume of 50%, the pre-formed emulsion was homogenized for 1.5 minutes at speed 5 using a Fisher Brand homogeniser.

5.3.4 Release of Oil Red

The polymerised emulsion can be frozen and freeze-dried to remove the solvents and yield a porous material. The organic nanoparticles could be formed in-situ within the macropores. The emulsions are frozen to lock the morphology and keep the structure during drying. The frozen emulsion was freeze-dried to produce porous structure with in-situ formation of organic nanoparticles.

5.3.4.1 Release of organic nanoparticles from disulphide crosslinked polymers using DTT

Release was performed using DTT as the redox agent. Solutions of DTT were prepared at the concentrations of 0.1, 0.2 and 1 wt% in pH 9 water, and bubbled with nitrogen for 10 minutes. Samples of the polymer (0.05 g) where cut and placed in a vial with a septa and flushed with nitrogen for 10 minutes. DTT solution (5ml) was added via a syringe to the vial. The vials were placed into a water bath at 50 °C.[24] Periodically the aqueous media was agitated 5 times to ensure uniform mixing of the suspensions and 500 µl of clear suspension was removed for UV analysis. The removed volume was replaced by fresh volume of

DTT. The collected samples were analysed for their UV absorption at room temperature.

Monitoring the release was performed using a 96-well multiplate reader. 200 µl of the released aqueous suspension was pipetted into a well of a 96-well flat bottomed polypropylene plate. The absorption peak was monitored by scanning from 200 to 800 nm in 2 nm steps. The height of the peak was subtracted from the baseline to give the absorption reading of each sample. The data points were normalized using:

$$M = \frac{A_t}{A_\infty} \qquad (1)$$

Were M is the normalized unit, A_t is the absorption at time t and A_∞ is the highest final absorption reading of all the readings. The final release time for particles after 2 hours at pH 2 was taken. It was confirmed with a controlled experiment that the absorption does not changed after a further reading 18 hours after this time.

The release rates were calculated by using Higuchi Model for release of molecules from an insoluble matrix (equation 1):

$$M = \frac{A_t}{A_\infty} = kt^{½} \qquad (2)$$

Were k is the rate constant and t is the time of the measurement. The regression function on Excel was used to calculate the R^2 for each release curve.

5.3.5 Release of organic nanoparticles from disulphide crosslinked polymers using TCEP

Release using DTT is a very restrictive way to break disulphide bonds as selective pH and selective temperatures are required. TCEP a phosphorous based compound can also be used to cleave disulphide bonds. Solutions of TCEP at the concentrations of 0.1, 0.2 and 1 wt% where prepared. Samples of the polymer (0.05 g) where cut and weighed. TCEP solution was added to the polymer, the temperature of the solution remained at room temperature. Periodically 200µl of the aqueous media was agitated 5 times to ensure uniform mixing and removed for UV analysis and analysed as mentioned in section 5.3.3.1. The removed volume was replaced with fresh TCEP.

5.3.6 Characterisation

The dried materials were sectioned to reveal the internal porous structures. The samples were adhered to an aluminium stub using a silver colloidal suspension and allowed to dry. A sputter coater (EMITECH K550X) was used to coat the samples with gold at 40 mA for 3 minutes. A Hitachi S-4800 field emission SEM was used to reveal the pore structure at 3 KV. The pore sizes and pore volumes of the dried materials were examined using a Micromereritics Autopore IV 9500 porosimeter. Samples were subjected to a pressure cycle starting at approx 0.5 psi, increasing to 60000 psi in predefined steps.

The OR nanoparticles where released into water by reaction with the reducing agent. The OR nanoparticles were released and an aqueous OR nanoparticle dispersion was formed. The OR nanodispersions where centrifuged for 15 minutes at 13000 rpm using an Eppendorf Centrifuge 5415D and the supernatant liquid was filtered through a 1 µm syringe

to remove the degraded polymer, OR nanoparticles were not precipitated during centrifuging as a clear red solution was still observed. The OR dispersions were analysed at 25^0C using a Malvern Zetasizer with a backscattering detection at 173°. The scattering intensity signal for the detector is passed through a correlator where this data is analysed by the software and give a size distribution. The size of the hydrated OR nanoparticles in water were obtained. Each measurement was repeated at least 3 times and the average data were used to plot the figures. 10µl of a diluted OR nanodispersion was dropped onto holey carbon filmed copper grids (400 mesh) and allowed to dry overnight. A scanning transmission microscopic (STEM) detector attached to the Hitachi S-4800 SEM was used to observe the dry OR nanoparticles at 30 KV.

Breaking of the disulphide bonds and therefore the formation of thiols were performed using DTT or TCEP, to prove the formation of thiols when using TCEP Ellmans stain was used. To prepared the stain[25]: 5,5'-dithiobis-(2-nitrobenzoic acid) (DTNB) (0.15g, 0.034 mmol) in 1:1 ethanol and 0.45 tris-HCl (150ml total). *Preparation of 1M tris-HCl* – Tris(hydroxymethyl)aminomethane (30.285g) was dissolved in distilled water (150ml) and acidified to pH 7.4 with concentrated HCl. The solution was made up to 250ml using distilled water. To prove the formation of the thiol, a drop of the released media was placed onto a TLC plate and submerged in the stain solution. The formation of the thiols was observed by a bright yellow spot where the drop was placed.

5.4 Results and Discussion

5.4.1 Preparation of disulphide crosslinker

The crosslinker, BAC, was synthesised according to the procedure given in 5.3.2. Figure 1 shows the 1H NMR spectrum for the synthesised crosslinker

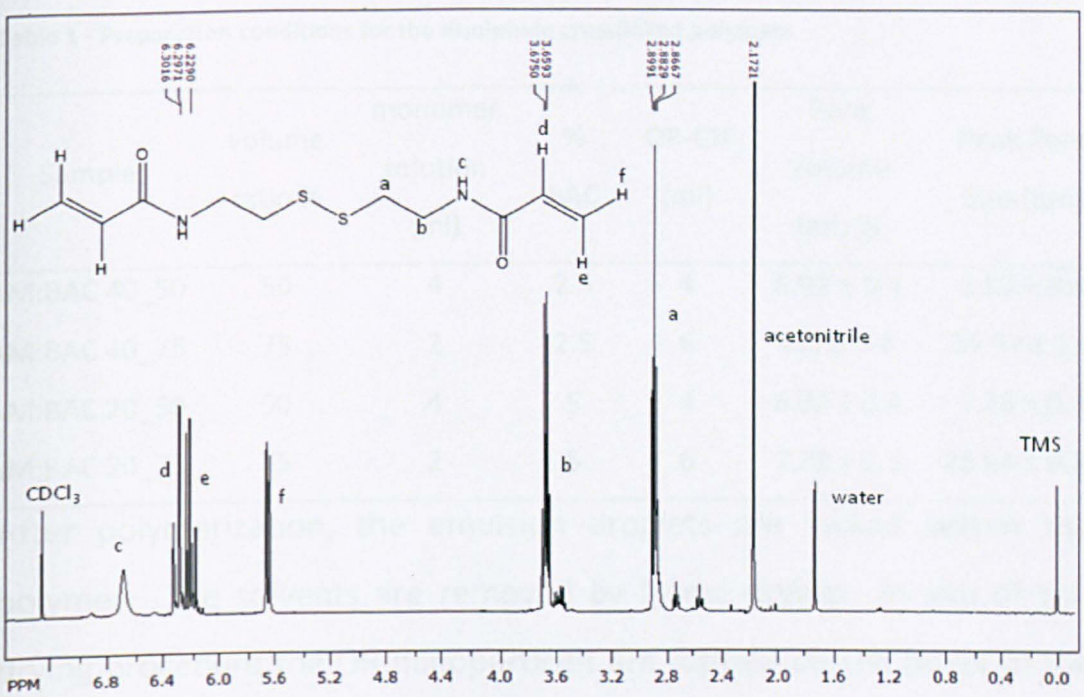

Figure 5-1 - 1H NMR spectrum for the synthesised crosslinker

1H NMR data (400MHz, $CDCl_3$): δ 2.85 (m, 4H, environment **a**), δ 3.7 (M, 4H, environment **b**), δ 5.62 (m, 2H, environment **f**), δ 6.2-6.4 (m, 4H, trans-H on alkene, environments **d and e**), δ 6.7 (s, 2H, $-NH^c$)

Mass spec: Found M/Z 292.38 $[C_{10}H_{16}N_2S_2O_2+Na]^+$

Elemental analysis: %C=45.64 (46% Theory) %H=6.11% (6.2% Theory), %N=10.28% (10.8% Theory)

5.4.2 Preparation of the Disulphide crosslinked polymer

Emulsion templated polymers can be prepared by polymerizing the continuous phase of an oil-in-water emulsion. The OR can be

solubilised in the oil phase and the interface stabilized by a surfactant like Triton X-405. The monomers and crosslinkers, together with initiators are present in the continuous aqueous phase. When placed into an oven above 60 °C the monomers react through free-radical polymerization and the emulsion is polymerized.

Table 1 - Preparation conditions for the disulphide crosslinked polymers

Sample	volume ratio %	monomer solution (ml)	% BAC	OR-CH (ml)	Pore Volume (mL/g)	Peak Pore Size (μm)
AM:BAC 40_50	50	4	2.5	4	6.99 ± 0.4	3.87 ± 0.4
AM:BAC 40_75	75	2	2.5	6	8.5 ± 0.4	25.97 ± 2.6
AM:BAC 20_50	50	4	5	4	6.95 ± 0.4	3.78 ± 0.4
AM:BAC 20_75	75	2	5	6	7.22 ± 0.3	25.94 ± 0.36

After polymerization, the emulsion droplets are locked within the polymer. The solvents are removed by freeze-drying. In situ of this drying procedure the OR nanoparticles are formed on the pores of the polymer through steps similar to emulsification-evaporation.[26] Table 1 shows the preparation conditions and the pore sizes and volumes for the prepared polymers at 20:1 And 40:1 crosslinking ratios, Figure 2 shows the morphology of the materials and the pore characterization through mercury porosimetry.

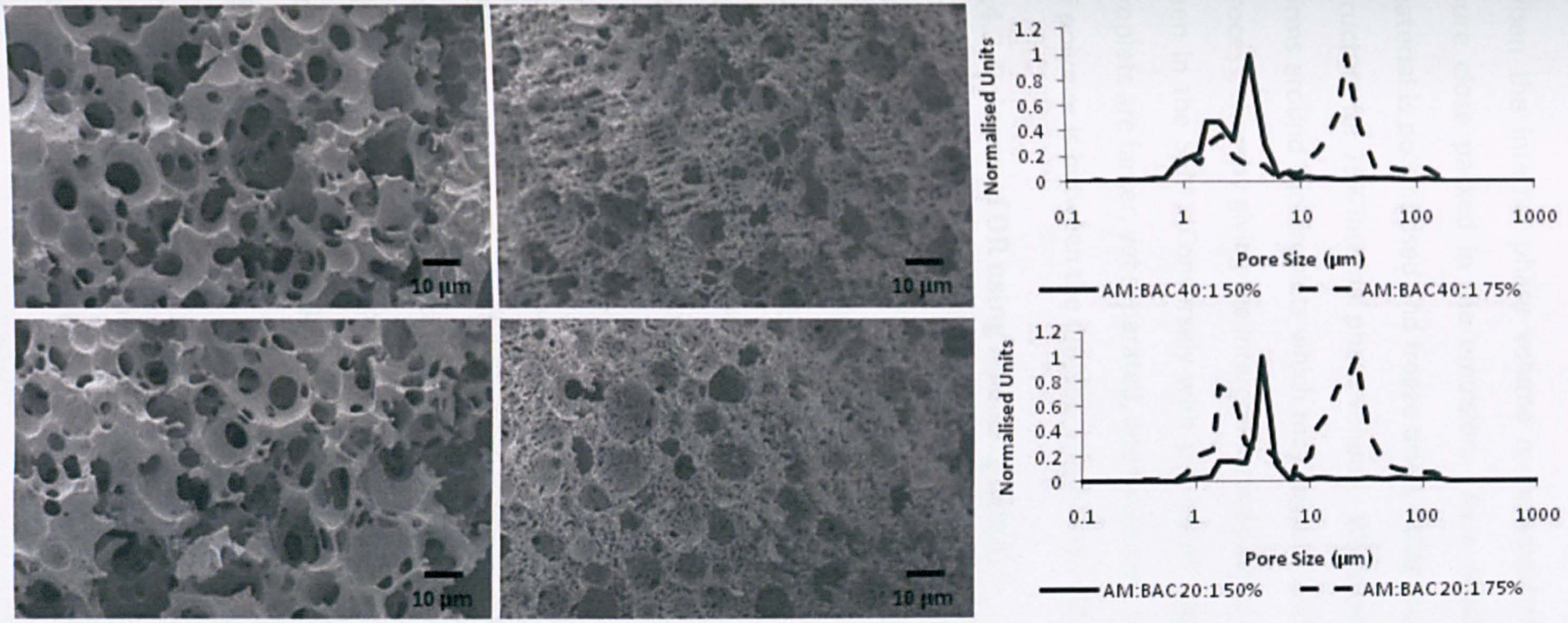

Figure 5-2 - SEM of the porous materials and the pore size characterisation by Hg intrusion

When the internal phase volume is increased the droplets become more close packed in the emulsion. As a result of this, when the material is polymerised and freeze dried, voids are seen in the polymer structure for 75% internal phase volume. When polymerised a thin film forms around the droplets which may rupture during the freeze-drying process, thereby giving the interconnected porous structure that can be seen in the SEM. Conversely with the lower volume percentage, the droplets are larger, yet separated, and when polymerised a thicker layer of polymer is between the droplets which does not get ruptured.

5.4.3 Release of OR using reducing agents

For all OR release using disulphide reducing agents. The OR can be seen to diffuse from the polymer, this is also observed by the solution becoming a clear red suspension of OR nanoparticles. As the disulphide bonds in the polymer become cleaved the material is seen to reduce in size and in some cases the material can break apart before eventually becoming completely dissolved.

5.4.3.1 Release of model dye

The porous materials loaded with OR can be placed into water. A control, where the polymer was placed into aqueous solution without the redox agent present confirmed that little OR was released through diffusion from the pores of the materials. The release of OR from the porous polymers where performed using DTT and TCEP as reducing agents.

5.4.3.2 Release of OR using DTT

DTT (also known as Cleland's reagent)[17] is a strong reducing agent. The reduction of a disulphide bond happens in two steps; both steps being

individual thiol-disulphide exchange reactions (see Mechanism 1). The intermediate is highly unstable and the lone thiol of the DTT prefers to close the ring to form the stable ox-DTT (a 6-membered ring with an internal disulphide bond). Closure of this ring leaves behind the reduced disulphide bonds.

The reducing capabilities of DTT are very limited owing to the fact that only the negatively charged S- thiolate is the reactive species, therefore the reaction is limited to pH values above pH7. DTT is also limited in the fact that it self-oxidises and multiple thiol-disulphide exchange reactions can occur.

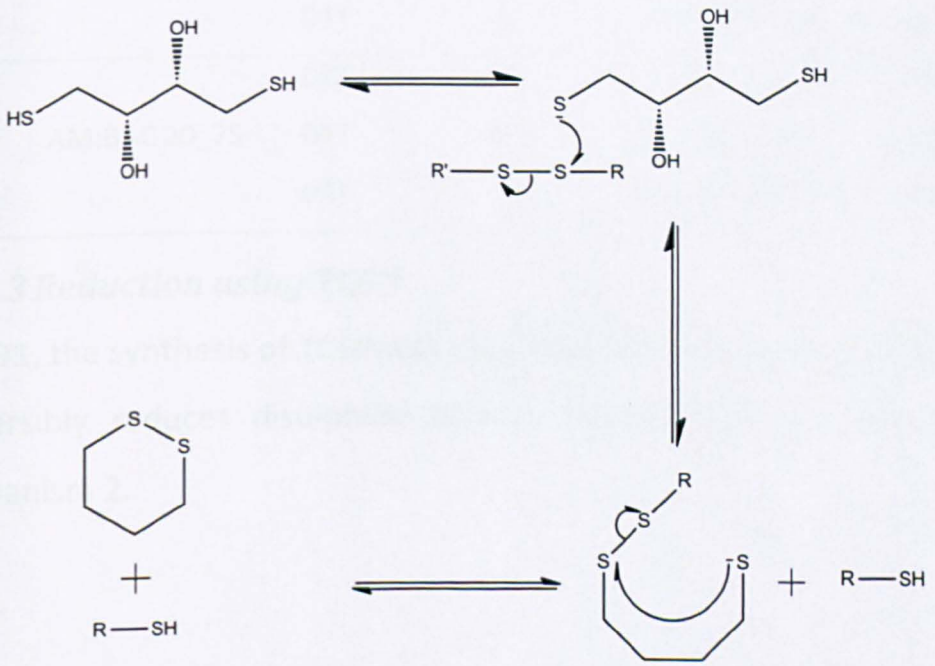

Scheme 1 - Reduction of a disulphide bond by DTT

The polymers where subjected to disulphide breaking by DTT, the release conditions for the release of OR are shown in table 2.

Table 2 - Release rates of Oil Red using DTT at pH 9

Sample ID	Sample	Redox reagent	Concentration of redox agent (wt%)	Release rate ($min^{-1/2}$)	R^2
SS1		DTT	0.1	0.0681 ± 0.006	0.9166
SS2	AM:BAC 40_50	DTT	0.2	0.0768 ± 0.006	0.9411
SS3		DTT	1	0.0952 ± 0.006	0.9371
SS4		DTT	0.1	0.1119 ± 0.017	0.8493
SS5	AM:BAC 40_75	DTT	0.2	0.1256 ± 0.016	0.8691
SS6		DTT	1	0.1418 ± 0.012	0.9161
SS7		DTT	0.1	0.0568 ± 0.008	0.8532
SS8	AM:BAC 20_50	DTT	0.2	0.0661 ± 0.011	0.8365
SS9		DTT	1	0.0789 ± 0.011	0.856
SS10		DTT	0.1	0.1044 ± 0.018	0.8321
SS11	AM:BAC 20_75	DTT	0.2	0.1179 ± 0.017	0.853
SS12		DTT	1	0.1322 ± 0.016	0.8951

5.4.3.3 Reduction using TCEP

In 1991, the synthesis of TCEP was described, this stoichiometrically and irreversibly reduces disulphide bonds according to the reaction in Mechanism 2.

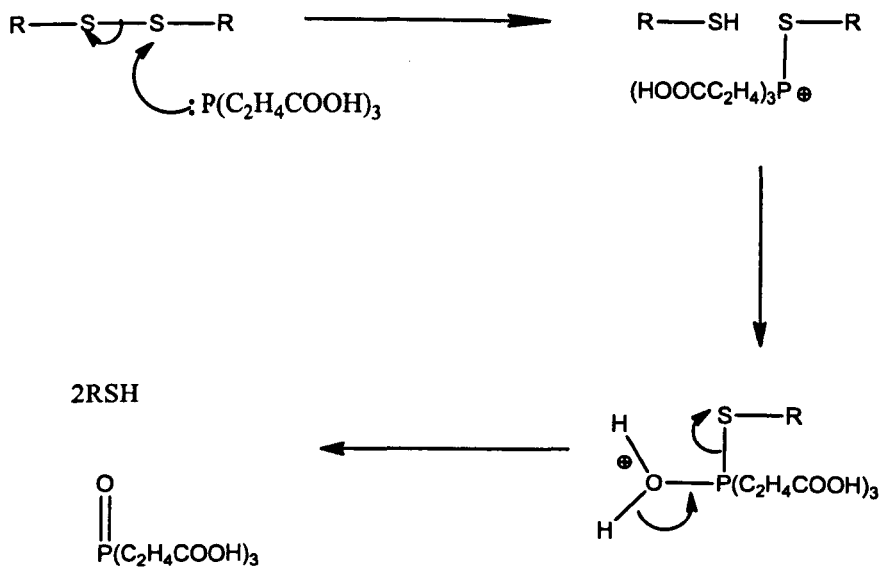

Scheme 2 - Reduction of a disulphide bond by TCEP

TCEP has been shown to be significantly more stable that DTT above 7.5 and a faster reductant below 8. TCEP can be a much more useful reducing agent than DTT over a much wider pH range (1.5-8.5)[27]. Release of OR using TCEP was performed in distilled water. The release rates are shown in Table 3.

Table 3 - Release Rates of Oil Red using TCEP at pH 7

Sample ID	Sample	Redox reagent	Conc^{n} of redox agent (wt%)	Release rate (min $^{-1/2}$)	R^2
SS13		TCEP	0.02	0.0181 ± 0.001	0.9731
SS14	AM:BAC 40_50	TCEP	0.2	0.0295 ± 0.001	0.9783
SS15		TCEP	1	0.0437 ± 0.001	0.9884
SS16		TCEP	0.02	0.0221 ± 0.001	0.9757
SS17	AM:BAC 40_75	TCEP	0.2	0.0336 ± 0.001	0.9656
SS18		TCEP	1	0.0563 ± 0.001	0.9783
SS19		TCEP	0.02	0.0154 ± 0.001	0.979
SS20	AM:BAC 20_50	TCEP	0.2	0.0248 ± 0.001	0.9767
SS21		TCEP	1	0.0384 ± 0.001	0.9806
SS22		TCEP	0.02	0.023 ± 0.001	0.9682
SS23	AM:BAC 20_75	TCEP	0.2	0.0323 ± 0.001	0.9654
SS24		TCEP	1	0.0472 ± 0.001	0.9845

5.4.3.4 Changing DTT concentration

Thiol-disulphide exchange reactions are reversible processes. In order for the reduction to occur, the DTT must be kept under nitrogen to ensure the DTT does not self-oxidise. The number of moles of DTT is in a large excess to that of the number of the moles of the disulphide bond (3.24×10^{-5} mole (0.1 wt% DTT) to 4.81×10^{-6} mol (40:1 Crosslinked polymer) Due to the large excess of the DTT the rate of reaction will not be changed significantly by concentration of DTT. This is exemplified by the release kinetics of OR from the polymers. Taking, for example, samples SS1, SS2 and SS3, the concentration of DTT is increasing from 0.1, 0.2 and 1wt% respectively. The release rates increase from 0.0681 to 0.0768 to 0.0952. This can be exemplified by looking at the examples in figure 3 where most of the OR nanoparticles are released before 120

minutes. As the mechanism of DTT reduction of disulphides is by thiol-disulphide exchange reactions, the oxidised-DTT (ox-DTT) can also partake in the mechanism with a previously cleaved disulphide bond which exists as a thiol. As the pH of the solution was quite high (pH 9), the presence of the thiolate (R-S- ion) is high (pKa ~8). As the overall concentration of the thiolate ion is high (also present from the cleaved disulphide bonds). The thiol-disulphide reactions can occur readily until all the disulphide bonds in the polymer have been cleaved.

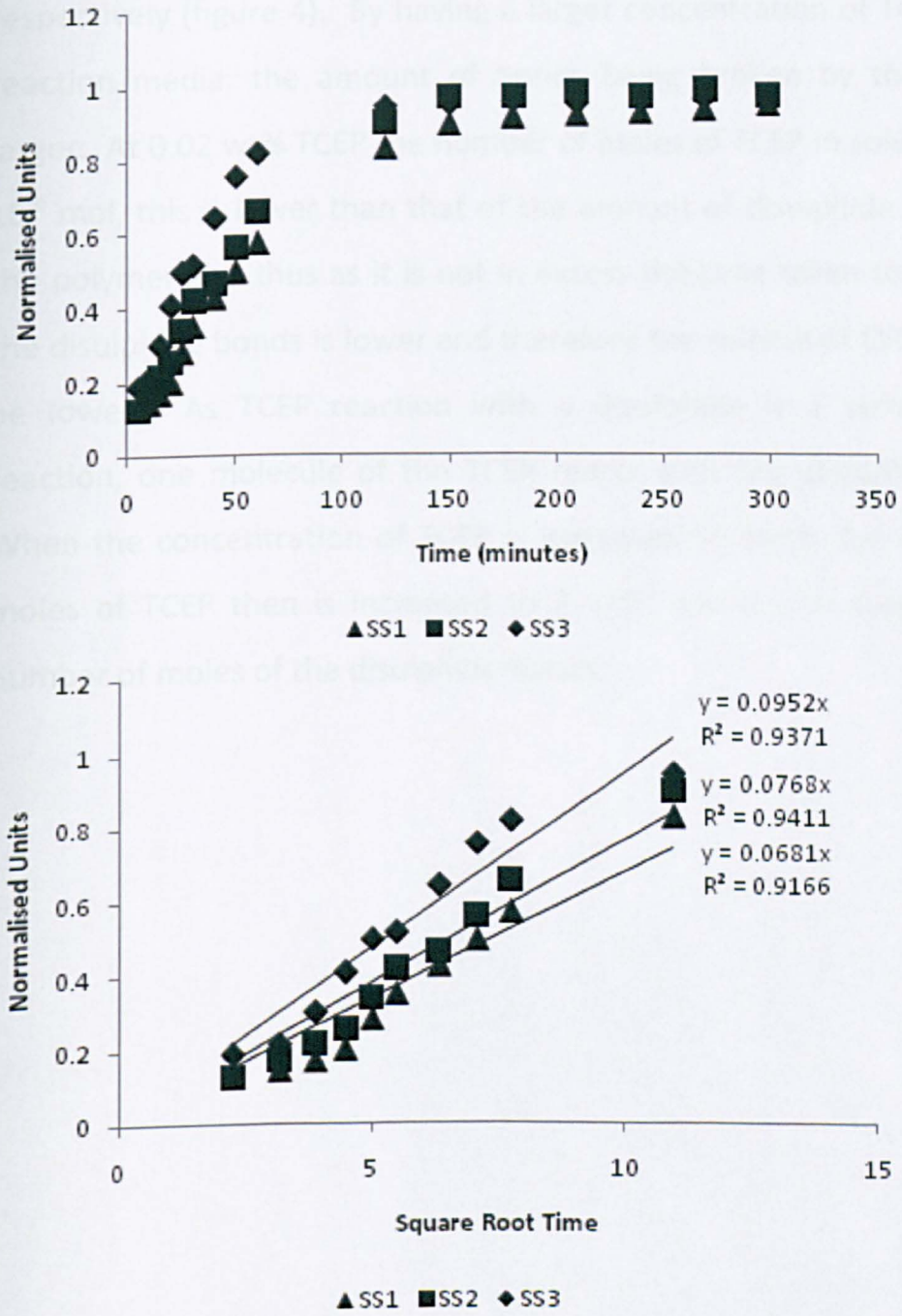

Figure 5-3 – Release profile and rate constant determination for samples SS1 SS2 and SS3.

5.4.3.5 Changing TCEP concentration

Conversely to changing the DTT concentration in the earlier section; the effect of TCEP on the release of OR is significant. Comparing samples: SS13, SS14 and SS15, the rate of OR release increases from 0.0181 to 0.0295 and 0.0437 for concentrations of 0.02, 0.2 and 1wt%

respectively (figure 4). By having a larger concentration of TCEP in the reaction media, the amount of bonds being broken by the TCEP is larger. At 0.02 wt% TCEP the number of moles of TCEP in solution is 4 x 10^{-6} mol, this is lower than that of the amount of disulphide bridges in the polymer and thus as it is not in excess the time taken to cleave all the disulphide bonds is lower and therefore the release of OR is seen to be lower. As TCEP reaction with a disulphide is a stoichiometric reaction, one molecule of the TCEP reacts with one disulphide bond. When the concentration of TCEP is increased to 1wt% the number of moles of TCEP then is increased to 2 x10^{4} which is in excess of the number of moles of the disulphide bonds.

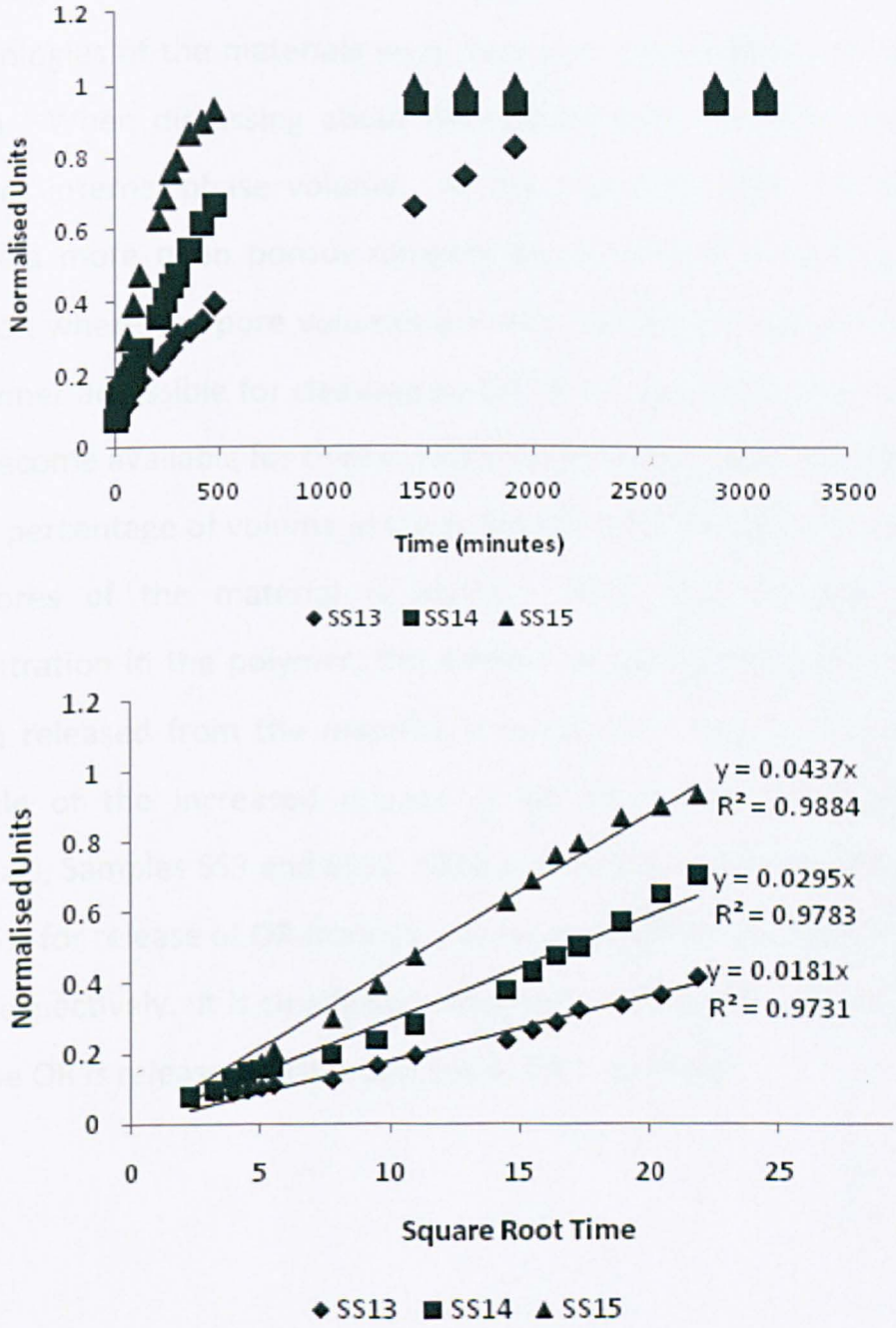

Figure 5-4 - Release profile and rate determination for samples SS13, SS14 and SS15

5.4.3.6 Changing internal phase volume

By changing the internal phase volume of the emulsions, the polymer prepared becomes more porous with an open network (see figure 1). With the polymers prepared with a 50% emulsion the pre-formed emulsion was homogenized due to rapid coalescence observed when

preparing the emulsions and consequently when polymerized the morphologies of the materials were very poor with a pore size of over 100μm. When discussing about OR release from the polymers with different internal phase volume. As the materials with 75% volume ratio is a more open porous network (as confirmed by SEM and Hg intrusion where the pore volumes are observed to be higher) the area of polymer accessible for cleavage by DTT is higher and therefore more sites become available for thiol-disulphide exchange. Also with having a higher percentage of volume in the pores the amount of OR available in the pores of the material is higher. With this increase in OR concentration in the polymer, the amount of nanoparticles of OR that can be released from the material is increased. Figure 5 shows an example of the increased release of OR from the higher porosity materials, Samples SS9 and SS12, SS19 and SS22 are the respective 50% and 75% for release of OR from 20:1 crosslinked polymers from DTT and TCEP respectively. It is clearly seen that with the highest volume phase, that the OR is release is faster and more OR is released.

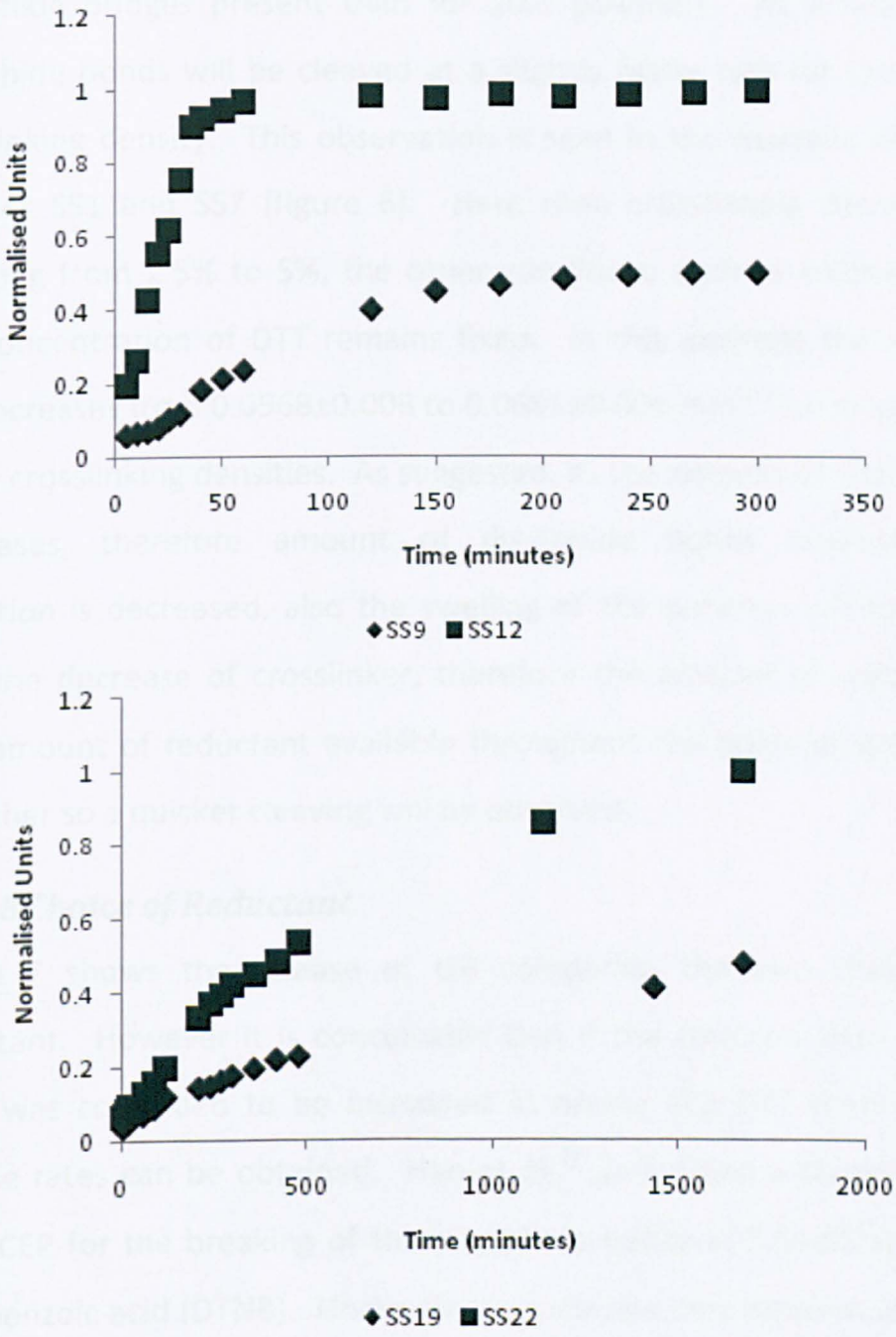

Figure 5-5 Release comparisons for 50% and 75% volume ratio of the polymer

5.4.3.7 Changing Crosslinking Density

By changing the crosslinking density of the polymer, the amount of disulphide bonds present in the polymer changes, the SEM images earlier show little change to the overall structure of the prepared materials. For 40:1 crosslinked polymers there are half as many

disulphide bridges present than for 20:1 polymers. As a result the disulphide bonds will be cleaved at a slightly faster rate for the lower crosslinking density. This observation is seen in the example of using samples SS1 and SS7 (figure 6). Here then crosslinking densities is changing from 2.5% to 5%, the other conditions such as volume ratio and concentration of DTT remains fixed. In this example the release rate increases from 0.0568±0.008 to 0.0681±0.006 $min^{-1/2}$ on decreasing of the crosslinking densities. As suggested, as the amount of crosslinker decreases, therefore amount of disulphide bonds available for reduction is decreased, also the swelling of the polymer will increase with the decrease of crosslinker, therefore the amount of water and thus amount of reductant available throughout the polymer work will be higher so a quicker cleaving will be observed.

5.4.3.8 Choice of Reductant

Figure 7 shows the release of OR comparing the two choices of reductant. However it is conceivable that if the concentration of the TCEP was continued to be increased in excess like DTT then similar release rates can be obtained. Han et al,[20] performed a study of DTT and TCEP for the breaking of the disulphide bonds in 5,5'-dithiobis-(2-nitrobenzoic acid (DTNB). Under their conditions they observe that the breaking of the disulphide bonds in DTNB using DTT at pH 9 is much quicker than that at TCEP at pH 7. The study covers a range of pHs for both redox reagents.

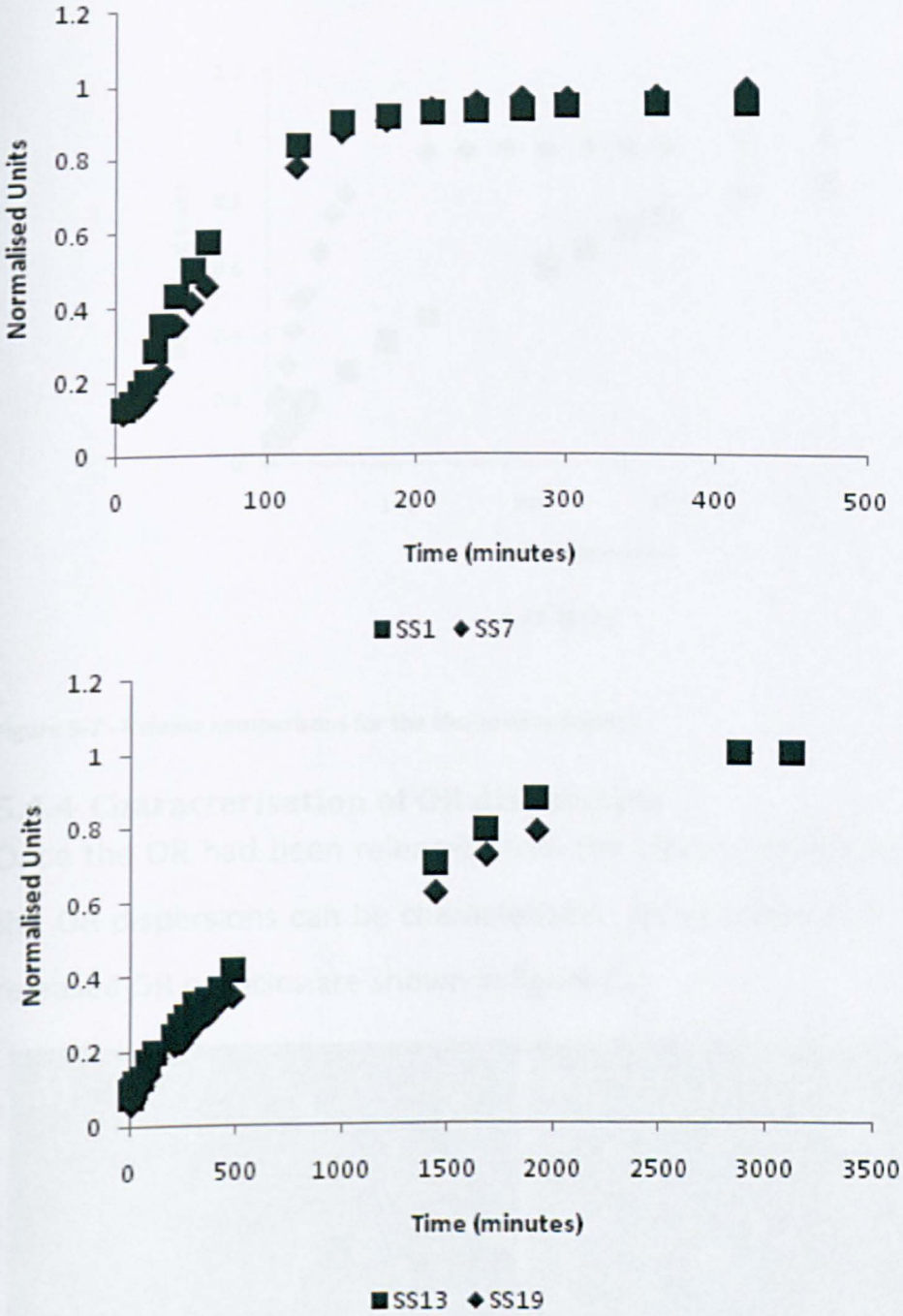

Figure 5-6 - Release comparisons for the amount of crosslinker in the polymer

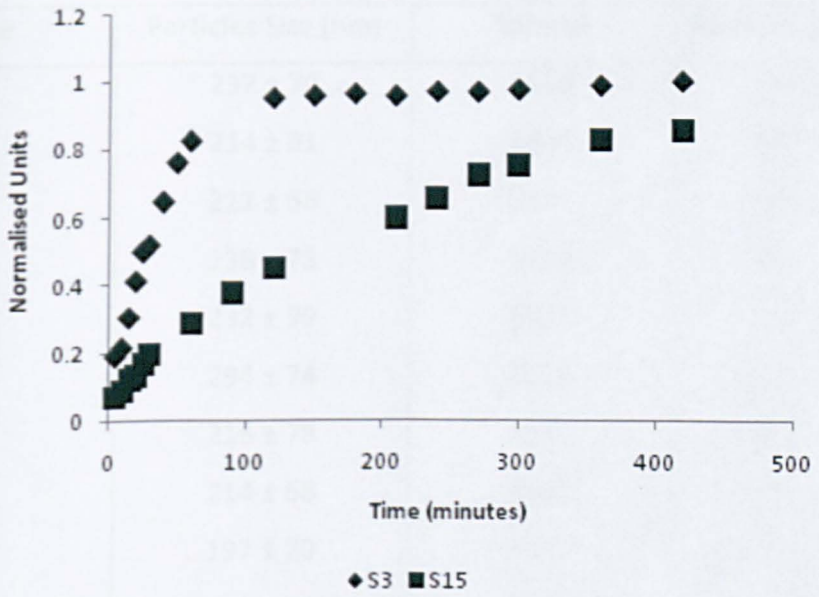

Figure 5-7 - Release comparisons for the choice of reductant

5.4.4 Characterisation of OR dispersions

Once the OR had been released from the cleaved disulphide polymer, the OR dispersions can be characterized. An example of a TEM of the released OR particles are shown in figure 8:

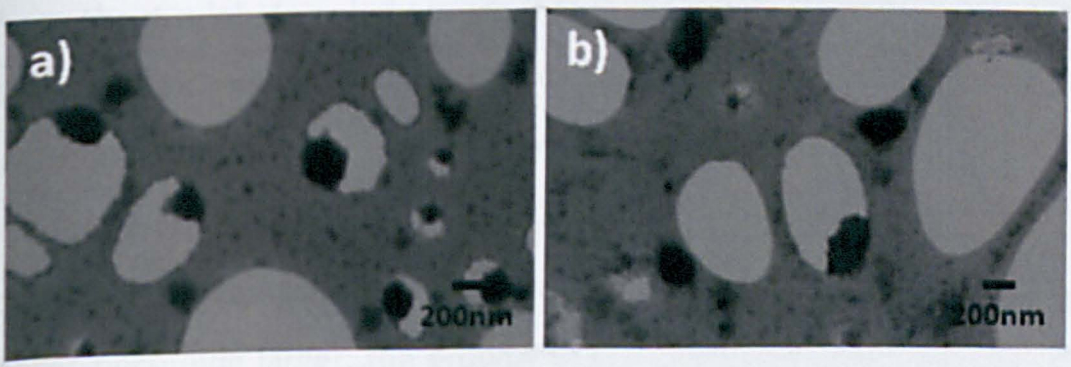

Figure 5-8 - TEM images of the nanoparticles a) from DTT b) from TCEP

The OR particles released from the polymers are in the region of 200nm. The particles released from the polymer can be examined by DLS analysis. Table 4 summarises the particles sizes of the OR from the polymer.

Table 4 - Particles size measurements of OR

Sample	Particles Size (nm)	Sample	Particles Size (nm)
SS1	237 ± 70	SS13	197 ± 57
SS2	214 ± 81	SS14	228 ± 76
SS3	212 ± 56	SS15`	207 ± 70
SS4	238 ± 73	SS16	239 ± 61
SS5	232 ± 99	SS17	216 ± 62
SS6	294 ± 74	SS18	217 ± 54
SS7	216 ± 78	SS19	185 ± 52
SS8	214 ± 68	SS20	179 ± 46
SS9	197 ± 70	SS21	200 ± 59
SS10	260 ± 72	SS22	211 ± 71
SS11	245 ± 63	SS23	216 ± 79
SS12	234 ± 60	SS24	217 ± 68

By DLS analysis the hydrated diameter of the OR nanoparticles is on average 210 nm. The summary of the particles sizes of OR released from the disulphide polymers are shown in table 4. Generally speaking, the particles sizes from 75% internal volume are larger than for 50 % internal volume. For example: samples SS7 and SS10 (50 % and 75 % respectively). The particles sizes are 216.0 and 260.2 nm. The larger particles size can be accounted for by the size of the interconnected pores becoming larger; the growth of the nanoparticles on the surface of the materials is less prohibited and could, therefore can grow larger than for a closed porous surface.

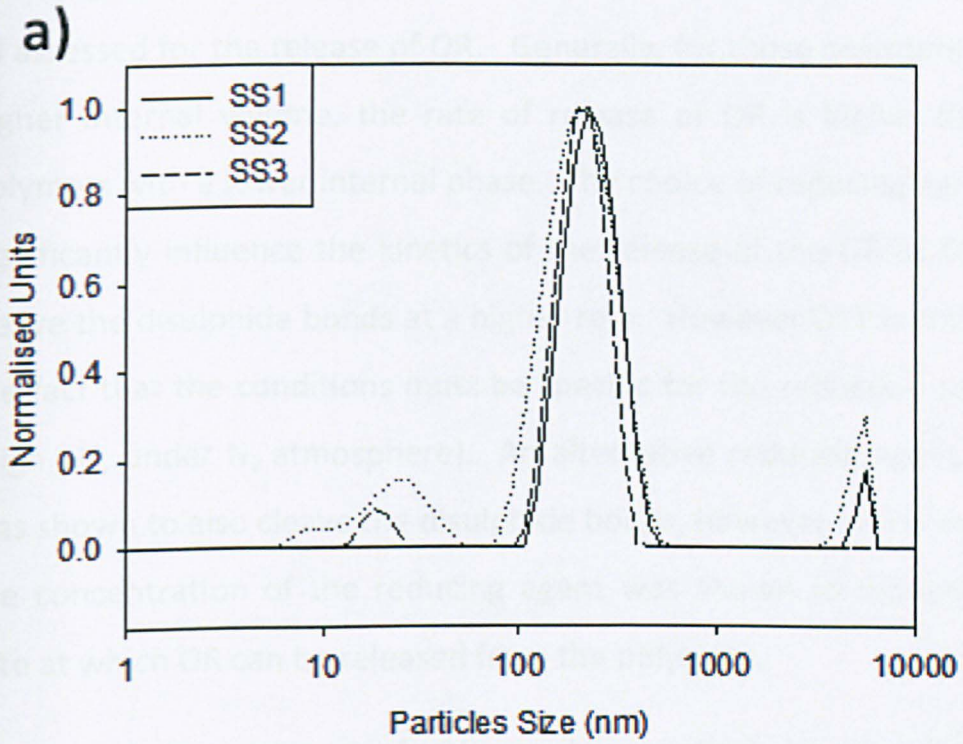

Figure 5-9 - Example of particle size distribution. Examples are for samples SS1, SS2 and SS3

For each respective sample conditions, the particles sizes remain experimentally the same. Figure 9 shows and example of the particle size characterisation. In each case it is confirmed that the size of the particles does not change significantly. Therefore the effect on the concentration of the reductant has little effect on particle size. The peaks observed at the lower range (approx 10nm) will be the presence of surfactant and/or polymer not removed by the centrifugation/filtration steps.

5.5 Conclusions

Oil Red has been shown to be released from emulsion templated polymeric structures with a degradable disulphide crosslinkage. The polymer can be degraded by using a reducing agent such as DTT and TCEP. The effects on choice of reducing agent, concentration of

reducing agent, internal phase volume and crosslinking densities where all assessed for the release of OR. Generally, for those polymers with a higher internal volume, the rate of release of OR is higher than for polymers with a lower internal phase. The choice of reducing agent can significantly influence the kinetics of the release of the OR as DTT can cleave the disulphide bonds at a higher rate. However DTT is limited by the fact that the conditions must be specific for the reduction to occur (high pH, under N_2 atmosphere). An alternative reducing agent, TCEP, was shown to also cleave the disulphide bonds, however in this instance the concentration of the reducing agent was shown to influence the rate at which OR can be released from the polymers.

In general the release of OR is characterised by the following observations (release rate in order of magnitude):

- Influence of internal phase volume: 75% volume ratio > 50% volume ratio
- Influence of redox reagent concentration: 1wt% >> 0.2wt% >> 0.02 wt% (TCEP); 1wt%>0.2wt%>0.1wt% (DTT)
- Influence on crosslinking density: 40:1 crosslink > 20:1 crosslink

5.6 References

1. Langer, R.; Vacanti, J. P. *Science* **1993**, *260*, 920-926.
2. Vinogradov, S. V.; Bronich, T. K.; Kabanov, A. V. *Advanced Drug Delivery Reviews* **2002**, *54*, 135-147.
3. Peppas, N. A.; Keys, K. B.; Torres-Lugo, M.; Lowman, A. M. *Journal of Controlled Release* **1999**, *62*, 81-87.
4. Oh, J. K.; Siegwart, D. J.; Lee, H.-i.; Sherwood, G.; Peteanu, L.; Hollinger, J. O.; Kataoka, K.; Matyjaszewski, K. *Journal of the American Chemical Society* **2007**, *129*, 5939-5945.

5. Denizli, A.; Kiremitci, M.; Piskin, E. *Biomaterials* **1988**, *9*, 363-366.
6. Edlund U.; Albertsson A. C. *Advances in Polymer Science* **2002**, *157*, 67.
7. Emilitri, E.; Ranucci, E.; Ferruti, P. *Journal of Polymer Science: Part A: Polymer Chemistry* **2005**, *43*, 1404-1416.
8. Bromberg, L.; Temchenko, M.; Alakhov, V.; Hatton, T. A. *Langmuir* **2005**, *21*, 1590-1598.
9. Hiratani, H.; Alverez-Lorenzo, C.; Chuang, J.; Guney, O.; Grosberg, A. Y.; Tanaka, T. *Langmuir* **2001**, *17*, 4431-4436.
10. Hiratani, H.; Miztani, Y.; Alverez-Lorenzo, C. *Macromolecular Biosciences* **2005**, *5*, 728-733.
11. Li, C.; Madsen, J.; Armes, S. P.; Lewis, A. L. *Angewandte Chemie International Edition* **2006**, *45*, 3510-3513.
12. Lees, W. J.; Whitesides, G. M. *Journal of Organic Chemistry* **1992**, *58*, 642-647.
13. Kakizawa, Y.; Harada, A.; Kataoka, K. *Journal of the American Chemical Society* **1999**, *121*, 11247-11248.
14. Getz, E. B.; Xiao, M.; Chakrabarty, T.; Cooke, R.; Selvin, P. *Analytical Chemistry* **1999**, *273*, 73-80.
15. Kice, J. L. *Chem. Res.* **1968**, *1*.
16. Parker, A. J.; Kharasch, N. *Chem. Rev.* **1959**, *59*, 583.
17. Cleland, W. W. *Biochemistry* **1964**, *3*, 480-482.
18. Netto, L. E. S.; Stadtman, E. R. *Arch. Biochem. Biophys* **1996**, *333*, 233-242.
19. Burns, J. A.; Butler, J. C.; Moran, J.; Whitesides, G. M. *Journal of Organic Chemistry* **1991**, *56*, 2648-2650.
20. Han, J. C.; Han, G. Y. *Analytical Biochemistry* **1994**, *220*, 5-10.
21. Ruegg, U. T.; Fudinger, J. *Methods in Enzymology* **1977**, *47*, 111-126.
22. Zelikin, A. N.; Quinn, J. F.; Caruso, F. *Biomacromolecules* **2006**, *7*, 27-30.
23. Lei, Q.; He, X.-W.; Zhang, W.; Li, W.-Y.; Zhang, Y.-K. *Analytical Chemistry* **2009**, *81*.
24. Yuting, L.; Armes, S.P.; McConwich, C. L., *Macromolecules,* **2006**, 39, 8, 2726-2728
25. Huffman, R. W.; Brown, D. M. *Journal of Organic Chemistry* **1991**, *56*, 6477-6479.
26. Reverchen, E, *Ind. Eng. Chem.* **2002**, 41, 2405

27. Han, S.-C.; He, W.-d.; Li, J.; Li, L.-Y.; Sun, X.-L.; Zhang, B.-Y.; Pan, T.-T. *Journal of Polymer Science: Part A: Polymer Chemistry* **2009**, *47*, 4074-4082.

6 CONCLUSIONS AND FUTURE WORK

6.1 Conclusions

This thesis has been based on emulsion templating for the release of organic micro- and nanoparticles. The porous materials where all produced from oil-in-water emulsions.

Firstly, porous poly(N-isopropylacrylamide) was prepared by emulsion templating and used to upload and release polymeric polystyrene colloids. The swelling capabilities and the water uptake of the crosslinked PNIPAM was used to upload the colloids, the colloids were observed to be on the pore walls of the PNIPAM polymer. The LCST of NIPAM was investigated and shown to release the colloids through multiple heating steps. The reproducibility of the uptake and release of colloids was demonstrated and the colloids where shown to not be altered by the upload and release procedures.

The next chapter follows up from an initial publication for water soluble emulsion templated materials by using Indomethacin as a model drug. The working example shows the production of an emulsion templated PVA/SDS system with IMC loaded into the pores of the material. The IMC nanodispersions can be observed by dissolving the monoliths rapidly into water. The effect on emulsion, pore size/volume and the nanodispersions hydrated particles size and zeta potential was observed by changing the polymer and surfactant concentrations and also the volume percentage. The PVA acts like a co-surfactant and therefore aids the stability of the emulsions whereas the surfactant SDS was shown to improve the morphologies of the pores and also decrease

the droplet size and the effect of these on the particles sizes where demonstrated.

Chapter 4 demonstrates using emulsion templated chitosan as a scaffold for the production of nanoparticles. The chitosan can be placed into differing pH ranges and showed a pH dependent release of organic nanoparticles of Oil Red and IMC. Due to the uncrosslinked nature of the chitosan and owing to its pKa, the release at lower pH is observed and the chitosan readily dissolves after a period of time. The release demonstrated the capabilities of using chitosan in different pHs for different release rates of the internal molecule.

Finally, Chapter 5 moves on to demonstrate release of OR from templated materials based on a disulphide bond as a crosslinker. Under normal conditions the OR can remain within the pores of the materials but upon addition of a redox reagent (DTT or TCEP) the disulphide bonds can be broken and the Oil Red can be released. The release rates for the different concentrations of the redox reagents, crosslinking densities of the disulphide crosslinker and the internal phase volume of the porous materials were demonstrated

6.2 Future Work

The possibilities of responsive materials are not limited to those presented in this thesis. Other stimuli can be investigated such as a response to light as an example: A polymeric network based on a 'ferrogel' could be implemented which modifies its shape in a magnetic field. A ferrogel is a gel, where a ferromagnetic material, such as magnetite (Fe_3O_4) particles dispersed in water was used in a network of poly(vinyl alcohol) crosslinked in by glutaraldehyde. The magnetic

particles were incorporated into chemically crosslinked poly(vinyl alcohol) hydrogels.[1]

Another example of a responsive system could be through response to light: Visible light-sensitive hydrogels have been prepared by introducing a light-sensitive chromophore (e.g. trisodiumsalt of copper chlorophyllin) to poly(N-iso-propylacrylamide) hydrogels. When light is applied to the hydrogel, the chromophore absorbs light which is then dissipated as heat by radiation increasing the temperature of the hydrogel. The temperature increase alters the swelling behaviour of poly(N-isopropylacrylamide) hydrogels.[2]

Other responsive systems include and are not limited to: Electric signals, Magnetic, Glucose, Pressure and specific ions

6.3 References

1. Zrinyi,M., Barsi, L., Buki, A., *Polymer Gels and Networks*, **1997**, 5, 415-427

2. Suzuki, A., Tanaka, T., *Nature*, **1990**, 346, 345-347

7 APPENDIX

7.1 pH dependent release of organic nanoparticles from chitosan monoliths

Table 7-1 - Summary of the release rates and particle characterisation of OR released from emulsion templated chitosan.

Sample	Sample Code	pH	Rate Constant ($min^{-½}$)	R^2	Particle Size (nm)	Zeta potential (mV)
1L-OR 50	C1	2	0.1063 ± 0.002	0.9769	214 ± 85	42.7 ± 12.7
1L-OR 50	C2	7	0.0083 ± 0.001	0.8589	134 ± 46	1.95 ± 2.4
1L-OR 50	C3	10	0.081 ± 0.004	0.9504	135 ± 43	-15.2 ± 1.4
1L-OR 80	C4	2	0.1535 ± 0.003	0.9835	203 ± 68	53.3 ± 11.7
1L-OR 80	C5	7	0.0385 ± 0.003	0.9323	174 ± 40	2.11 ± 2.6
1L-OR 80	C6	10	0.1109 ± 0.005	0.9562	124 ± 32	-10.8 ± 1.6
1M-OR 50	C7	2	0.1305 ± 0.010	*0.9271*	*191 ± 77*	*44.8 ± 14.6*
1M-OR 50	C8	7	0.0083 ± 0.002	0.8174	119 ± 27	2.65 ± 3.0
1M-OR 50	C9	10	0.1015 ± 0.011	0.893	122 ± 41	-14.8 ± 2.4
1M-OR 80	C10	2	0.1756 ± 0.006	0.9658	175 ± 52	55.6 ± 15.4
1M-OR 80	C11	7	0.0327 ± 0.004	0.8921	191 ± 35	2.59 ± 1.6
1M-OR 80	C12	10	0.0901 ± 0.003	0.9674	149 ± 37	-12.2 ± 3.1
1H-OR 50	C13	2	0.1553 ± 0.016	0.8971	188 ± 53	42.6 ± 12.6
1H-OR 50	C14	7	0.0096 ± 0.002	0.8343	194 ± 44	2.15 ± 1.6
1H-OR 50	C15	10	0.1052 ± 0.014	0.8673	110 ± 28	-15.1 ± 2.5
1H-OR 80	C16	2	0.16 ± 0.005	0.9684	186 ± 39	52.8 ± 13.4
1H-OR 80	C17	7	0.03 ± 0.004	0.8831	196 ± 50	1.16 ± 2.1
1H-OR 80	C18	10	0.1026 ± 0.008	0.9219	117 ± 37	-12.9 ± 4.2

Table 7-2 - Summary of the release rates, particle size and zeta potential measurements for release of IMC from emulsion templated chitosan

Sample	Sample Code	pH	Rate Constant ($min^{-½}$)	R^2	Particle Size (nm)	Zeta potential (mV)
CH1L-IMC 50	C19	2	0.1287 ± 0.004	0.9633	253 ± 71	13.7 ± 5.4
CH1L-IMC 50	C20	7	0.0501 ± 0.001	0.9719	152 ± 69	2.54 ± 3.0
CH1L-IMC 50	C21	10	0.081 ± 0.003	0.959	202 ± 58	-10.8 ± 4.1
CH1L-IMC 80	C22	2	0.1425 ± 0.007	0.933	277 ± 99	24.7 ± 8.4
CH1L-IMC 80	C23	7	0.0335 ± 0.003	0.912	203 ± 63	3.39 ± 3.1
CH1L-IMC 80	C24	10	0.0678 ± 0.001	0.9798	241 ± 63	-3.85 ± 2.6
CH1M-IMC 50	C25	2	0.1358 ± 0.002	0.9868	255 ± 152	22.8 ± 10.2
CH1M-IMC 50	C26	7	0.0506 ± 0.001	0.9777	157 ± 82	6.14 ± 3.2
CH1M-IMC 50	C27	10	0.0751 ± 0.001	0.9885	216 ± 74	-10.1 ± 5.6
CH1M-IMC 80	C28	2	0.1306 ± 0.021	0.8361	293 ± 122	25 ± 11.6
CH1M-IMC 80	C29	7	0.0302 ± 0.001	0.992	214 ± 80	7.41 ± 4.1
CH1M-IMC 80	C30	10	0.0532 ± 0.001	0.9775	252 ± 74	-6.64 ± 2.3
CH1H-IMC 50	C31	2	0.1454 ± 0.003	0.9786	273 ± 110	23.5 ± 10.7
CH1H-IMC 50	C32	7	0.0409 ± 0.001	0.9783	163 ± 89	6.03 ± 3.9
CH1H-IMC 50	C33	10	0.0656 ± 0.002	0.9716	222 ± 100	-11.7 ± 4.6
CH1H-IMC 80	C34	2	0.142 ±v 0.018	0.87	299 ± 116	19.5 ± 9.5
CH1H-IMC 80	C35	7	0.0249 ± 0.001	0.9646	215 ± 90	7.22 ± 3.6
CH1H-IMC 80	C36	10	0.0516 0.003	0.9423	263 ± 71	-6.67 ± 4.1

7.2 Disulphide crosslinked emulsion templated polymers and the Redox Controlled release of Organic nanoparticles

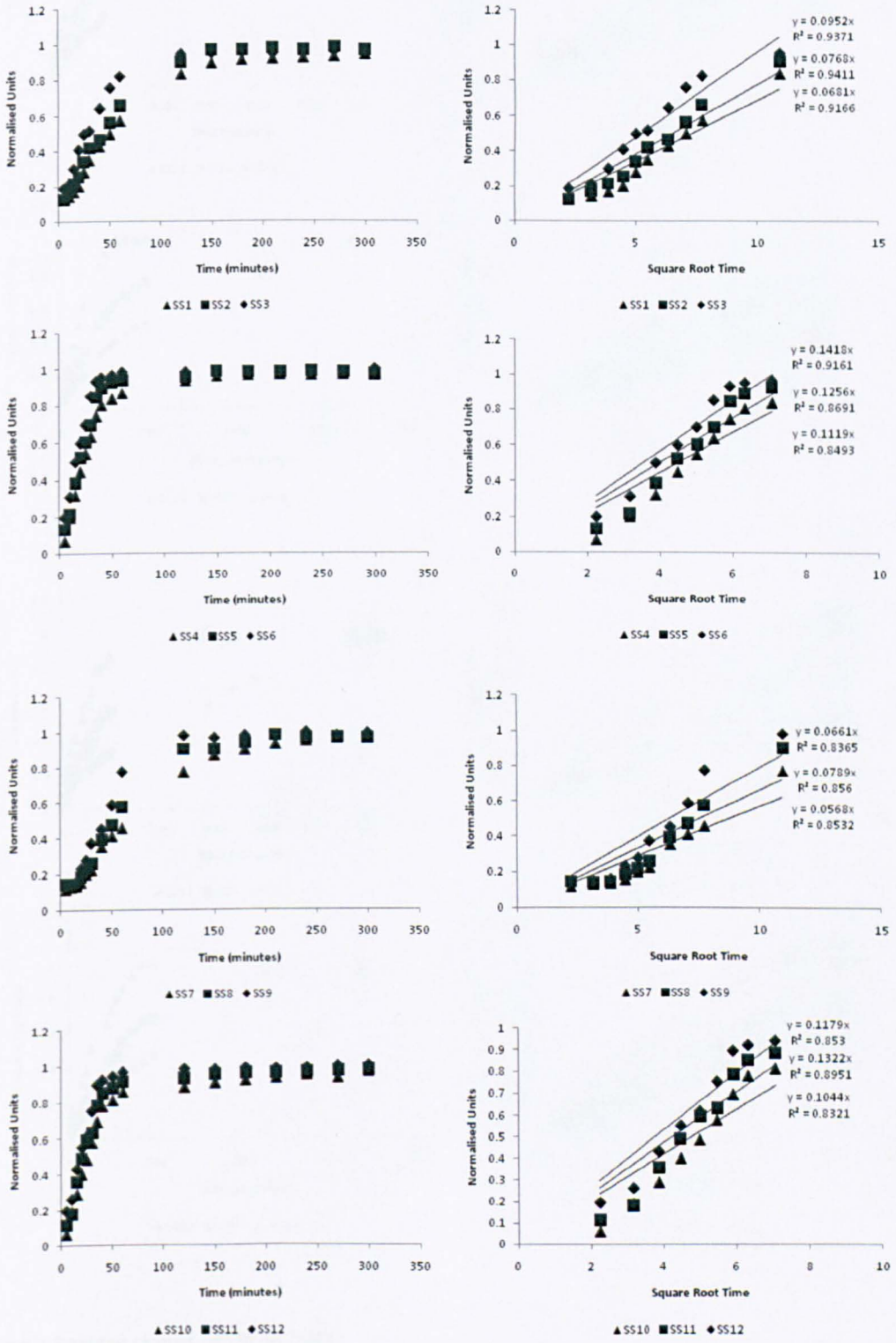

Figure 1 - Release charts of OR by DTT

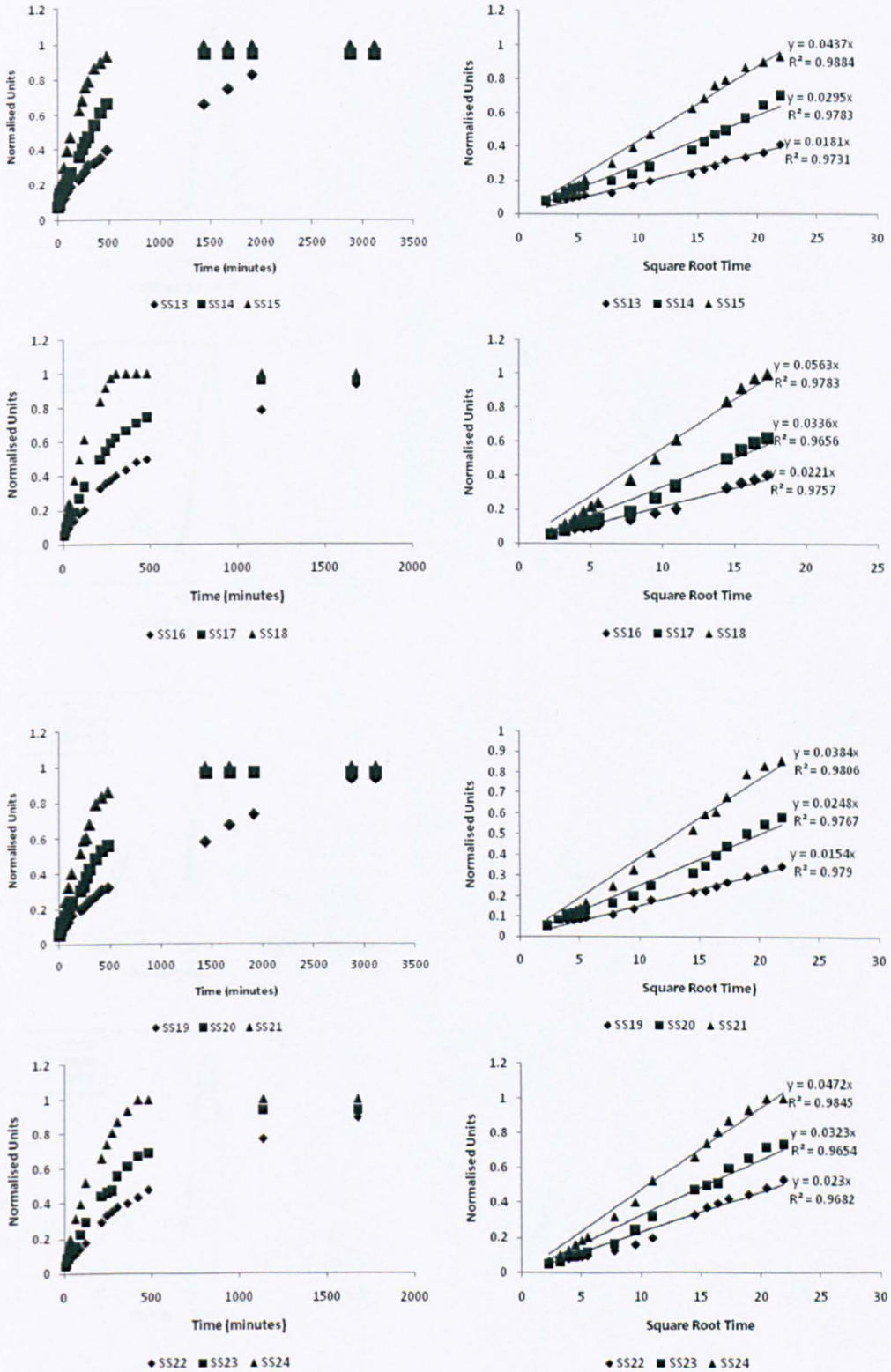

Figure 2 Release chares of OR by TCEP

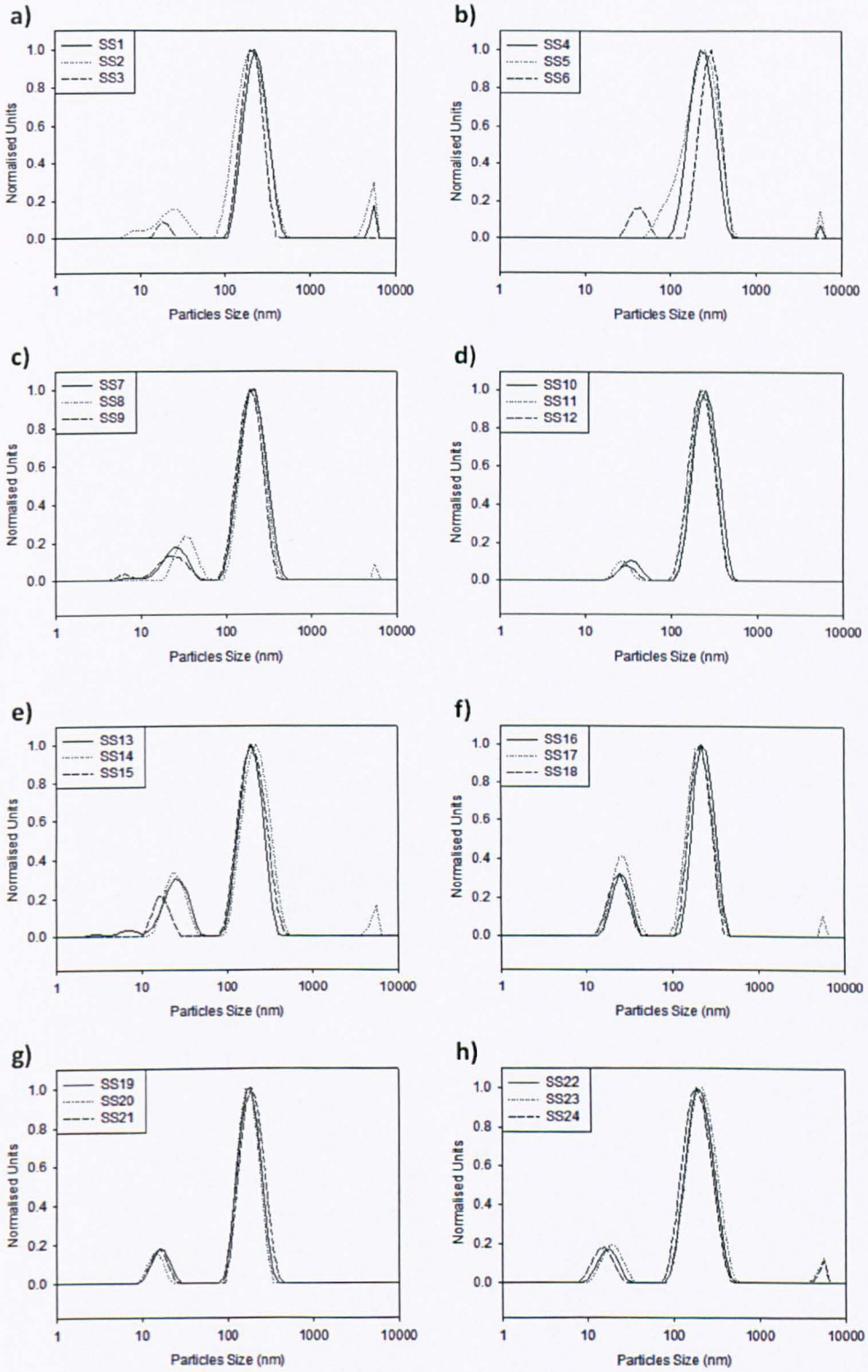

Figure 3 - Particle size distributions for OR